OCTOBER, 1995

FOURTH
REPORT

Australian Mineral Industries Research Association Limited
ACN 004 448 266

Faulting and Mineralisation in Western Tasmania

- P291A -

THE UNIVERSITY OF TASMANIA
CENTRE FOR ORE DEPOSITS AND EXPLORATION STUDIES

CENTRE FOR ORE DEPOSIT AND EXPLORATION STUDIES

STRUCTURE AND MINERALISATION OF WESTERN TASMANIA

AMIRA PROJECT P.291A
Fourth Report
October 1995

UNIVERSITY OF TASMANIA

CONTENTS

SUMMARIES

Lithogeochemistry
— R.F. Berry, D. Selley and M.J. White

The whole rock chemistry of the sedimentary rocks of the Mt Read Volcanics were compared to see if they were useful in distinguishing sedimentary sources sufficiently well to support a basin analysis. The chemical data was also investigated to demonstrate whether it could be used to solve some difficult lithostratographic correlation problems.

The trace element chemistry indicates that at least four sources can be readily discern. These are a low Ti basalt (MUC and Hellyer basalt), an intermediate Ti basalt (from normal Crimson Creek Formation) and a very high Ti basaltic suite (unknown source for Tyndall Group), and a felsic source. The separation of the felsic source into several groups may be possible with more Th data. The Precambrian basement source signature lies in the middle of these four types and cannot be detected unless it is a dominant component such as in the Stitt Quartzite. It is best detected by the presence of rounded zircon and tourmaline (and detrital mica).

The preliminary investigation indicated whole rock chemistry may be very useful in distinguishing a range of different rock types. The Animal Creek greywacke and Farrell Slate are clearly distinct from Dundas Group. The EQPS has a lower Ti/V than CVC volcaniclastics. The Tyndall Group was separated by high Ti/Th. These relationships need more data for a proper assessment but they are very encouraging.

Sedimentological evidence for Cambrian growth faults on the eastern side of the Dundas Trough, western Tasmania — Matt White

Geological evidence in the Anthony River area suggests that Cambrian movement was apparent on what is referred to as the Selina fault, during upper Tyndall Group (Middle to Late Cambrian) time. This is consistent with observations of Keele (1991) and Berry & Keele (1993), who interpreted a normal fault on the contact of the Tyndall Group and the Eastern Quartz-phyric sequence in this area. A southern bounding possible transfer fault may have constrained Tyndall Group deposition into a small fault-bounded basin. Reverse movement on the fault involving east-block upward movement is another possibility.

Progress Report 4: Detecting Cambrian structures in the Mount Read Volcanic Belt using sulfur isotopes
— sulfur isotopes of growth faults
— Garry J. Davidson and Paul Kitto

Sulfur isotope results from Cambrian growth faults can be tentatively divided according to fault style and fluid history. Those containing base-metal sulfides have values similar to known base-metal deposits in the Mount Read Volcanics (Carters Prospect). These consistently vary from north ($\delta^{34}S$ = 5–9‰) to south ($\delta^{34}S$ = 7–15‰) in the belt (Solomon et al., 1988). Those faults with small displacements, likely original Normal fault geometries, and pyrite rather than base-metal sulfides in the alteration assemblage, contain heavy sulfur (e.g. Comstock-Zig Zag Hill, $\delta^{34}S$ > ~20‰). Some of these have tentatively been identified at the margins of large base metal deposits, such as Rosebery. Thirdly, faults that lie sub-parallel to stratigraphy, are extensively sericite-chlorite altered, and are defined by wide shear zones (e.g. Moxons Saddle), have $\delta^{34}S = 0 \pm 5$‰, and may represent deep rock-buffered fluid circulation, although this conclusion requires confirmation of a Cambrian origin, because these values overlap those expected from Devonian magmatism. These conclusions are very preliminary, and will require detailed work on each scenario in the coming field season.

Fluid inclusion microthermometry of Cambrian and Devonian fault structures
— Paul A. Kitto

Geochemical and isotopic signatures associated with Cambrian and Devonian fault structures
— Paul A. Kitto

Lithogeochemistry

R.F. Berry, D. Selley and M.J. White

Centre for Ore Deposit and Exploration Studies, Geology Department, University of Tasmania

ABSTRACT

The whole rock chemistry of the sedimentary rocks of the Mt Read Volcanics were compared to see if they were useful in distinguishing sedimentary sources sufficiently well to support a basin analysis. The chemical data was also investigated to demonstrate whether it could be used to solve some difficult lithostratographic correlation problems.

The trace element chemistry indicates that at least four sources can be readily discern. These are a low Ti basalt (MUC and Hellyer basalt), an intermediate Ti basalt (from normal Crimson Creek Formation) and a very high Ti basaltic suite (unknown source for Tyndall Group), and a felsic source. The separation of the felsic source into several groups may be possible with more Th data. The Precambrian basement source signature lies in the middle of these four types and cannot be detected unless it is a dominant component such as in the Stitt Quartzite. It is best detected by the presence of rounded zircon and tourmaline (and detrital mica).

The preliminary investigation indicated whole rock chemistry may be very useful in distinguishing a range of different rock types. The Animal Creek greywacke and Farrell Slate are clearly distinct from Dundas Group. The EQPS has a lower Ti/V than CVC volcaniclastics. The Tyndall Group was separated by high Ti/Th. These relationships need more data for a proper assessment but they are very encouraging.

INTRODUCTION

A major aim of the combined ARC-AMIRA project is to define the basin geometry for the Mount Read Volcanics. A structural model was put forward in P291 which is being used as a template for this analysis. The project has looked at the heavy mineral suite as a guide to what sources are available to the basin at each stage in its genesis. Samples have been analysed from:

Cycle 1: Denison Group biostratigraphic correlates
All the units which are Idamean or younger.

Cycle 2: Tyndall cycle of deposition
upper Boomerangian/Mindallyian

Cycle 3: Yolande Cycle of deposition
Undillian/lower Boomerangian (pre- to syn-granite intrusions).

Heavy mineral distribution places constraints on the basin architecture. In addition, if certain sources only become available during the history of the belt a separation of the stratigraphy should be possible. However the separation and study of heavy minerals has proven a very time consuming exercise. The chemistry of the bulk rocks may be sufficient to discriminate different rock types and to recognise the different source types. In order to test this all the samples collected for heavy mineral analysis were

by XRF. This data set was combined with a similar set of whole rock analyses on sandstones of the Dundas area, Crimson Creek Formation and Oonah Formation analysed by Mr D. Selley and a group of sandstones from the Tyndall Group analysed by Mr M. White for his PhD project.

The results discussed below are heavily dependent on work that is formally outside the AMIRA project but made available to the AMIRA sponsors in a pre-publication form. The geochemistry of the Tyndall Group reported here is entirely within the PhD program of Matt White and outside the AMIRA project. The Dundas area, Stitt Quartzite and Oonah Formation samples, and arguments about the distinction of Crimson Creek from Dundas Group, and Concert Schist from Dundas, and the sandstones from Moores Pimple from Dundas Group all form part of the PhD program of Dave Selley which is formally outside the AMIRA project. Analyses from the Que River Shale, Eastern quartz phyric sequence and many volcanic rocks were made available to us on the basis that rights of first publication were retained by the people concerned. Many of the ideas summarised here were developed in extensive discussion with Joe Stolz and Tony Crawford. The results here could not have been achieved without this discussion. The AMIRA project has generated the data from the Animal Creek greywacke, CVC sandstones, Yolande River Group and northern Dundas Group. The major contribution of the AMIRA project reported here is to bring the diverse data sources together to achieve a basin-wide view of the sediment geochemistry.

SUMMARY OF PROVENANCE DATA FROM HEAVY MINERALS

1. The Tyndall Group is distinguished by high Fe oxide contents in heavy mineral separates (magnetite, hematite and ilmenite plus the oxidised equivalents). The total heavy mineral suite is high, about 1% of sample. The rocks have low zircon and tourmaline in the separates, possibly due to dilution effects. The high oxide content appears to be typical of all of the Tyndall Group and is not limited to the lower andesitic part. The Tyndall Source can be from defined as FeTi oxides >> euhedral zircon, Fe > Ti and apatite is > 0.01 * zircon.

2. The Animal Creek Greywacke has a distinctive association of high chromite, high TiO_2, very low Fe oxides, high zircon, tourmaline and apatite content. High rounded zircon content, about 0.15 ¥ chromite, apatite > euhedral zircon, high tourmaline, chromite>TiO_2 and Ti > Fe. The Yolande River samples from the Strahan Road have high chromite, apatite ~ zircon and Ti >Fe, but the chromite < TiO2.

3. In contrast the Tyennan region, as exemplified by the Sticht Range has a high proportion of rounded zircons, no chromite, and low Fe oxides, low abundance of euhedral zircon, TiO_2 >> Fe oxides.

4. Volcanogenic Yolande River Group are dominated by euhedral zircon with low apatite and tourmaline. There is no chromite and TiO_2 abundance is less than a third of the zircon. The FeTi oxide contents are extremely low reflecting a very felsic composition. The most volcanogenic CVC sample has TiO_2~ euhedral zircon and apatite/euhedral zircon of 0.3. The one White Spur correlate studied is similar to this CVC sample.

In the following section groups of samples have been lumped together for ease of discussion. These are:

- Westcott Argillite includes all the Rosebery Group above the Stitt Quartzite,
- The Dundas Group includes samples from Dundas and from the Southwell Subgroup and Husskisson Group,
- Animal Creek Greywacke includes samples from the Farrell Slate,
- Moores sandstones and mudstones are from presumed Precambrian exposed on Moores Pinnacles,
- Tyndall Group includes the samples from the Mt Cripps Formation and Jukes conglomerate.

These groupings reflect the most likely correlations.

GEOCHEMISTRY

The whole rock composition of the samples is shown in Table 1. These were combined with the 43 other sandstone analyses that were available. An analysis of the covariance (Table 2) shows that there are essentially three groups of correlated elements. These are

1. Ca Fe Mn Mg Na P Sr
   — possibly carbonate veining
2. Cr V Ni (Ti Fe Mg)
   — basaltic source
3. Th Si K La Ce Nd Zr Ba Rb Pb
   — felsic source

For the purposes here it is more significant to look at the less mobile elements. In this regard the Group 2 elements represent a basic component (Western source– Crimson Creek Formation) and the Group 3 elements represent a felsic component (direct contribution from middle Cambrian felsic volcanics). The elements with the largest variance from these groups are:

Group 2 — Cr and Ni
and Group 3 — Th, Ba K.

Given considerations of mobility the preferred measure of the basic group could be Cr Ni or V but the felsic endmember is perhaps best indicated by Th or La.

A principal component analysis of the 14 less mobile elements shows that 74% of the variance can be represented in a single vector and 87% in two vectors. The results of this classification are shown in Figure 1. The Axis 1 vector is dominated by Cr and Ni (+ve direction) and Th and the LREE elements in the –ve direction (Table 3). Thus basic sources are to the right and felsic sources to the left. The Axis 2 vector is dominated by TiO_2, V, P and Sc to positive direction and Cr, Th and LREE in the negative direction. As expected the volcaniclastic sandstones all plot in the left hand side of the diagram while the micaceous sandstones and generally all the Dundas Group sandstones plot with positive scores on Axis 1 to the right of the diagram. The Yolande River Group which includes a range in volcaniclastic component spreads from one side of the diagram to the other.

A very important feature is displayed on the vertical axis. Among the volcaniclastic sandstones the younger suit of Tyndall sandstones has a distinctly higher score on axis one than the CVC and EQPS and Yolande River Group. Among the sandstones dominated by a basaltic source there is also a trend to higher Axis 2 scores. In general high Axis 2 scores represents the southern population around Dundas, while Dundas correlates from Boco Road and the Cradle Mountain Link Road have low Axis 2 scores. This may reflect a decrease in the relevant source material (c.f. variation in Ti/V below). The Dundas sandstones have high Axis 2 scores because of there very high TiO_2 and elevated P_2O_5 while the higher scores for Tyndall Group sandstones is caused by the moderate TiO_2 and V at very low Ni and Cr contents reflecting a mixing line to a high Ti source. The is no evidence in this data for Tyndall Group sources contaminating the Dundas Group.

The very low Axis 2 scores for older parts Animal Creek Greywacke and Yolande River Group reflect the low TiO_2 and V at elevated Cr reflecting a more mature composition as suggested from the previous study or the absence of a Crimson Creek source (c.f. Ti/Th below). The interpretation from the heavy mineral suite was that the change with time in the Dundas Group reflected a change from a low relief deeply weathered western source to a western source which was less weathered. This was used to explain the shift from TiO_2 to Fe oxides with time. Alternatively the transport process included a high energy stage for the early rocks but less so for the latter sandstones that are much less mature (except the Stitt Quartzite).

The Stitt Quartzite has low Cr and Ni reflecting the absence of a basaltic source. It lies very close in composition to Oonah sandstones which are the probable source of these rocks.

The Sticht Range Formation plots close to the Stitt Quartzite reflecting a lack of a basaltic or felsic volcanic source component. The sample 94/42 looks extremely similar to SQ1 and 93/4 which are Stitt Quartzite of similar maturity. These two samples also have a similar pattern of heavy minerals including the ratio of rounded to euhedral zircons. When looking at the heavy mineral suite alone this correlation was missed. No chromite was detected in the Sticht Range Formation which overweighed all other considerations of similarity. The cluster analysis (Fig. 3 of Berry & Fulton 1985) links 93/42 to 93/4 as the most similar sample. Cluster analysis of the whole rock chemistry also places 93/42 with 93/4 as the most similar sample and these were both linked with

Table 1. Whole rock chemistry of sandstones.

Ident	SiO2	TiO2	Al2O3	Fe2O3	MnO	MgO	CaO	Na2O	K2O	P2O5	La	Ce	Nd	Nb	Zr	Sr	Cr	Ba	Sc	V	Y	Rb	Th	Ni	Pb
Yolande R Gp																									
94/26	81.04	0.19	10.87	1.20	0.00	0.60	0.02	0.08	3.41	0.06	48	105	47	12	205	6	16	956	8	10	37	138	20	7	127
94/27	83.73	0.41	6.16	2.72	0.01	2.77	0.03	0.09	0.98	0.04	16	38	16	8	176	9	521	177	11	59	19	38	5	82	7
94/28	74.54	0.24	14.52	0.86	0.00	0.30	0.03	4.58	3.43	0.05	72	148	65	16	223	83	2	767	5	9	35	115	29	2	59
94/29	74.71	0.46	11.37	3.11	0.06	1.73	0.04	1.38	4.54	0.08	24	60	27	16	217	67	57	2249	7	64	27	172	26	26	41
94/32	58.33	0.78	21.19	3.66	0.01	2.48	0.17	0.08	8.11	0.18	96	202	87	32	362	20	122	1452	12	115	58	270	56	33	14
94/33	69.73	0.24	16.42	2.51	0.00	0.94	0.01	0.16	6.35	0.03	66	133	56	17	205	12	3	761	9	15	36	292	31	6	6
94/38	55.68	1.37	19.44	8.86	0.01	3.76	0.00	0.09	4.02	0.16	24	56	20	9	168	12	180	1115	55	396	14	163	6	115	19
94/39	72.40	0.60	16.33	1.15	0.00	0.67	0.02	0.14	4.29	0.07	94	193	87	21	341	30	11	1271	10	36	47	186	30	6	33
CVC																									
94/34	82.01	0.25	9.95	1.30	0.00	0.67	0.01	0.05	3.12	0.05	63	123	45	13	204	6	21	605	5	31	32	107	28	13	121
94/35	78.74	0.16	10.56	2.26	0.02	0.63	0.03	0.23	5.31	0.04	50	107	49	11	210	13	2	1266	7	3	40	202	19	2	5
Sticht Range																									
94/42	91.74	0.23	3.82	0.68	0.01	0.57	0.05	0.04	1.22	0.04	15	39	19	6	277	4	12	128	2	14	18	45	6	4	12
EQPS																									
94/21	67.09	0.49	12.35	9.15	0.15	2.94	0.50	0.03	3.18	0.09	33	67	32	14	292	11	24	851	14	70	25	127	18	10	5
Tyndall Gp																									
94/17	62.37	0.88	15.85	6.56	0.02	1.92	0.14	0.81	6.47	0.14	52	85	42	15	232	85	33	1277	21	183	34	202	15	10	12
94/18	71.71	0.63	13.48	3.63	0.02	0.52	0.05	5.14	1.98	0.10	44	76	35	14	213	71	21	499	10	93	23	44	16	6	4
94/20	68.85	0.61	13.47	7.02	0.03	1.28	0.16	0.03	4.96	0.14	56	104	41	13	256	12	58	1120	17	127	36	188	17	13	24
94/30	70.57	0.46	14.41	3.69	0.02	1.51	0.04	0.45	4.23	0.08	59	90	58	13	263	38	5	912	15	72	39	156	17	4	2
94/31	55.88	1.11	17.24	10.12	0.07	4.99	0.14	2.66	2.51	0.07	19	35	16	8	140	106	31	607	40	305	15	100	2	8	3
94/36	67.46	0.51	16.05	4.71	0.10	1.14	0.01	0.16	4.27	0.04	14	28	18	18	303	8	11	1499	14	60	35	183	19	6	31
94/37	72.70	0.35	13.82	3.49	0.02	1.07	0.01	0.04	5.35	0.03	46	90	38	13	201	28	6	904	8	43	25	225	13	3	7
94/41	72.77	0.42	12.67	4.04	0.02	0.81	0.08	3.60	3.48	0.07	41	79	36	14	215	91	17	1088	9	79	30	100	15	7	19
Stitt Quartzite																									
SQ1	93.60	0.26	3.59	0.28	0.01	0.20	0.01	0.01	1.11	0.02	15	39	15	6	273	8	36	294	3	22	17	46	5	4	8
SQ2	90.30	0.37	5.68	0.41	0.01	0.27	0.03	0.03	1.73	0.03	24	57	24	8	290	9	34	386	4	28	24	70	9	6	60
94/4	89.20	0.31	4.88	1.94	0.01	0.71	0.07	0.06	1.21	0.04	25	63	28	8	346	9	24	220	4	23	33	50	10	10	32
ccf																									
94/24	56.98	2.80	15.53	11.82	0.13	3.15	0.12	0.68	1.96	0.07	64	138	69	32	305	56	199	222	37	307	67	86	12	110	4
Dundas Gp																									
94/3	82.39	0.30	7.80	2.44	0.08	1.64	0.04	0.04	2.30	0.05	15	40	13	7	96	6	52	505	7	115	16	102	10	23	392
94/8	62.48	0.74	18.05	4.36	0.01	3.02	0.01	0.06	4.52	0.02	27	56	24	15	160	13	225	491	25	190	20	195	13	59	50
94/9	72.22	0.44	14.38	3.07	0.06	1.24	0.00	0.04	3.66	0.08	143	221	123	16	292	7	6	1920	10	30	108	165	24	5	211
94/19	65.84	0.45	8.56	6.06	0.09	9.70	1.19	0.85	0.89	0.08	29	45	29	8	143	43	930	962	18	102	46	32	6	461	10
94/23	76.42	0.45	11.40	2.84	0.01	0.73	0.03	2.20	3.11	0.07	32	70	29	10	192	39	34	1012	10	51	23	71	13	13	25
Animal Creek Ge																									
94/1	74.91	0.38	6.48	5.52	0.17	4.45	1.88	0.15	0.70	0.10	16	36	20	7	154	24	606	134	13	80	21	30	6	96	4
94/2	70.12	0.48	9.54	5.11	0.07	5.05	1.68	0.04	1.92	0.12	24	51	22	10	194	42	391	313	16	93	23	84	9	123	32
94/11	75.00	0.44	8.84	5.71	0.05	4.28	0.01	0.06	1.40	0.08	27	55	27	9	177	13	376	262	13	76	21	55	10	116	20
94/12	80.92	0.37	6.80	4.18	0.02	3.68	0.04	0.15	0.89	0.08	15	39	18	7	159	9	584	158	13	73	16	33	6	110	11
94/13	75.17	0.48	12.28	3.37	0.01	1.36	0.13	0.61	3.40	0.10	57	122	52	13	239	22	179	793	12	74	33	140	18	62	42
94/14	76.20	0.48	8.88	4.77	0.03	3.89	0.01	0.15	1.56	0.06	22	49	21	10	189	12	390	310	13	89	21	60	10	108	8
94/15	76.93	0.46	7.90	4.62	0.02	4.25	0.03	0.03	0.88	0.08	22	46	22	8	229	9	824	158	16	101	22	34	9	142	33
Westcott Argillite																									
94/5	58.64	2.54	13.92	12.53	0.14	2.00	0.03	0.62	2.48	0.14	68	90	46	30	305	23	203	496	31	271	53	114	12	209	16
94/6	60.27	1.14	15.26	9.16	0.03	4.40	0.20	0.45	2.64	0.16	33	70	34	18	205	22	292	218	25	194	34	111	13	124	36
94/7	62.36	1.06	17.02	6.23	0.02	3.10	0.01	0.10	3.66	0.11	50	104	52	19	209	19	232	255	28	178	37	153	14	76	28
94/22	48.08	3.43	17.05	15.64	0.24	4.28	0.59	1.99	1.77	0.32	29	68	35	33	304	67	215	279	48	410	56	167	7	120	7

Table2 Covariance matrix for all sandstones after Aitchison centred log ratio transformation.

	SiO2	TiO2	Al2O3	Fe2O3	MnO	MgO	CaO	Na2O	K2O	P2O5	La	Ce	Nd	Nb	Zr	Sr	Cr	Ba	Sc	V	Y	Rb	Th	Ni	Pb
SiO2	0.4																								
TiO2	-0.1	0.3																							
Al2O3	0.1	-0.1	0.1																						
Fe2O3	-0.3	0.1	-0.1	0.4																					
MnO	-0.3	-0.1	-0.1	0.1	1.3																				
MgO	-0.2	0.1	-0.1	0.4	0.1	0.5																			
CaO	-0.7	0.2	-0.3	0.4	0.7	0.4	3.6																		
Na2O	-0.3	0.0	0.1	0.1	0.4	-0.2	1.3	3.0																	
K2O	0.3	-0.3	0.2	-0.3	-0.3	-0.3	-1.1	-0.5	1.0																
P2O5	-0.1	0.1	-0.1	0.1	0.0	0.0	0.5	0.2	-0.2	0.2															
La	0.2	-0.1	0.1	-0.2	-0.1	-0.2	-0.6	-0.2	0.3	-0.1	**0.3**														
Ce	0.2	-0.1	0.1	-0.2	-0.1	-0.2	-0.7	-0.3	0.3	-0.1	**0.3**	0.3													
Nd	0.2	-0.1	0.1	-0.2	-0.1	-0.2	-0.6	-0.2	0.3	-0.1	**0.3**	0.3	0.3												
Nb	0.1	0.1	0.0	-0.1	0.0	-0.1	-0.3	-0.1	0.0	0.0	0.1	0.1	0.1	0.1											
Zr	0.3	0.0	0.1	-0.2	-0.2	-0.2	-0.5	-0.1	0.2	-0.1	0.2	0.2	0.2	0.1	0.3										
Sr	-0.1	0.0	0.0	0.0	0.2	-0.1	1.0	1.3	-0.3	0.1	-0.1	-0.1	-0.1	0.0	0.0	1.1									
Cr	-0.3	0.3	-0.4	0.3	-0.4	0.6	0.2	-1.1	-0.6	0.2	-0.4	-0.4	-0.4	-0.1	-0.4	-0.7	**2.4**								
Ba	0.2	-0.3	0.2	-0.3	-0.1	-0.3	-0.8	0.0	0.7	-0.2	**0.3**	0.3	0.2	0.0	0.2	-0.1	-0.9	0.9							
Sc	-0.2	0.1	0.0	0.2	0.0	0.2	0.3	0.1	-0.2	0.1	-0.2	-0.2	-0.1	0.0	-0.2	0.0	0.2	-0.1	0.3						
V	-0.3	0.3	-0.1	0.3	-0.2	0.3	0.3	-0.2	-0.4	0.1	-0.3	-0.3	-0.2	0.0	-0.2	-0.1	**0.9**	-0.4	0.2	0.6					
Y	0.2	0.0	0.0	-0.1	0.0	-0.1	-0.3	-0.2	0.1	-0.1	0.2	0.2	0.2	0.1	0.2	-0.1	-0.3	0.1	-0.1	-0.2	0.1				
Rb	0.3	-0.2	0.1	-0.3	-0.2	-0.2	-1.0	-0.7	0.9	-0.2	**0.3**	0.3	0.2	0.0	0.2	-0.4	-0.4	0.5	-0.2	-0.3	0.1	0.9			
Th	0.3	-0.2	0.1	-0.3	-0.1	-0.3	-0.9	-0.3	0.5	-0.2	**0.3**	0.3	0.3	0.1	0.3	-0.2	-0.6	0.4	-0.2	-0.4	0.2	0.4	0.5		
Ni	-0.4	0.3	-0.4	0.4	-0.1	0.6	0.3	-1.0	-0.6	0.1	-0.4	-0.4	-0.4	-0.1	-0.5	-0.6	**2.1**	-0.8	0.2	0.7	-0.2	-0.4	-0.5	**2.0**	
Pb	0.3	-0.2	0.0	-0.4	-0.3	-0.3	-1.2	-1.0	0.3	-0.2	0.2	0.3	0.2	0.0	0.2	-0.6	0.1	0.2	-0.3	-0.2	0.1	0.4	0.4	0.1	1.8
	SiO2	TiO2	Al2O3	Fe2O3	MnO	MgO	CaO	Na2O	K2O	P2O5	La	Ce	Nd	Nb	Zr	Sr	Cr	Ba	Sc	V	Y	Rb	Th	Ni	Pb

Fig. 1 — First two eigenvectors for all sandstones based on immobile elements. The analysis used Aitchison log-ratio transformation and a centred covariance table.

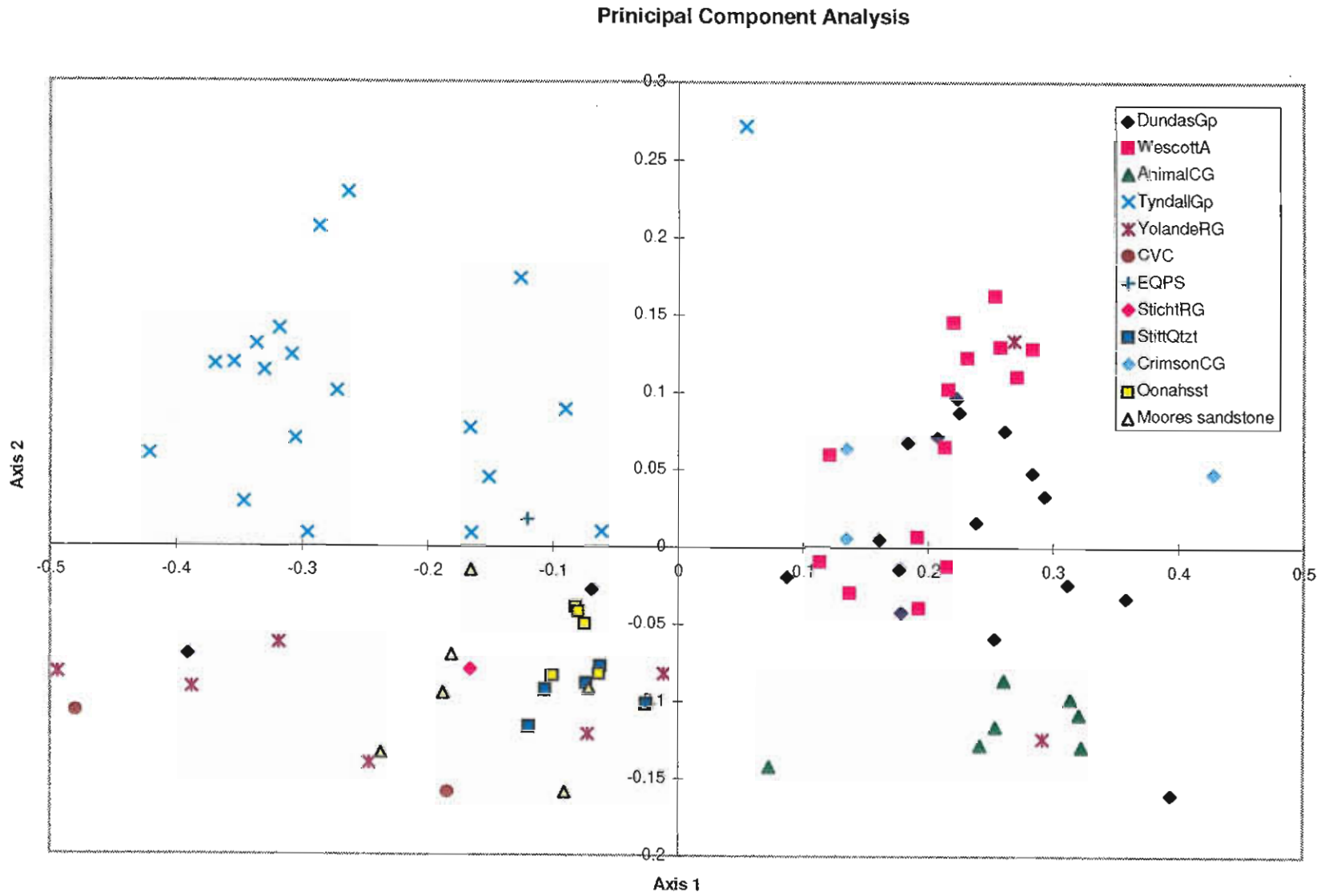

Table 3 — Eigenvectors scores in Principal Component analysis and component loadings of first three eigenvectors for 14 least-mobile elements in all sandstones.

Axis	Eigenvalue	Percentage of total	Cumulative percentage
1	5.305	73.96	73.96
2	0.916	12.77	86.73
3	0.261	3.64	90.37

Eigenvectors (Component Loadings)

	Axis 1	Axis 2	Axis 3
TiO_2	0.07	0.35	–0.39
Al_2O3	–0.16	0.15	0.35
P_2O5	0.02	0.30	–0.15
La	–0.21	–0.19	0.08
Ce	–0.21	–0.20	0.00
Nd	–0.20	–0.16	–0.01
Nb	–0.09	0.06	–0.20
Zr	–0.21	–0.06	–0.47
Cr	0.59	–0.33	–0.14
Sc	0.05	0.42	0.49
V	0.22	0.37	0.07
Y	–0.14	–0.07	–0.10
Th	–0.26	–0.35	0.33
Ni	0.53	–0.27	0.17

Oonah Sandstone and Stitt Quartzite. The only distinction of Sticht Range Formation from Stitt Quartzite that we have found is the presence of small amounts of chromite in the latter

The individual Yolande River Group sample with high Axis 2 score is a micaceous sandstone (94/38) from the Strahan road. It has extremely high TiO_2 content with only moderate Ni and Cr. The high Axis 2 score would normally be a Tyndall Group signature but this rock still has Cr and Ni contents an order of magnitude higher than Tyndall Group sandstones which puts it in the Dundas field.

The statistical analysis suggests that the best elements to show the chemical variations are Ti, La, Zr, Cr, V, Ni and Th. Figure 2 shows Cr/Zr vs Ti/V. As expected the Dundas Group (including Animal Creek greywacke and Westcott Argillite) have high Cr/Zr typical of a basaltic source. For comparison a few examples of igneous rocks are show on the same diagram (Fig. 3). All these rocks plot close to the position of Crimson Creek basalts. The micaceous Yolande River Group also plot in this range. Tyndall Group sandstones have lower Cr/Zr reflect their derivation from a andesitic to rhyolitic source. The EQPS sandstone have a lower Ti/V content than Tyndall Group suggesting a more calc-alkaline source for these rocks. This is partly supported by the position of the EQPS volcanics (Fig. 3) which have a high proportion of dacites with lower Ti/V than equivalent CVC and this may indicate some relation to the Hellyer basalts which occupy a similar part of the stratigraphy. The Crimson Creek sandstones are identical to the Westcott Argillite on this plot. The Stitt Quartzite, Oonah Formation, Sticht Range Formation and the Moores sandstone all plot close together on this diagram.

There are three outlying Dundas Group rocks. The sample with low Ti/V suggestive of EQPS is the sample from the Browns Road sequence. This sample has a Ti/V substantially below normal CVC suite 1 lavas. This is more like the Suite 3 lavas including the Hellyer basalt. The sample from the Husskisson Group on the Pieman Road has a Ti/V of 53 and a Cr/Zr of 0.18 which is similar to Stitt Quartzite. The third sample (Cr/Zr 0.02, Ti/V 88) is a volcaniclastic rock from the Boco Road which is more properly considered a White Spur correlate.

A similar range of variations is shown by Ni/La versus Ti/Th (Fig. 4). The vertical axis is again a measure of basic versus felsic endmembers. The Animal Creek greywacke, Yolande Trend is very distinct here with a mixing line towards rhyolites from a depleted basaltic endmember. This low Ti/Th suggests a calc-alkaline source such as the low Ti tholeiites of the ophiolite or perhaps the Hellyer basalt (although this is probably to young to be a source for the Animal Creek greywacke). The Dundas sandstones show a spread in Ti/Th from the depleted source of the ACG to the relatively enriched source of the Crimson Creek Formation. The Crimson Creek Formation does not appear to be available to the basin during Animal Creek–Yolande time. The Tyndall Group sandstones have high Ti/Th and lie on a trend towards a source with a very high Ti/Th, higher than the Crimson Creek sandstone source region.

Fig. 2 — Trace element variation in all sandstones

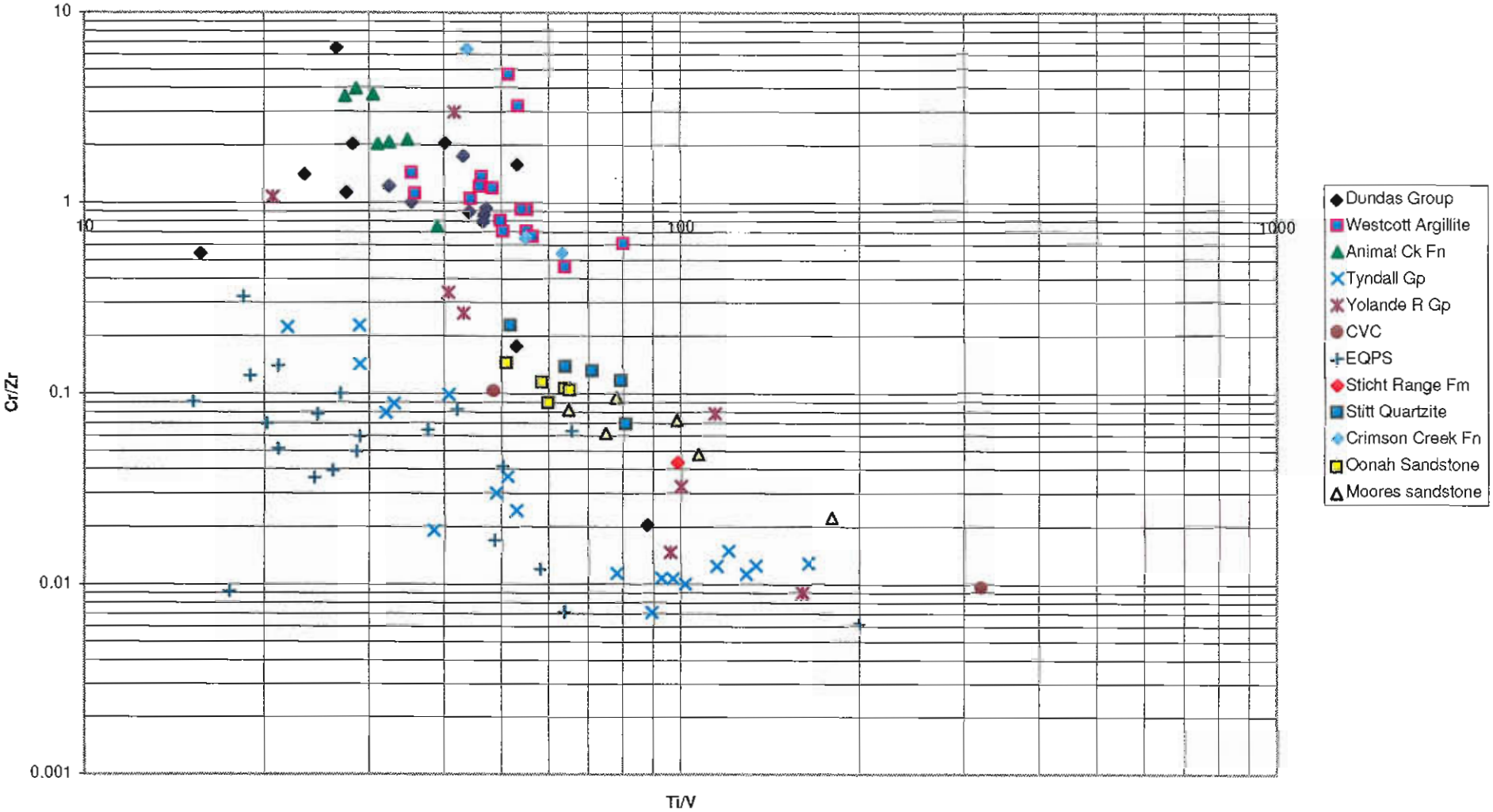

Fig. 3 — Trace element variation in some representative igneous compositions

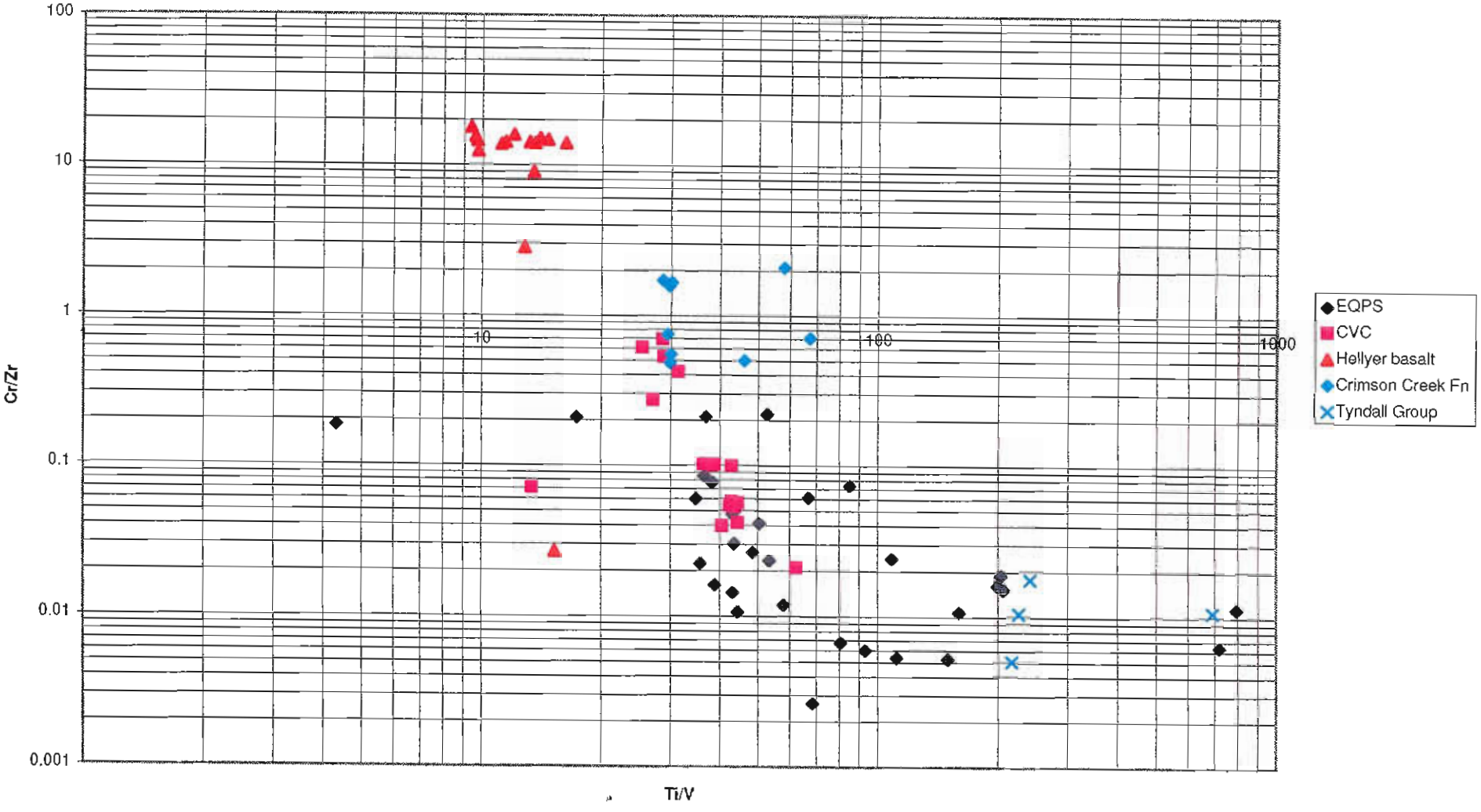

Fig. 4 — Trace element variation in all sandstones

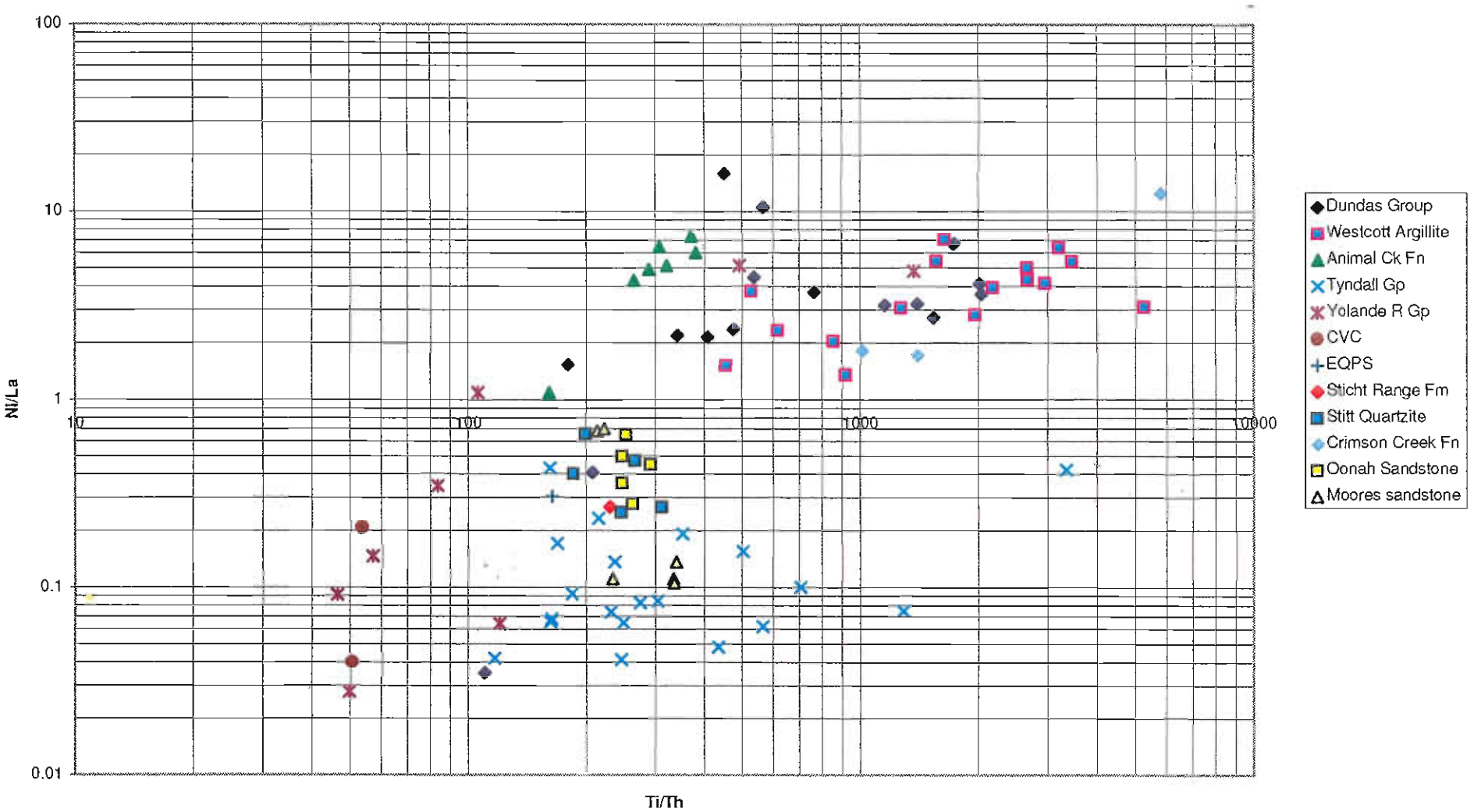

The Precambrian basement, Stitt Quartzite, Sticht Range Formation and the Husskisson Group sandstone form a distinct cluster. The Moores sandstones plot near this group with a trend towards the Tyndall Group. The Yolande River Group that plots close to Tyndall Group (Ni/La 0.06 Ti/Th 120) is from the Strahan Road. The Browns Road sequence sample lies close to the Animal Creek greywacke trend as does the Southwell subgroup sample from the Cradle Mountain Link road (a micaceous sandstone shown as Dundas Group). The Crimson Creek Formation source appears to have a much higher Ti/Th as this trend of sandstones forms a linear array (including the Westcott Argillite) projecting to Ti/Th of 6000 compared to the 500 for the Animal Creek trend.

Given that Ni is concentrated in glass and olivine and Cr is concentrated in chromite the ratio of Ni/Cr is strongly influence by mineralogical maturity of the sediments. The Figure 5 shows Cr/Zr versus Ni/Cr. The most mature sandstones at any Cr/Zr value are to the left. Not surprisingly mature sandstones such as the Stitt Quartzite and the Animal Creek greywacke plot to the left. The unusual situation her is that EQPS rocks range to very high Ni/Cr values.

DISCRIMINANT ANALYSIS

The analysis above makes several groups very clear. The Dundas Group is dominated by a basaltic source for the sandstones and can be separated from Tyndall Group, EQPS, CVC sandstones and Precambrian basement on Cr/Zr alone. Tyndall Group sandstones are separated from Yolande River Group and CVC sandstones on the Axis 2 vector of the principal component analysis or more simply by Ti/Th.

Tyndall Group versus Eastern Quartz–phyric Sequence

The problem in discriminating Tyndall Group from Eastern Quartz–phyric Sequence is that we do not have access to Th data for the EQPS. It is not clear if a Ti/Th vector will also discriminate EQPS from Tyndall Group.

With the available data set, we have not been able to find a single set of elements that will discriminate EQPS from Tyndall Group sandstones. A discriminant analysis was applied with the following results:

Discriminant scores

EQPS mean = 32.0
Critical value for distinguishing groups = 28.7
Tyndall Group Mean = 25.4

Discriminant loading

Variable	Constant	Prot. added
log(TiO2/Zr)	–40.1	–20.5
log(Al2O3/Zr)	15.7	27.9
log(P2O5/Zr)	7.59	19.5
log(Nb/Zr)	8.66	16.3
log(Cr/Zr)	–.423	–1.18
log(Sc/Zr)	17.1	27.7
log(V/Zr)	3.65	20.4
log(Y/Zr)	–4.76	–8.86
log(Ni/Zr)	2.94	18.7

Here the two data sets were separated at the 99% confidence level. This separation is shown in Figure 6 using this discriminant function except for the Cr value which added nothing of significance.

Crimson Creek Formation from Dundas Group Sandstones

The Crimson Creek sandstones and the Dundas Group sandstones both have a high proportion of basaltic detritus derived from the Crimson Creek basalts. They are very similar in composition on the basis of most elements and overlap on all the diagrams. The principle distinction recognised from chromite was that the Dundas Group samples have 20% of chromites with Cr# > 80 which we expect must come from the ophiolites. As far as we are aware there are no chromites in this range in the Crimson Creek but this needs to be investigated further.

The ophiolites also contain basalts with low Ti/V contents. Thus the Dundas Group sandstones may show a spread to lower Ti/V contents than sandstones from the Crimson Creek Formation. Crimson

Fig. 5 — Trace element variation in all sandstones

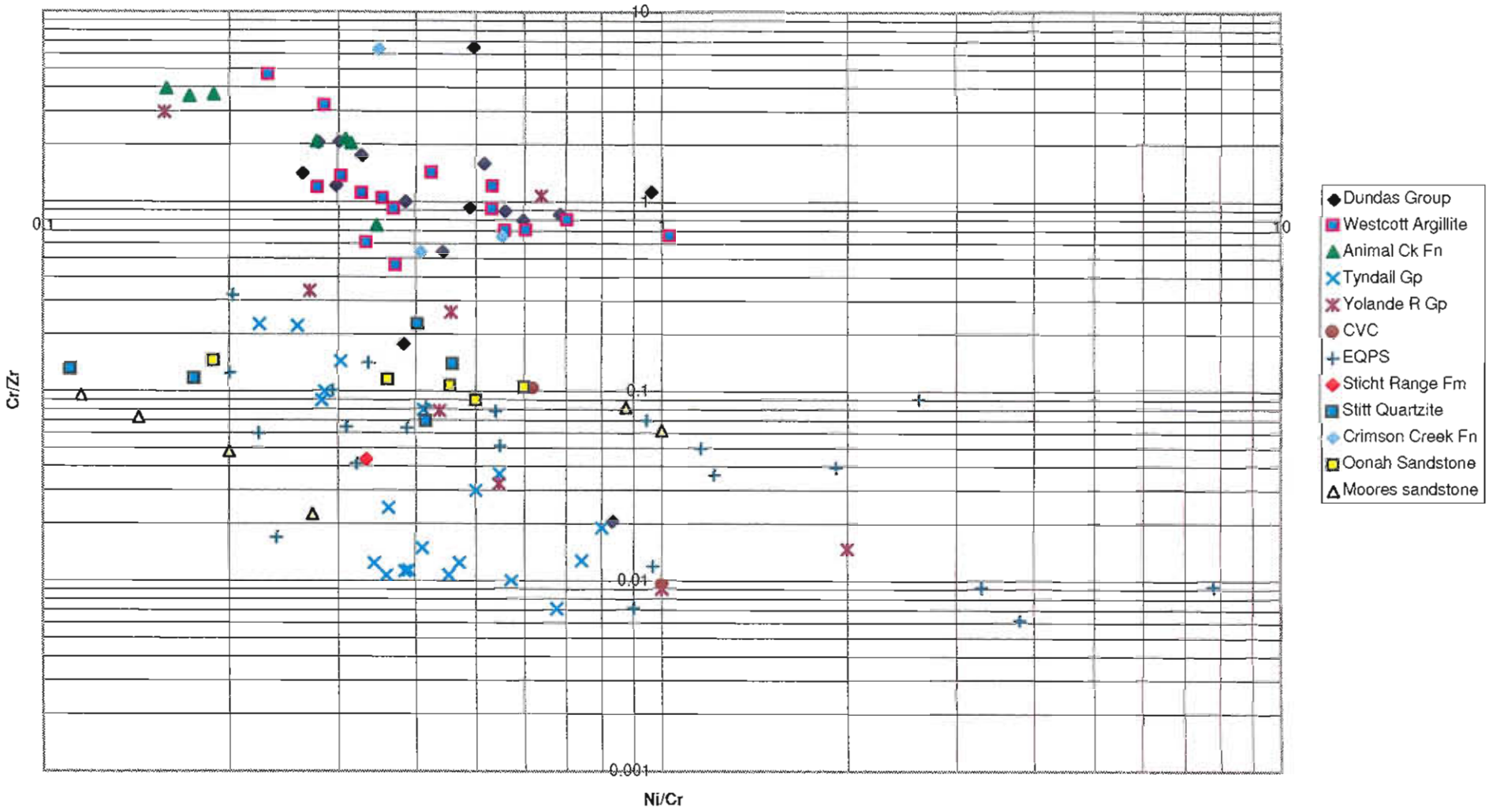

Fig. 6 — Discriminant analysis of Tyndall Group from EQPS. The discriminant function used is:
$-40.1 * \log(TiO_2/Zr) + 15.7 * \log(Al_2O_3/Zr) + 7.59 * \log(P_2O_5/Zr) + 8.66 * \log(Nb/Zr) + 17.1 * \log(Sc/Zr) + 3.65 * \log(V/Zr) - 4.76 * \log(Y/Zr) + 2.94 * \log(Ni/Zr)$

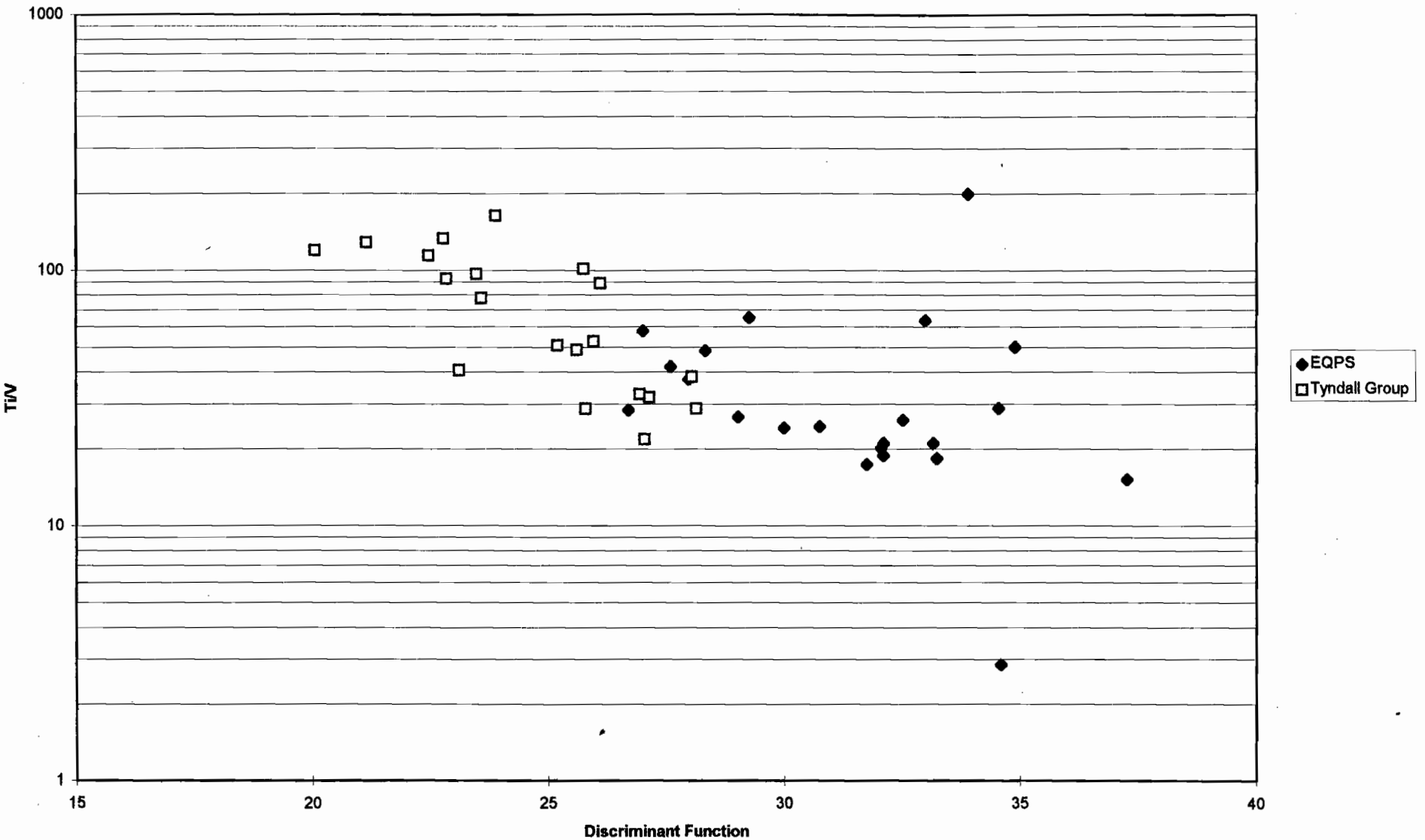

Creek basalts have a Ti/V from 30 to 70 with an average around 45. We do not have much data from the Crimson Creek sandstones, but the three samples included here have Ti/V from 43 to 62. Taking 40 as a demarcation line, for samples with Cr/Zr>0.5, 50% of Dundas Group sandstones and 15% of Westcott Argillite lie below this value, as do all the Animal Creek greywackes. The Dundas samples with this low Ti/V signature include samples from the Red Lead and Razorback sandstones but not Fernfields sandstone. The samples with low values from the Westcott Argillite group are two samples, out of three, from Higgins Creek. It is possible that a similar discrimination will be possible using Ti/Th when more data is available. This ratio spreads the data over an order of magnitude with the Crimson Creek sandstones at the high end of the range reflecting the undepleted character of the rift tholeiites in this formation.

Animal Creek from other Dundas

Animal Creek greywackes are clearly differentiated from Dundas Group on the Axis 2 of the principal component analysis. This distinction is reflected in the low Ti/Th of these sandstones which correlates very well with the observed presence of detrital mica. The few Dundas Group rocks that plot at this low Ti/Th are also micaceous greywackes of the Browns Road sequence and the Southwell Subgroup. The Animal Creek greywacke lies on a trend back towards Cr/Zr of 5 and Ti/V of 20 which is too refractory for the Crimson Creek Formation and this is also reflected in the Ti/Th values. Probably this component is an ophiolitic source as indicated by the presence of very refractory chromite.

Yolande River Group versus Dundas

Most of the Yolande River Group samples lie on a trend between Animal Creek greywacke and a CVC rhyodacite on Figure 4. There are two samples that lie off this trend. These are both from the Strahan road. The micaceous sandstone shows a more typical Dundas composition and the volcaniclastic has a high Ti/Th more like the dacite to andesite signature of the Tyndall Group or perhaps the EQPS. Since the position of this stratigraphic section is in doubt, no firm conclusions can be drawn at this stage. The dramatic similarity between Yolande River Group and Animal Creek greywacke has potential implications for the stratigraphy. The low Ti/Th of these sandstones correlates very well with the observed presence of detrital mica. However this signature cannot be ascribed to either the Tyennan or the Oonah Formation

Lavas

While the analysis of coherent volcanics within the Tyndall Group and the Eastern Quartz -phyric Volcanics lies outside the scope of this project there is a database available in scattered locations of these rocks. We accumulated ten analyses of Tyndall Group lavas from M. White (pers. comm.), Crawford et al. (1992) and McNeill & Corbett (1992), and 49 analyses off the Eastern Quartz-phyric Volcanics from Crawford et al. (1992), A. Stolz (pers. comm.), S. Hunns (pers. comm.) and McNeill & Corbett (1992). There is a startling difference between these two data sets. The Tyndall Group coherent igneous rocks are all rhyolites with TiO_2 ~ 0.2% and FeO total ~ 2.4%. In contrast, the Eastern Quartz-phyric Volcanics (including quartz porphyries) are less evolved and are dominated by dacitic composition (Fig. 3). Four of the 49 samples have rhyolitic compositions close to the Tyndall Group volcanic rocks. There are less analyses which include Zr but these also indicate the Zr/Ti of the all the Tyndall Group coherent lavas are close to 0.2 and well within the field for rhyolites. Crawford & Whitford (in Crawford et al. 1992) have indicated these evolved Tyndall Group lavas have a very high component in crustal melt and these very evolved compositions are consistent with the Nd isotopic evidence. In making this distinction the Tyndall Group igneous rocks were screened to exclude volcaniclastic compositions such as AR4 in Crawford et al. (1992) which are dacitic in composition possible reflecting crystal sorting.

Recognition of coherent igneous rocks of dacitic composition is a possible mechanism to recognise EQPS within areas previously mapped as Tyndall Group. This analysis emphasizes the fact that the Murchison and Darwin Granitoids are part of the EQPS cycle and not related to Tyndall volcanism. In the CVC database of A. Crawford (pers. comm.) there

are only 4 rhyolites similiar to the Tyndall Group from 136 rocks (about 3%) although there is a sampling bias against rhyolites in that study.

Mudstone geochemistry

The analysis of mudstones has not been a part of the AMIRA project. However it is useful at this stage to report on work being carried on by graduate students at CODES. This is principally the work of Dave Selley but includes analyses from other graduate student theses (White in prep, Sinclair 1994). A total of 83 mudstone analyses were available for consideration. All these included major elements plus La, Zr, Sr, Cr, Ba, Sc, V, Y, Rb, Ni and Pb. Two analyses were discarded because of apparent problems with Ni analyses. The covariance analyses for the remaining 81 mudstones is shown in Table 4. The variance is dominated by CaO, and to a lesser extent Na_2O and Pb. The groups of correlating elements are:

1. Ca, Mn, P, Ni — this association suggests calcite veining.
2. Pb, K, Ba, Rb — representing K feldspar
3. Na, Sr — related to seawater interaction
4. Cr, Ni, Ti, V — basaltic source
5. Zr, La, Y, Al (,Si) — felsic source

The major element chemistry is dominated by the variability to Group 1 elements. In order to minimise alteration effects a principal component analysis of the less mobile elements was carried out. The major variance in these elements can be represented by two eigenvectors (Table 5). The first eigenvector has a felsic source in the positive direction and a basaltic source in the negative direction. The second eigenvector has P in the positive direction and La, Cr and V in the negative direction. The distribution of rock types is shown in Figure 7. All the cycle 1 and 3 mudstones have a similar composition. The Que River Shales representing the oldest suite are lower in axis 2 than Dundas Group mudstones but there is a large overlap. In contrast the Tyndall mudstones are extremely enriched in felsic material compared to all other mudstones considered.

The Oonah Formation mudstones, Concert Schists and Moores mudstones all trend off to higher felsic and lower P composition suggesting they are all part of the basement to the Dundas Group or were directly source from the basement at a time when basaltic sources were not dominating the basin. The Crimson Creek Formation trends to more basaltic composition consistent with its being one end-member of the sources feeding the basin.

The variance in this data set is dominated by the differences between Dundas Group mudstones and all other compositions. In order to see the internal variations in the Dundas Group and correlates the analysis was repeated on only these samples.

Considering only the less mobile elements, the total variance in the system is very small. The major groups of correlating elements are:

1. Ti, Sc, (P) — ?magnetite, cpx
2. V — ?contrast between calc-alkaline and tholeiitic sources
3. La, Al, Zr, Y — felsic
4. Ni, Cr — basaltic

The first eigenvector is groups 1 and 4 in the positive direction and group 3 in the negative direction (Fig. 8). The larger basaltic component in the Dundas area leads to a spread to higher values on this vector with the Westcott Argillite having the highest values. The second eigenvector is group 2 in the positive direction and groups 1 and 3 in the negative direction. The Dundas area is much higher in Group 1 and 3 elements but not in V which leads to the spread in vector 2. The lower ratio of Ti/V in the source reflects the absence of Crimson Creek Formation rocks from the source region. This statistical summary suggests a good measure of the variation in Dundas mudstones will be Ti/V versus Cr/Zr or Ni/La.

These elements are shown in Figure 9. The Que River Shale shows a spread in Ti/V ratios to very low values, whereas the Dundas area mudstones have a more consistent value around 45. The possible sources for this signature are also show for comparison. The Hellyer basalt suite and the MUC basalts have values low enough to be considered a direct source for this signature. In contrast the Dundas area mudstones are very close to the value of Crimson Creek basalts as are Crimson Creek sandstones. All the Dundas mudstones and correlates including the Que River shale have a very consistent Cr/Zr of 1. This value is very uniform and close to average basalt compositions. It is well above the value found in dacitic volcanics from the Mt Read volcanics which is close to 0.1. Overall these elements suggest that basaltic compositions are very important in the

Table 4 — Covariance table for mudstones after Aitchison centred log ratio transformation.

	SiO2	TiO2	Al2O3	Fe2O3	MnO	MgO	CaO	Na2O	K2O	P2O5	La	Zr	Sr	Cr	Ba	Sc	V	Y	Rb	Ni	Pb
SiO2	0.14																				
TiO2	-0.05	0.23																			
Al2O3	0.10	0.04	0.12																		
Fe2O3	-0.05	0.07	-0.04	0.18																	
MnO	-0.12	-0.04	-0.14	0.19	0.71																
MgO	-0.07	0.04	-0.07	0.10	0.17	0.16															
CaO	-0.35	-0.39	-0.53	0.06	0.76	0.27	3.30														
Na2O	0.04	0.03	0.06	0.07	0.27	-0.02	-0.09	1.45													
K2O	0.15	-0.07	0.15	-0.15	-0.34	-0.16	-0.73	-0.30	0.49												
P2O5	-0.04	0.08	-0.04	0.03	0.00	0.04	0.22	-0.06	-0.13	0.21											
La	0.12	-0.01	0.13	-0.08	-0.19	-0.11	-0.60	0.04	0.22	-0.07	0.21										
Zr	0.12	0.06	0.14	-0.04	-0.12	-0.08	-0.60	0.15	0.14	0.00	0.16	0.22									
Sr	0.05	-0.01	0.08	-0.09	-0.08	-0.10	-0.19	0.45	-0.01	-0.07	0.13	0.13	0.49								
Cr	-0.19	0.18	-0.11	0.05	-0.06	0.13	0.18	-0.52	-0.13	0.10	-0.17	-0.18	-0.24	0.60							
Ba	0.20	-0.23	0.12	-0.15	-0.20	-0.18	-0.34	0.07	0.37	-0.17	0.20	0.12	0.12	-0.40	0.58						
Sc	0.01	0.11	0.05	0.01	-0.09	-0.01	-0.35	0.01	0.03	0.02	0.03	0.06	0.01	0.06	-0.05	0.08					
V	-0.14	0.14	-0.07	0.03	-0.09	0.07	0.01	-0.39	-0.10	0.07	-0.13	-0.15	-0.19	0.43	-0.31	0.06	0.45				
Y	0.11	0.05	0.13	-0.05	-0.15	-0.08	-0.59	0.11	0.15	-0.01	0.16	0.19	0.12	-0.15	0.13	0.06	-0.12	0.18			
Rb	0.09	-0.02	0.12	-0.12	-0.31	-0.11	-0.66	-0.32	0.39	-0.09	0.18	0.10	-0.03	0.00	0.22	0.04	-0.01	0.12	0.36		
Ni	-0.23	0.11	-0.19	0.16	0.18	0.19	0.59	-0.39	-0.28	0.10	-0.27	-0.28	-0.32	0.52	-0.43	0.00	0.36	-0.24	-0.16	0.67	
Pb	0.09	-0.35	-0.03	-0.18	-0.34	-0.16	0.00	-0.67	0.32	-0.20	0.01	-0.13	-0.27	-0.08	0.31	-0.15	0.06	-0.12	0.20	-0.10	1.76
	SiO2	TiO2	Al2O3	Fe2O3	MnO	MgO	CaO	Na2O	K2O	P2O5	La	Zr	Sr	Cr	Ba	Sc	V	Y	Rb	Ni	Pb

Fig. 7 — Principal component analysis of immobile elements in mudstones.

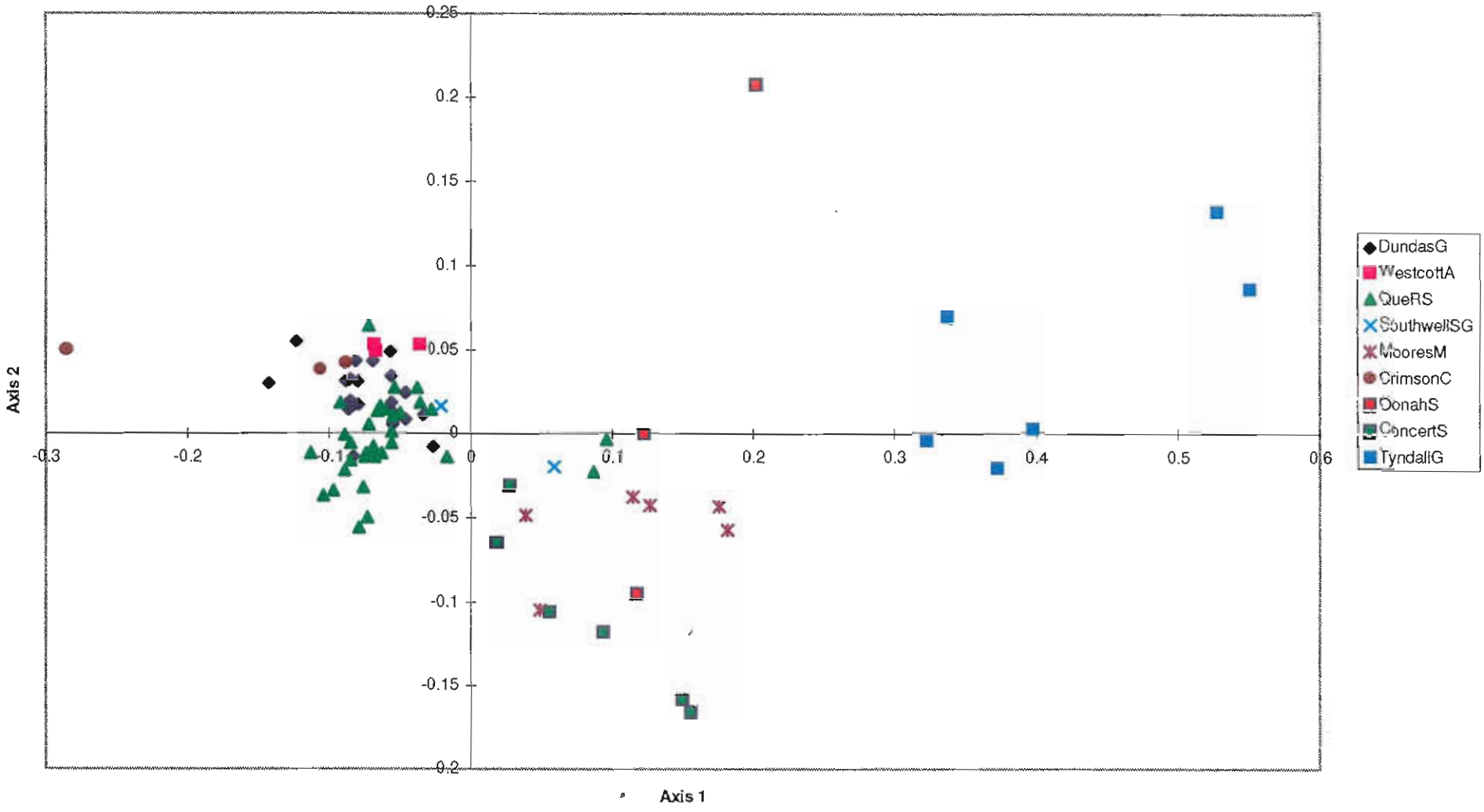

Fig. 8 — Principal component analysis of immobile elements in Dundas and Que River mudstones.

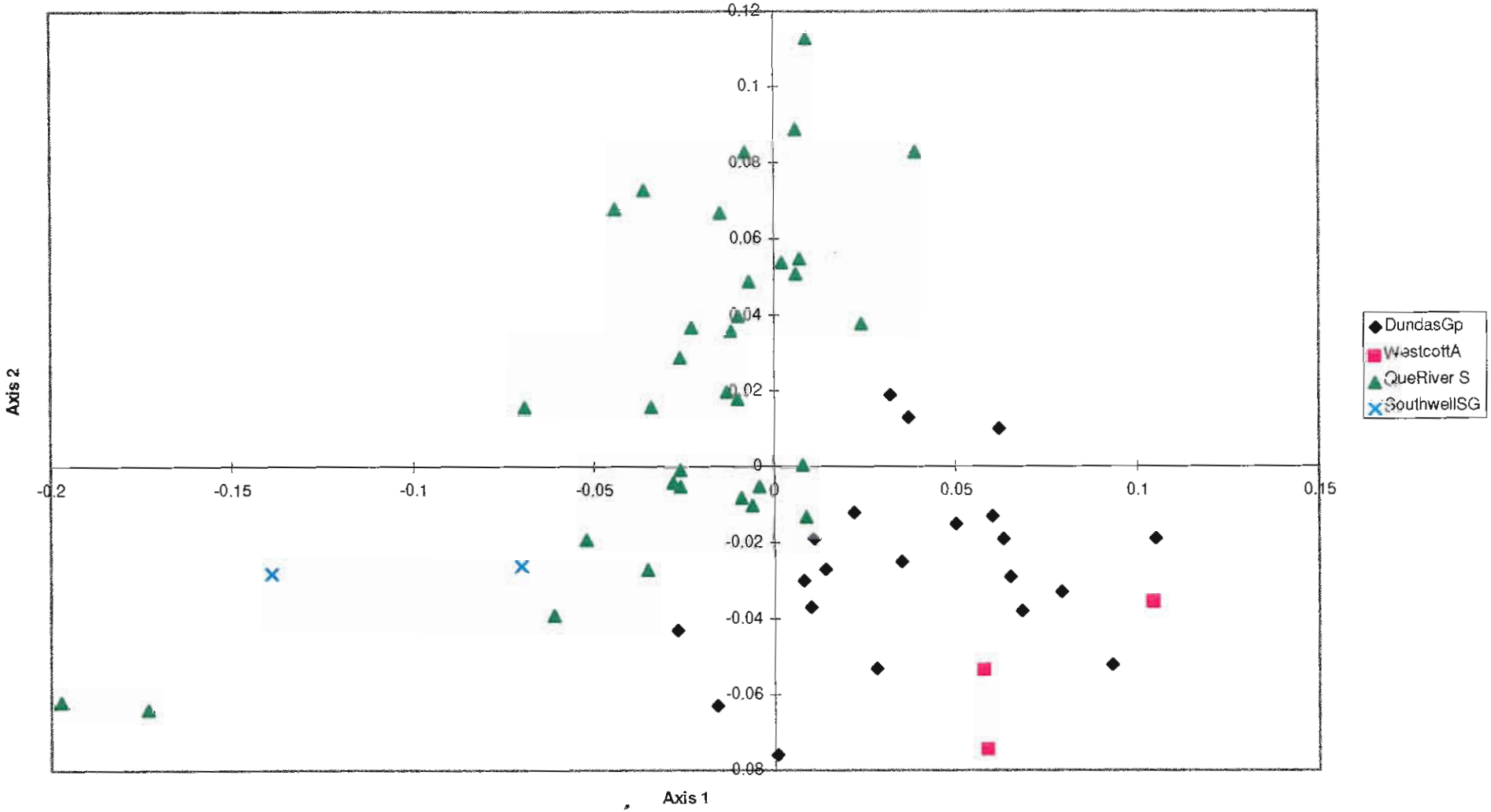

Fig. 9 — Trace element variation in mudstones.

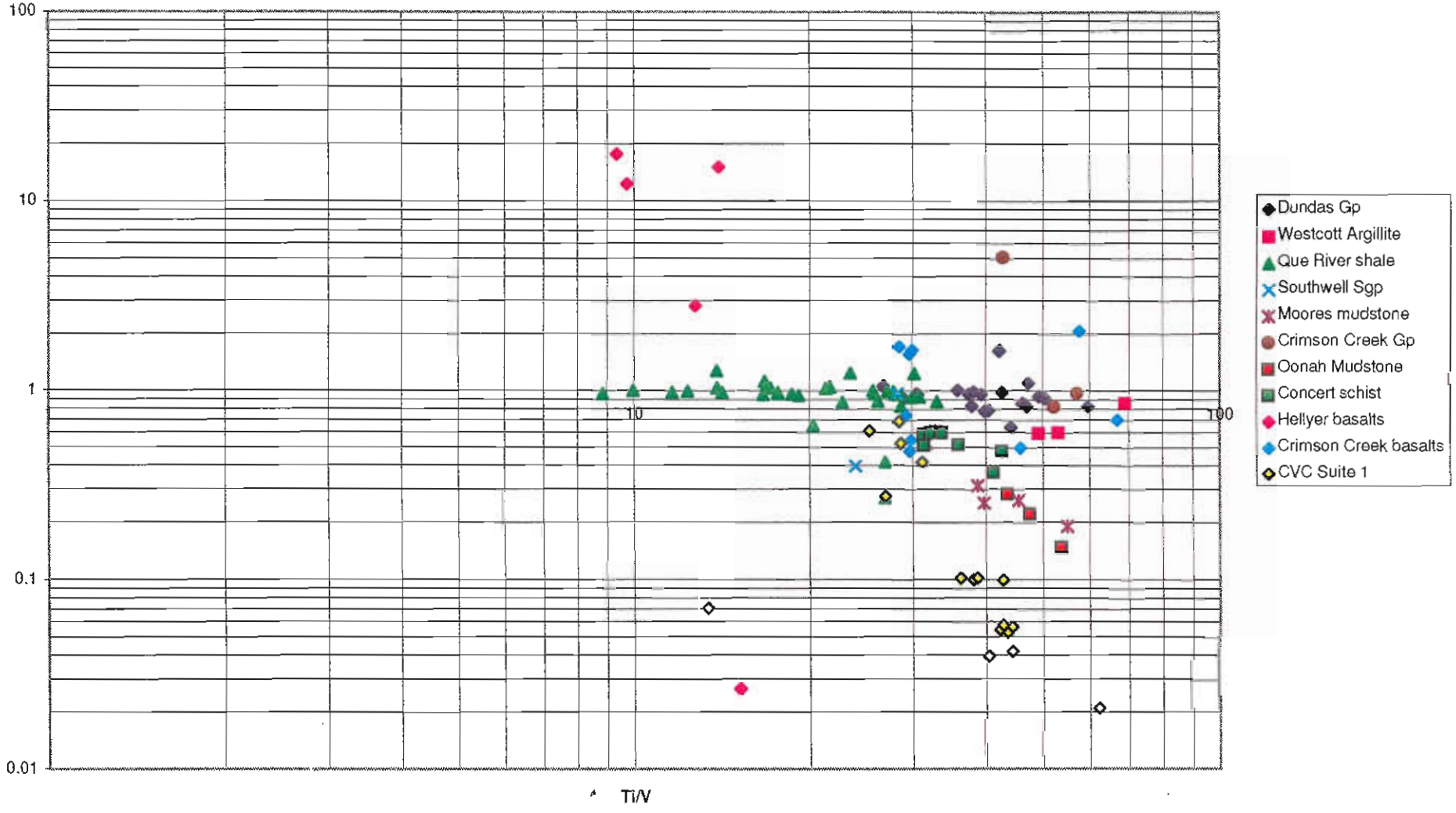

Table to be supplied at meeting

Table 5 — Eigenvector scores for principal components in analysis based on less mobile elements.

generation of mudstones in much of the basin. Alternatively the Cr/Zr value is constrained by the crystal chemistry of one of the mudstone components. In the northern samples, the mudstones from the Southwell Subgroup and two of the Que River shales have lower Cr/Zr, and these rocks are at the high end of the range in K and Al contents, and at the low end of the Fe and Mg range. This suggests the contaminant is illite rather than dacitic glass. It is unlikely that illite is constraining the Cr/Zr ratio. This trend is not found within Dundas Group mudstones.

The mudstones from the Moores Pimple area and those from the Oonah Formation and Concert Schists have a Cr/Zr substantially below those of the all the measured Dundas mudstones. They form a discrete group in many elements. The Tyndall Group mudstones have typical Cr/Zr for a more evolved source such as Tyndall volcanic rocks. This is compatible with the environment where they are found.

CONCLUSIONS

The major aim of this section was to compare the efficacy of a basin analysis using whole rock geochemistry with that of the heavy minerals. The present analysis suggests that a combination of major and trace element analysis produces a statistically superior method which is more useful in defining sediment sources in almost all cases. Features of heavy minerals that are superior to whole rock chemistry are:

1. Presence of chromite with Cr# > 80 to define the Dundas sandstones from Crimson Creek sandstones.
2. The ratio of rounded to euhedral zircons as an indicator of a basement source component.
3. Presence of tourmaline indicating a basement source component

Features of whole rock chemistry that are superior to heavy minerals are:

1. Separation of different types of basaltic component based on Ti/Th and Ti/V.
2. The close similarity of Precambrian units, Sticht Range Formation and Stitt Quartzite.
3. Statistically superior data with less problems in operator error and counting statistics. The resulting data is more homogeneous and easier to analyse.
4. Much cheaper to generate.

The whole rock chemistry is superior except for distinguishing Crimson Creek Formation from Dundas Group and for recognising a small component of basement.

REFERENCES

Berry, R.F. & Fulton, R., 1995. Heavy minerals, provenance and lithostratigraphy. AMIRA P291A report 3, 1–19.

Crawford, A.J., Corbett, K.D. & Everard, J.L., 1992. Geochemistry of Cambrian volcanic-hosted massive-sulfide-rich Mount Read Volcanics, Tasmania, and some tectonic implications. *Econ Geol.* 87, 597–619.

McNeil, A.W. & Corbett, K.D., 1992. Geology of the Tullah–Mt Block area. Mt Read volcanics project report 2. Tasmania Dept Mines, Hobart 19pp.

Sinclair, B.J., 1994. Geology and geochemistry of the Que River Shale, western Tasmania. Unpubl. BSc (Hons) thesis University of Tasmania.

White, M.J., in prep. Volcanic facies analysis of the Cambrian Tyndall Group, Mount Read Volcanics, western Tasmania. Unpubl. PhD thesis, University of Tasmania.

Sedimentological evidence for Cambrian growth faults on the eastern side of the Dundas Trough, western Tasmania

Matt White

Centre for Ore Deposit and Exploration Studies, Geology Department, University of Tasmania

INTRODUCTION

Four areas on the eastern side of the Dundas Trough within the Mount Read Volcanics were investigated with the aim of finding sedimentological evidence, to confirm the presence of Cambrian growth faults interpreted by Berry & Keele (1993). Cambrian growth faults have been proposed along both the western and eastern sides of the Dundas Trough and also within the trough (Berry and Keele 1993). These faults are important as they record a period of Middle Cambrian extension which has led to extensive volcanism and hydrothermal alteration/mineralisation (Berry & Keele 1993). Transfer faults were also active during this period of extension and accommodated for variations in extension along the trough. The western side of the Dundas Trough was studied in detail by Bull (1994, 1995) who found sedimentological evidence to support the presence of a north–south syn-depositional growth fault and associated WNW-trending transfer fault to the west of Rosebery. Cambrian growth faults are also thought to exist on the eastern side of the trough (Berry & Keele 1993). The aim of this study is to find sedimentological evidence to support this interpretation.

During extension, active growth faults have a significant control on clastic sedimentation. This is most obvious in modern subaerial rift systems (e.g. East African Rift; Baker 1986). In relatively deep subaqueous settings, the effects of growth faults on sedimentation are less obvious due to the quiet subwavebase conditions limiting erosion and reworking (cf. Bull 1995). Recognising Cambrian growth faults in the Dundas Trough is difficult and requires detailed structural and sedimentological analysis. Sedimentological methods that help to define growth faults include (1) regional lithofacies analysis which may reveal thickness variations across the growth fault, (2) identification of distinctive components in clastic facies on the down-thrown side of the fault indicating that components were sourced from the up-thrown side of the fault-block, and (3) palaeocurrent analysis which determines the provenance direction. Method 2 above was largely used for this project to test the structural interpretations of Berry & Keele (1993). Due to the massive nature of the deposits in these areas, (where transportation processes were largely by subaqueous high-density sediment gravity flows), no palaeocurrent indicators were identified.

The areas studied for this project were the Moxon Saddle–Henty area, the Northern Anthony Road–Murchison Gorge area, the Hanging Rock area and the Anthony River area (Fig. 1). The inferred Cambrian growth-fault structure at Moxon Saddle (which occurs to the east of the Henty Fault Zone and strikes north–south) merges with the Henty Fault Zone to the north, and then diverges away from it again to the northeast in the Murchison area (Fig. 1). This structure probably extends further north, passing close to the Hanging Rock area (Fig. 1) and may continue further north to the Mount Cripps region (Berry & Keele 1993). This fault is interpreted as a growth fault (west block down) which was active in

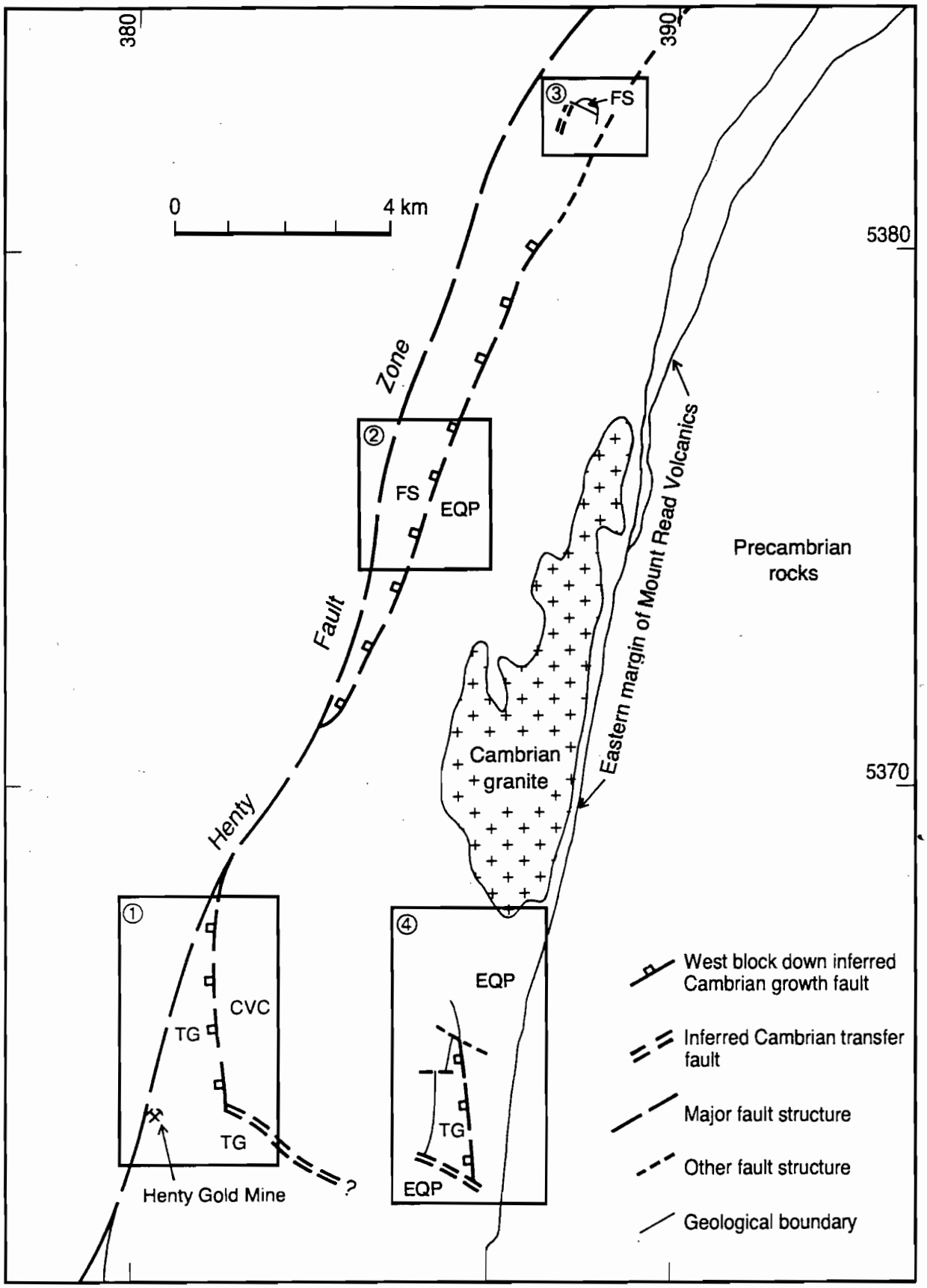

Fig. 1 — Location diagram showing the four areas studied for this project. (1) Moxon Saddle–Henty area; (2) Northern Anthony Road–Murchison area; (3) Hanging Rock area; and (4) Anthony River area. TG = Tyndall Group, CVC = Central Volcanic Complex, EQP = Eastern quartz-phyric sequence, FS = Farrell Slate sequence. Geology from Berry & Keele (1993), Corbett & McNeill (1988).

the Cambrian during the period of extension (Berry & Keele 1993). The inferred growth fault probably represents the Cambrian stage of movement on the Henty Fault. Areas close to the main Henty Fault Zone were not studied as significant post-Cambrian activity on the Henty Fault (Berry 1989) has largely overprinted evidence for Cambrian activity. Another probable Cambrian growth fault structure occurs to the east of Moxon Saddle around the Anthony River–Mount Selina area. This structure was also investigated. An east–west transfer linking these two major growth faults is possible but unlikely.

MOXON SADDLE–HENTY AREA

Moxon Saddle

The Moxon Saddle area lies approximately 2 km NNE of the Henty Gold Mine (Fig. 2). RGC Limited hold a mining lease and exploration licence over these areas and have recently carried out detailed grid mapping and sampling at Moxon Saddle (Boyd 1994). The Henty Fault Zone (HFZ) in this area, comprises a NNE- trending, steeply west-dipping, thick (>100 m thick in places) fault zone containing highly distorted, foliated, sericite-chlorite altered mudstone, sheared Central Volcanic Complex rocks and other fault zone facies which record a complex history of fault movements (Berry 1989). Felsic to mafic volcanic rocks of the Central Volcanic Complex (CVC) occur to the west of the HFZ (Figs 2, 3). To the east of the HFZ is a wedge-shaped area of Tyndall Group rocks comprising dominantly coherent rhyolite, along with minor lenses of crystal-, lithic-rich volcaniclastic pebbly sandstone (Figs 2, 3). The Tyndall Group 'wedge' is fault bounded to the east by rocks of the CVC (Figs 2, 3) comprising mainly feldspar-phyric volcanic facies (McNeill 1987, Jenkins 1991) including lavas and possible pumice-bearing volcaniclastic units. This east-bounding fault (informally referred to as Moxons fault) merges with the Henty Fault Zone to the north around 5368600N (see Fig. 1). Moxons fault has been interpreted as a Cambrian growth fault structure associated with the Henty Fault system (Berry & Keele 1993) with a west-side-down configuration. The Tyndall Group was explored in this area for components which may have been derived from the east.

The Tyndall Group in the Moxon Saddle area is dominated by quartz-feldspar porphyritic coherent volcanic rock interpreted as rhyolite lava. Flow banding textures (1–3 cm thick and laterally continuous) are observed in outcrop and are generally planar with minor occurrences of mesoscopic open flow-folding. The banding orientation varies over the area but is generally steeply dipping to the south and west (see McNeill 1987). Autobrecciation textures are observed but are uncommon in these rocks, and patchy chlorite alteration forms pseudobreccia textures in places. The phenocryst content varies from about 5% to approximately 25% and phenocryst size also varies (quartz is up to 6 mm in places). These rocks correlate to the rhyolite lavas in the Henty Canal area to the south which occur stratigraphically within the Comstock Formation (White & McPhie, in prep).

The eastern contact of the Tyndall Group (referred to as Moxons fault) comprises a wide (50–100 m thick), north-trending, steeply west?-dipping shear zone with feldspar-phyric rocks of the CVC occurring to the east. Approaching the fault contact, the NNW-trending, steeply west- dipping cleavage foliation increases in intensity. Around the position of the inferred fault the rocks are strongly silica-sericite-pyrite altered, strongly weathered and the foliation is very intense, completely destroying the primary texture of the rock. The shear foliation is subparallel to the regional cleavage foliation suggesting a Devonian age for the shearing. Jenkins (1991) inferred a Devonian age for the last (and possibly only) movement on this fault structure. Earlier Cambrian movement may have occurred on this fault, but no structural evidence for this was observed by the author. Sulfur isotope work on this fault is proposed by Davidson & Kitto (1995) to test if a Cambrian signature is present.

Thin lenses of pebbly volcaniclastic sandstone occur within the Tyndall Group rhyolite sequence close to the eastern contact of Moxons fault (located by Boyd 1994) and may represent redeposited volcaniclastic facies adjacent to a Cambrian fault scarp. Samples from these volcaniclastic units were taken for microscopic analysis. One clastic lens (Lens A) occurs well within the lava sequence (Fig. 2) consisting of quartz-feldspar crystal-rich volcaniclastic sandstone with minor amounts of lithic fragments (<5%), and minor magnetite grains (characteristic of the Comstock Formation, White & McPhie, in

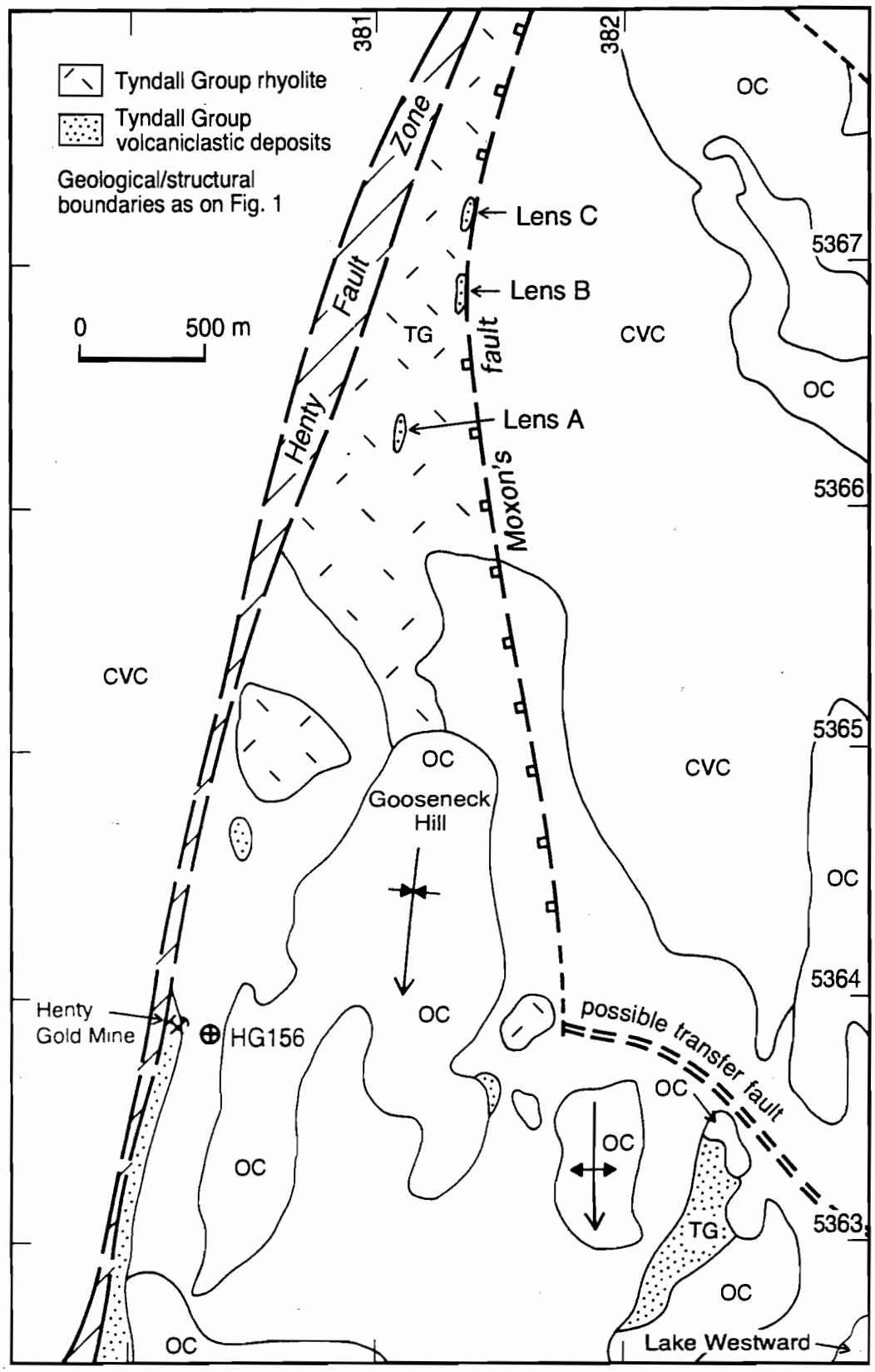

Fig. 2 — Geological sketch map of the Moxon Saddle–Henty area showing the position of the inferred Cambrian growth fault (Moxons fault) and possible associated transfer fault. TG = Tyndall Group, CVC = Central Volcanic Complex, OC = Owen Conglomerate. Geology from McNeill (1987), Berry & Keele (1993), herein.

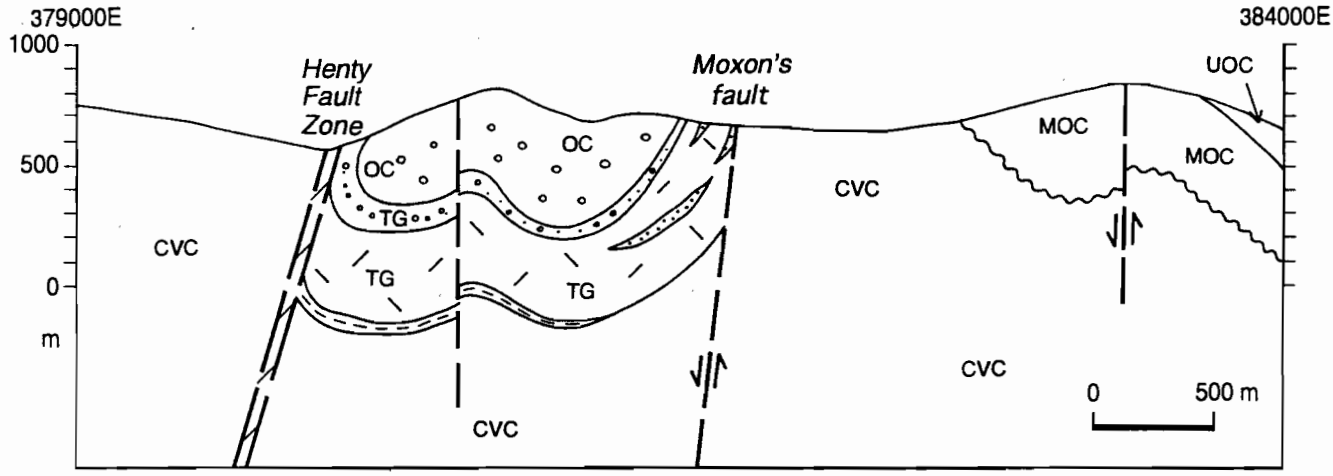

Fig. 3 — East–west cross-section interpretation sketch of the Moxon Saddle–Henty area at 5364000 N. TG = Tyndall Group, CVC = Central Volcanic Complex, OC = Owen Conglomerate, MOC = Middle Owen Conglomerate, UOC = Upper Owen Conglomerate. Geology from McNeill (1987), herein.

prep). The lithic clasts are dominantly pebble size and consist of quartz-feldspar porphyry (rhyolite lava) clasts, green sericite altered clasts and fine grained cream coloured siliceous (cherty) aphyric clasts. Two pebbly volcaniclastic sandstone lenses (Lens B, Lens C) occur further north on the eastern limit of the Tyndall Group, up against the fault contact (Fig. 2). These rocks are strongly foliated (as they lie adjacent to the fault), are strongly silica-sericite-chlorite altered, and moderately weathered making precise interpretation difficult. They consist of crystal-lithic sandstone with approximately 10–20% lithics and abundant quartz, feldspar with minor magnetite. The lithics comprise angular pebble size quartz-feldspar porphyritic (rhyolite) clasts, silica-sericite-hematite altered clasts, creamy silica altered aphyric clasts and very rare feldspar-phyric hematite altered clasts. The presence of clastic units on the eastern margin of the Tyndall Group, adjacent to the fault is consistent with a growth fault interpretation. Some of the aphyric clasts and rare feldspar-phyric clasts may have been sourced from the CVC rocks to the east. However, the lack of diagnostic CVC clast types indicating an easterly source, and the absence of palaeocurrent indicators strongly limits this interpretation.

Lake Westward

Tyndall Group facies also occur 2–3 km SSE of Moxon Saddle, just northwest of Lake Westward and near the southeastern side of Gooseneck Hill (see Fig. 2). These exposures comprise Tyndall Group volcaniclastic breccia/conglomerate and sandstone facies, typical of the upper Tyndall Group. In this area, the Tyndall Group is conformably overlain by the Lower Owen Conglomerate with a thin (1–5 m wide) transitional zone (of mixed Precambrian and volcanic provenance) on the contact (Jukes Conglomerate; see McNeill 1987). The Tyndall Group volcaniclastic conglomerate beds are dominantly massive with planar diffuse stratification in places and are generally several metres thick. Pebbly sandstones associated with the conglomerate beds are diffusely stratified and in places are lensoidal, showing low angle truncations and minor cross-bedding. Planar bedded fine to medium sandstone beds (cm thick) were also observed. The conglomerate beds contain subangular to subrounded pebble to boulder sized clasts in a sandy matrix. The clast type is almost entirely quartz-feldspar porphyritic rhyolite (similar to the Tyndall Group lavas further north) and the matrix is a coarse quartz-lithic sandstone, with sericite ± hematite

alteration. The conglomerates also contain rare red hematite-silica clasts and rare creamy-white siliceous clasts. The most likely source of this facies is the Tyndall Group rhyolite lava complexes, which occur lower in the Tyndall Group (Comstock Formation) and are exposed further north at Moxon Saddle. Some of the rhyolite clasts in the conglomerate are subrounded to rounded and have probably been reworked in above-wavebase environments prior to deposition. The eroded lava debris probably initially deposited in an series of alluvial fans or fan delta systems adjacent to normal fault scarps. Some of the diffusely stratified and cross-stratified volcaniclastic units near Lake Westward may represent this style of deposition. Much of the lava-derived debris was then redeposited downslope into deeper parts of the basin and possibly along the basin axis, in subaqueous sediment gravity flows.

Henty Drill Hole

A Henty drill hole (HG156), drilled vertically as the new Henty shaft pilot hole, intersects the Tyndall Group sequence in the footwall of the Henty Gold Mine, approximately 2 km SSW of Moxon Saddle (see Fig. 2). The sequence in the hole is similar to the Tyndall Group sequence at Moxon Saddle. A number of volcaniclastic conglomerate/breccia and sandstone units occur in the sequence along with rhyolite lavas and associated autoclastic breccias. The hole was logged to check if the volcaniclastic facies contain distinctive components that suggest an easterly provenance. A summary of the drill hole log is given (Fig. 4). The hole passes through an inclined synclinal structure, firstly up-sequence through the Tyndall Group into the Owen Conglomerate (positioned in the core of the syncline), then back down-sequence again into the upper Tyndall Group volcaniclastic units and finally down into the underlying Tyndall Group rhyolite sequence (Fig. 4). A fault slice of Owen Conglomerate occurs in the Tyndall Group sequence near the top of the hole.

Volcaniclastic lithic breccia/conglomerate and sandstone facies occur in the hole stratigraphically underlying the Owen Conglomerate (upper part of the Tyndall Group) (see Fig. 4). The breccia/conglomerate facies are both clast- and matrix-supported and contain angular to subrounded (and minor rounded), pebble to cobble size clasts. The clast population is dominated by rhyolite clasts that have a similar texture to the massive rhyolites at Moxon Saddle. The facies also contains minor proportions of feldspar ± altered-ferromagnesian phyric intermediate volcanic clasts, aphyric chlorite-sericite altered clasts and cherty siliceous clasts. The intermediate volcanic clasts are similar in texture to typical CVC rocks and may have been derived from the CVC to the east. CVC facies are also widespread to the west of the Henty Fault Zone, but their present position is due to significant post-Cambrian movements on the Henty Fault Zone. No palaeo-current indicators were observed in the hole, therefore provenance direction for the intermediate clasts cannot be confidently determined, however an easterly source is most likely.

Structural Models

1. The erosion of Tyndall Group rhyolite lavas, implied by the abundance of rhyolite-derived clastic units to the south of Moxon Saddle, may be due to erosion of lavas originally deposited on the eastern side of Moxons fault, (up-thrown side of normal fault). The east–west transfer (proposed by Berry & Keele 1993) at the south end of Moxons fault may also have controlled deposition. In other words, the northeast block which once contained Tyndall Group lava facies, probably shed eroded lava debris to the south and west, depositing the rhyolite-derived volcaniclastic deposits in a basin on the downthrow side of the two faults (Fig. 5). This interpretation is consistent with the regional distribution of facies observed in the Anthony Road/Henty area further south (data collected previously from PhD project work). In these areas, rhyolite lava and lava-derived clastic units thin out southward, but the Tyndall Group stratigraphy actually thickens to the south, possibly indicating deepening of the basin to the south away from the proposed growth fault. Post-Middle Cambrian compressional deformation events (Delamerian and Devonian events) have produced macroscopic folds and re-activated Cambrian faults and probably caused an inversion on Moxons fault causing the steep

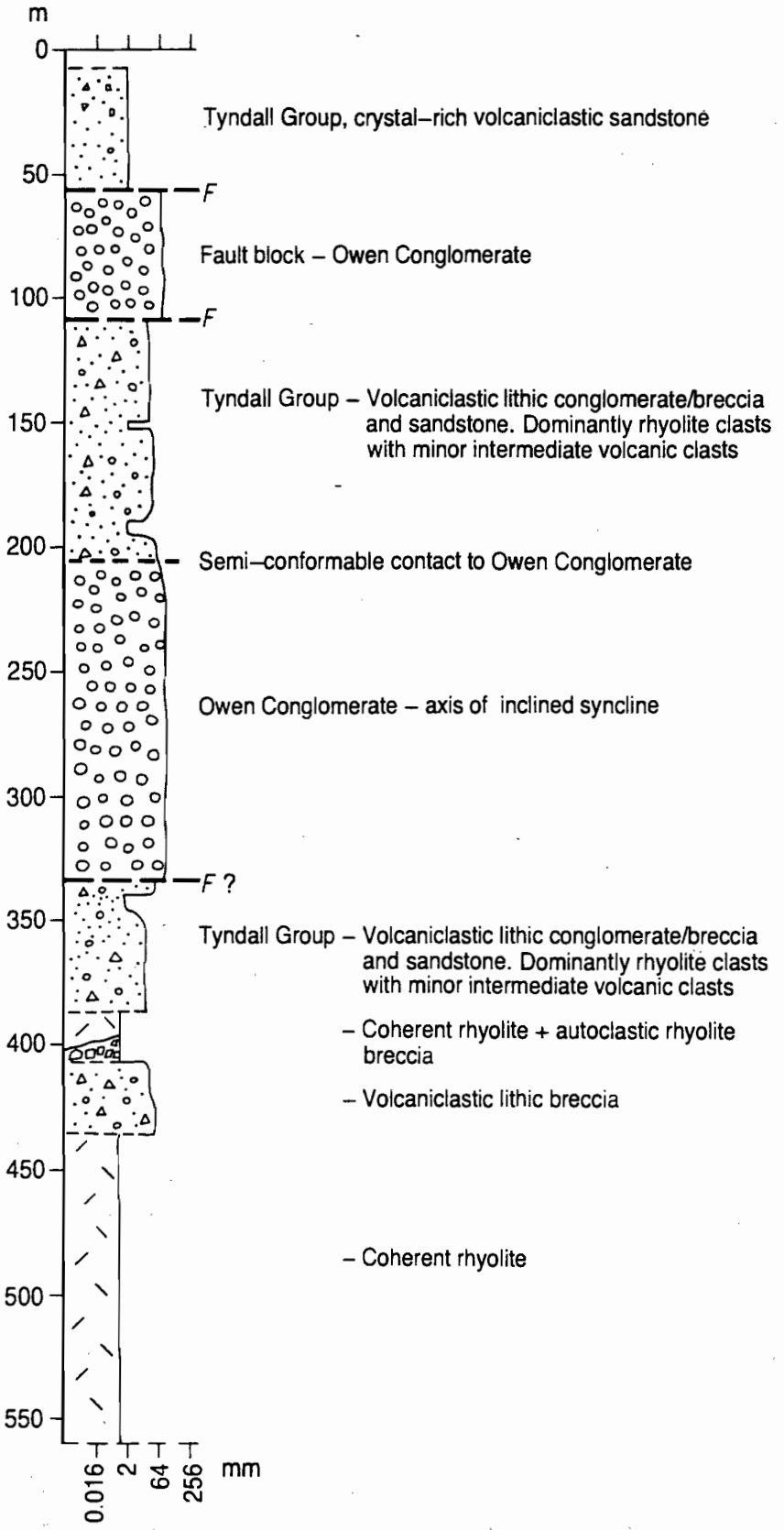

Fig. 4 — Diamond drill log summary of the Henty shaft pilot hole HG156. See Figure 2 for collar location.

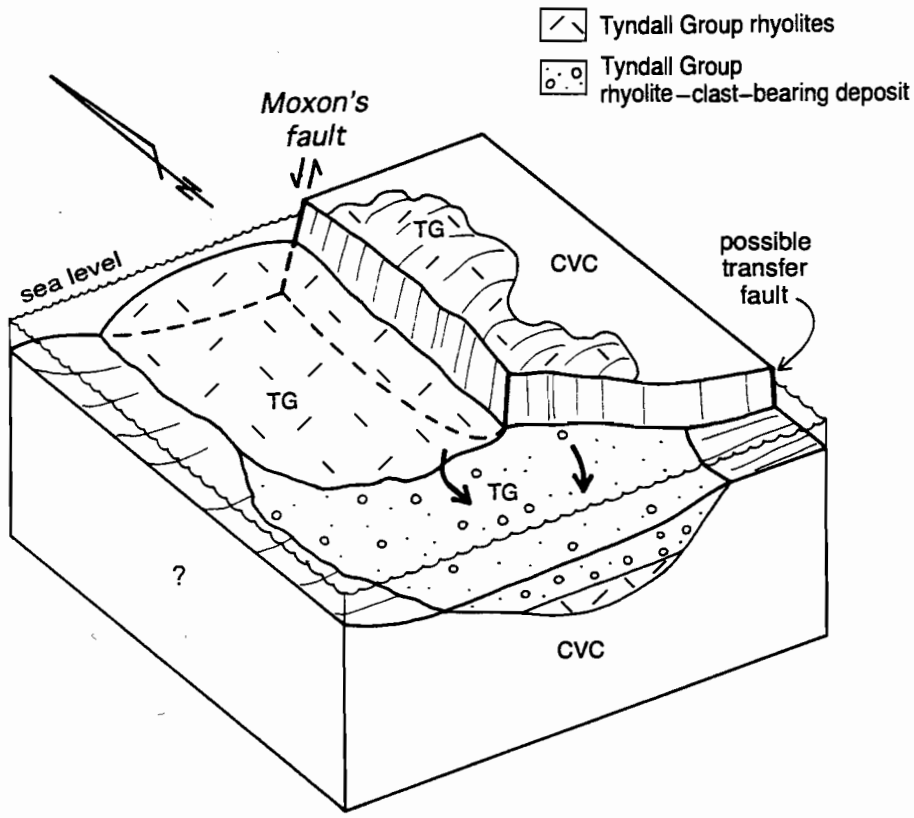

Fig. 5 — Schematic block diagram depicting the preferred model for Tyndall Group deposition in the Moxon Saddle–Henty area. The diagram shows a normal growth fault (Moxons fault) and possible transfer fault controlling deposition of the rhyolite-clast-bearing volcaniclastic units of the Tyndall Group. TG = Tyndall Group, CVC = Central Volcanic Complex.

bedding and flow banding dips observed in the Tyndall Group rocks.

2. Another possibility is that Moxons fault was originally an east-dipping reverse fault that underwent movement during late Tyndall Group time (Middle Cambrian to Late Cambrian). In this model, rhyolite lava on the eastern side of the fault was uplifted during late Tyndall Group time and shed rhyolite lava debris and some CVC clasts into a depocentre to the west and south. Like model 1), this model requires relative uplift of the eastern block. The reverse movement may have occurred during the Late Cambrian Delamerian compressional deformation events proposed by Berry & Keele (1993). However, the Delamerian events are thought to have occurred after Tyndall Group time.

3. Another possible model involves only Devonian deformation and requires no Cambrian fault activity. In this model the deposition of rhyolitic volcaniclastic units were simply sourced from emergent rhyolite lava complexes. Erosion of the rhyolites was initiated as the rhyolite complexes emerged into above-wavebase environments due to constructional growth. In this model the position of clastic facies adjacent to the Moxons fault are purely coincidental and movement on Moxons fault is entirely Devonian in age.

All the above models are valid, however the first model (model 1 above) is most favoured, where deposition of the Tyndall Group is controlled by a Cambrian normal growth fault (Fig. 5). This model best explains the distribution of the volcanic facies in the Moxon Saddle–Henty area, and also accounts for the presence of volcaniclastic lenses adjacent to Moxons Fault and occurrence of intermediate volcanic clasts (possibly derived from the CVC to the east) in the volcaniclastic facies in the upper part of the Tyndall Group at Henty. Sulfur isotope work (proposed by Davidson & Kitto 1995) may help to

confirm that there was Cambrian movement on Moxons fault and structural analysis of fault movements may help to confirm whether Moxons fault was originally normal or reverse.

NORTHERN ANTHONY ROAD–MURCHISON AREA

Volcanic and volcaniclastic units in the Farrell Slate sequence along the northern part of the Anthony Road, approximately 1–2 km south of the Murchison Highway junction, and along the Murchison Dam Road were also assessed for this study (Fig. 1). The contact between the Eastern-quartz phyric sequence (EQPS) (or Murchison Volcanics, Polya 1981) and the younger Farrell sequence is interpreted as a west-dipping inverted Cambrian normal growth fault (Berry & Keele 1993), which records Cambrian movement associated with the Henty Fault system. The fault shows strong reverse movement but juxtaposes younger (Farrell) rocks over older (EQPS) rocks, a common attribute of an inverted normal fault (Berry 1993). This area was selected for analysis to see if sedimentological evidence can be found to support a normal growth fault model. The Farrell volcaniclastic units were investigated for components that indicate an easterly provenance (e.g. EQPS clasts or granite clasts etc.).

On the Anthony Road the EQPS is dominated by orange to green, quartz ± feldspar phyric, chlorite-sericite-feldspar-silica altered coherent volcanic and lesser volcaniclastic facies. The unit mapped by McNeill (1987) as 'Ctct' is interpreted by Berry (pers. comm.) to be part of the west-facing Farrell Slate sequence rather than part of the EQPS as interpreted by McNeill & Corbett (1992). The NNE-trending contact to the east-facing?, lava-dominated sequence of the EQPS is interpreted as an (inverted) Cambrian growth fault. The unit mapped as 'Ctct' (McNeill 1987) consists of a light green to white quartz-feldspar phyric volcanic unit with evenly distributed quartz crystals up to 5 mm across set in a silica-feldspar-sericite altered matrix/groundmass. McNeill & Corbett (1992) interpret these rocks as pumice-, lava-clast bearing volcaniclastic rocks. This interpretation is consistent with my observations, although some areas may contain coherent volcanic facies showing a pseudoclastic texture. The groundmass and/or matrix is strongly quartz-feldspar-sericite altered with green pumiceous or wispy pseudoclastic textures, and is also moderately foliated. Minor occurrences of white pebble size, finely quartz-feldspar porphyritic lithics occur in places in the volcaniclastic facies. The provenance of these clasts is difficult to determine, but are probably locally-derived intraclasts as their texture and alteration assemblage is similar to that in the surrounding rocks. Relatively crystal-rich (quartz-feldspar) facies are observed in places and are interpreted as volcaniclastic sandstone facies. No obvious green-orange chlorite-feldspar altered EQPS clasts or granite clasts were found, indicating an easterly provenance.

Exposed further north along the Murchison Dam Road are green chlorite altered, quartz-feldspar crystal-lithic bearing volcaniclastic units within the Farrell Sequence just to the west of the proposed Cambrian growth fault. This unit also contains silica-feldspar altered quartz-feldspar phyric volcanic clasts, and although the alteration of the groundmass in the clasts is different to that in the EQPS, it is possible that they were derived from the EQPS to the east. The clasts appear similar to some of the Tyndall Group rhyolites further south but are unlikely to have been derived from that group as the Farrell sequence is probably older than the Tyndall Group. In summary, the provenance of these clasts is undefined, however their presence is consistent with a Cambrian growth fault structure at the position inferred by Berry (pers. comm.).

HANGING ROCK

The Hanging Rock area is located about 500 m east of Mackintosh Dam and was accessed by canoe from the western shore of Lake Mackintosh. At Hanging Rock, undifferentiated units of the Farrell Slate sequence (which includes slate, non-volcanic sandstone and volcaniclastic sandstone/breccia facies) were identified by Corbett & McNeill (1986). The Farrell sequence was investigated for any evidence suggesting the presence of a Cambrian growth fault located to the east (inferred by Berry & Keele 1993). The inferred Cambrian growth fault is the northern continuation of the inferred growth fault located on the Murchison Dam Road which occurs on the contact between the Eastern-quartz phyric

sequence (or Murchison Volcanics) and the younger Farrell Slate sequence (Fig. 1). Therefore this area was selected for analysis, to check for presence of components in the Farrell volcaniclastic units that indicate an easterly provenance.

The sequence at Hanging Rock contains three lithofacies. A sequence of turbiditic graded sandstone and mudstone occur at the western limit of the exposure and are comparable to the Farrell Slates further west around the Murchison dam spillway. These rocks are moderately tightly folded on the western limit of the exposure and also strongly sheared. The coarsest beds consist of granule sandstone comprising dominantly angular to subrounded grey chert clasts (2–6 mm) and some feldspar. To the east, after a gap of no exposure is a large area of porphyritic textured intermediate to mafic volcanic rock (probably andesite or basalt). To the east of this unit is an exposure of polymict volcaniclastic pebble/cobble conglomerate and sandstone. This unit contains a high proportion of chert clasts with lesser mafic volcanic clasts in the western most exposure. The mafic clasts have a similar texture to the massive andesite/basalt unit to the west and may have eroded from that unit. This implies a easterly younging direction. Towards the east the unit crudely fines to pebbly sandstone and quartz-feldspar phyric volcanic clasts become more dominant. The sandstone and the matrix within the conglomerate is quartz-rich with additions of feldspar and cherty lithics. At the western most limit of this unit, the pebbly sandstone shows excellent preservation of planar diffuse stratification and well developed trough cross-stratification indicating an easterly facing. Current directions were not measured as trough axes could not be identified due to the lack of suitable three-dimensional exposure. This unit is unconformably overlain by siliciclastic conglomerate and sandstone of the Owen Conglomerate. The contact is very sharp, with no evidence of faulting. An angular discordance of approximately 47° was measured. The underlying volcaniclastic unit is not like typical facies of the Farrell Slates, and is more like units of the Jukes Conglomerate around Mount Jukes. In summary, no evidence for an eastern source was identified.

ANTHONY RIVER AREA

The Anthony River area, around Lake Plimsoll and Mount Selina contains a wedge-shaped body of Tyndall Group volcaniclastic conglomerate and sandstone facies (Fig. 6). The area was briefly investigated two years ago, for my PhD project work on the Tyndall Group. During that time, the Anthony Power Tunnel was briefly assessed and the Mount Selina–Anthony River area was mapped, mainly to investigate the types of facies present in the Tyndall Group rocks. The Tyndall Group facies in this area correlate with the upper Tyndall Group (White 1994). The area was re-visited to establish the nature of the eastern boundary of the Tyndall Group (to the Eastern quartz-phyric sequence) and to investigate clast types in the Tyndall Group conglomerates in order to establish their provenance.

The wedge-shaped body of Tyndall Group is fault bounded to the south. This fault boundary comprises a cross-cutting, ESE-striking (sub-vertical?) contact, at a high angle to bedding in the Tyndall Group, with older Eastern quartz-phyric sequence rocks exposed to the south (Fig. 6). This fault probably represents a Devonian fault as it trends subparallel to other Devonian structures in the area. However, a Cambrian normal/transfer fault may have existed at this location prior to Devonian reactivation (see below).

The western contact of the Tyndall Group 'wedge' passes into siliciclastic units of the Middle Owen Conglomerate with possible lenses of Jukes Conglomerate in places at the base (McNeill 1987). Bedding attitudes are similar across this boundary suggesting a semi-conformable to disconformable contact. A few kilometres north, in the Anthony Power Tunnel, the same contact is highly irregular and sharp, and represents an irregular erosional contact. This is to be expected, as units of the Middle Owen Conglomerate lie directly on the Tyndall Group, and the Lower Owen Conglomerate is missing, implying some time break between these units. The contact is therefore interpreted as an erosional (parallel) disconformity.

The eastern contact of the Tyndall Group to the EQPS is interpreted as a fault contact (herein referred to as Selina fault) (Figs 6, 7) as strong shearing and intense chlorite-pyrite alteration is present at the

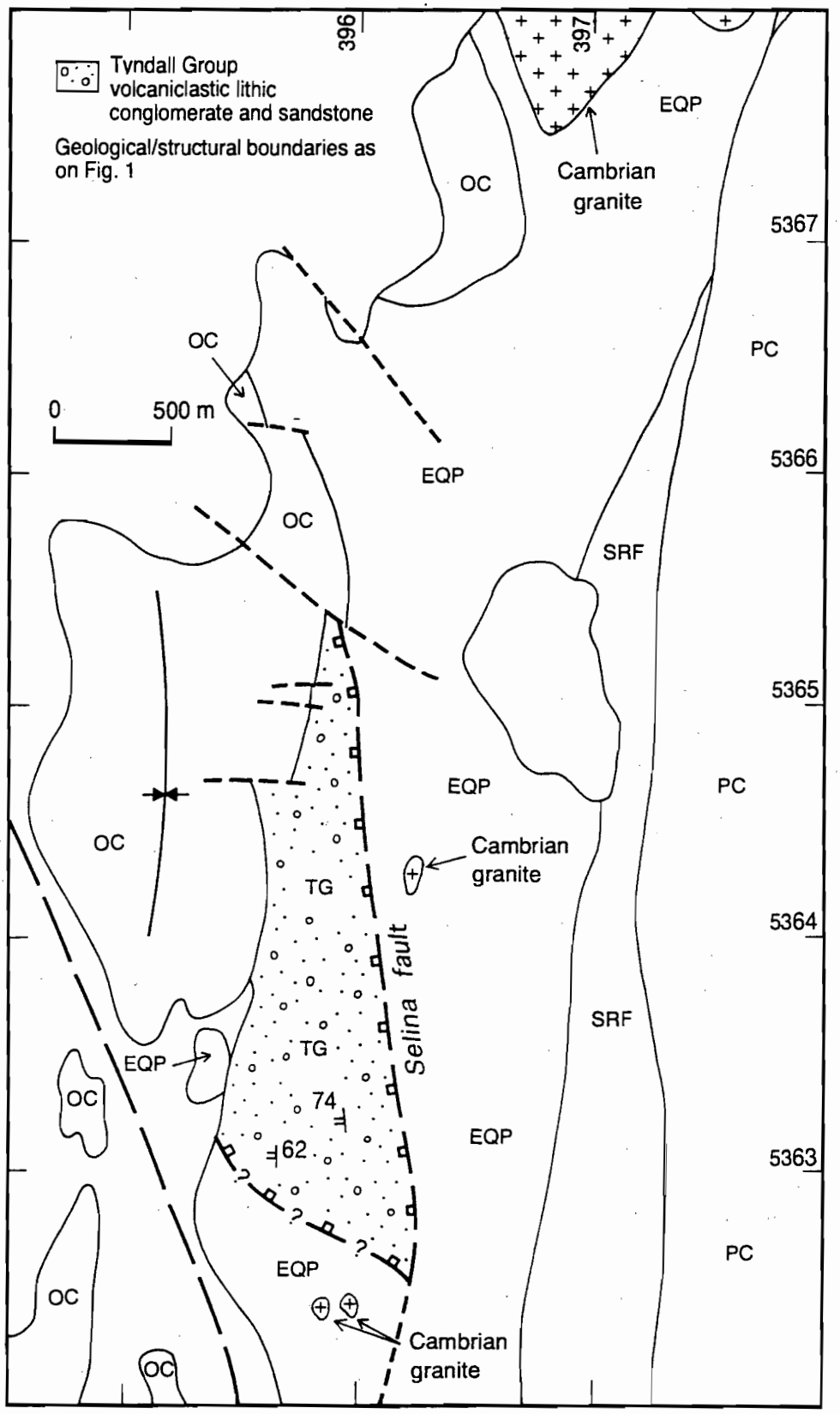

Fig. 6 — Geological sketch map of the Anthony River area showing the position of the inferred Cambrian growth fault (Selina fault). TG = Tyndall Group, EQP = Eastern quartz-phyric sequence, SRF = Stitch Range Formation, PC = Precambrian rocks, OC = Owen Conglomerate. Geology from McNeill (1987), herein.

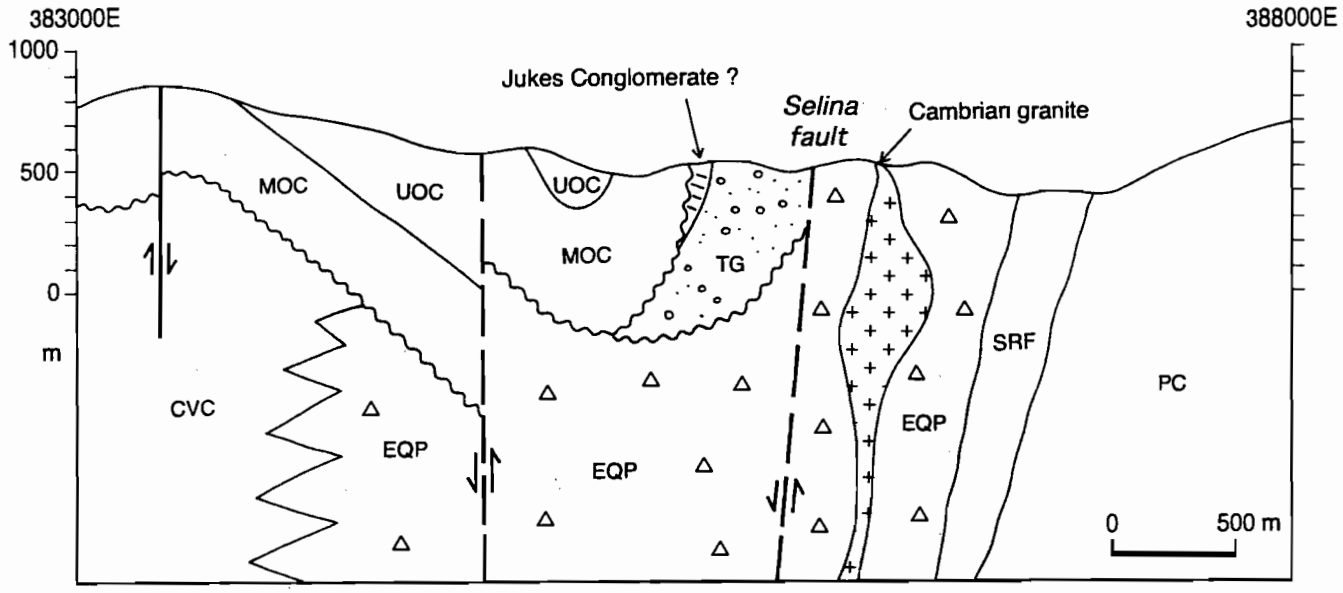

Fig. 7 — East–west cross-section interpretation sketch of the Anthony River area at 5364000 N. TG = Tyndall Group, CVC = Central Volcanic Complex, EQP = Eastern quartz-phyric sequence, SRF = Stitch Range Formation, MOC = Middle Owen Conglomerate, UOC = Upper Owen Conglomerate. Geology from McNeill (1987), herein.

contact in exposures in the Anthony River. A few kilometres further north in the Anthony Tunnel, this contact consists of a strong shear zone (approximately 5–10 m wide) that required concrete lining for tunnel support. This fault probably represents a Cambrian growth fault with a west side down configuration. It was probably reactivated in the Devonian, as the regional cleavage associated with Devonian folding is intense and sub-parallel to the fault attitude. The Tyndall Group facies wedge out or thin to the north (Fig. 6), possibly due to (1) primary lateral thickness changes controlled by basin architecture; (2) the effect of the west-bounding erosional disconformity; or (3) the east-bounding fault (Selina fault) displacing part of the Tyndall Group during Devonian reactivation. Number 1 above is the most likely option as the overlying Middle Owen Conglomerate also thins to the north (see McNeill 1987). The Tyndall Group rocks adjacent to this fault were searched for sedimentological evidence that suggests an eastern source.

The Tyndall Group in this area comprises polymict volcaniclastic conglomerate and pebbly sandstone, typical of the upper Tyndall Group (White 1994). Grainsize ranges from cobble/boulder clast-supported conglomerate to coarse sandstone, with sandy matrix-supported pebble/cobble volcaniclastic sandstone being the most common facies. The beds are generally thick to very thick and massive (m to 10's m thick) showing diffuse planar stratification in places. The deposits are poorly sorted and clasts vary considerably in size and shape. Well rounded clasts are common indicating reworking above wave base prior to deposition, with some additions of subrounded to subangular and lesser angular types. The clast population is diverse, comprising dominantly quartz-feldspar (felsic) porphyritic volcanic clasts, granite clasts, and undifferentiated hematite altered clasts, with minor sedimentary intraclasts, metamorphic Precambrian basement-derived quartzite, feldspar-ferromagnesian (intermediate) porphyritic clasts other undifferentiated altered clasts. The matrix is medium to very coarse sand largely comprising quartz crystals and lithic fragments. The strong Devonian regional cleavage foliation has strongly deformed and attenuated the clasts in places, creating a false type of clast alignment and/or imbrication and modifying primary clast shapes. Within 100 m of the east bounding fault (Selina fault), the foliation is intense and clasts have been very strongly attenuated and flattened.

Provenance of the Tyndall Group and structural model

The most interesting and most obvious lithics in the Tyndall Group conglomerates are the large granite boulder clasts, which are well exposed around the Anthony Saddle Dam. The granite clasts are up to 1 m across and are, on average, larger than the other clasts implying proximity to source. The clasts are subrounded to moderately rounded and have a typical granite to microgranite texture, very similar the Murchison Granite exposed to the north and east. The Murchison Granite intruded the EQPS (exposed to the east of the Tyndall Group) prior to deposition of the Tyndall Group. Granite clasts are also found in the Tyndall Group around Mount Darwin suggesting post-granite age for the Tyndall Group (Corbett 1979). The presence of large granite clasts in the Tyndall Group in the Anthony River area, close to the position of the inferred Cambrian fault is good evidence to suggest that the granite was eroded, shedding debris east, into a basin to the west across a normal-fault-scarp margin (Figs 7, 8). Although the southern extent of the Tyndall Group is probably marked by a Devonian fault, a Cambrian east–west transfer may have existed near this southern margin of the Tyndall Group and also controlling deposition into the basin (Fig. 8). Uplift of the EQPS and intruded granite associated with the transfer fault may also have occurred.

Another interesting component in the Tyndall Group conglomerates in this area is the abundance of quartz-feldspar phyric volcanics similar in appearance to the EQPS to the west. This is also consistent with an easterly provenance. One of these clasts observed at the Anthony saddle dam, shows a cleavage foliation oblique to the regional cleavage foliation, suggesting deformation and cleavage development prior to erosion and re-deposition into the conglomerate. This is also seen at Mount Darwin, where randomly oriented cleaved clasts appear in the Tyndall Group volcaniclastic units (Corbett 1979). This is good evidence for a pre-upper Tyndall Group Cambrian deformation event.

One problem with the normal growth fault model is that the eastern block requires substantial uplift to contribute rounded granite clasts into the basin. The granite was emplaced into the EQPS at considerable

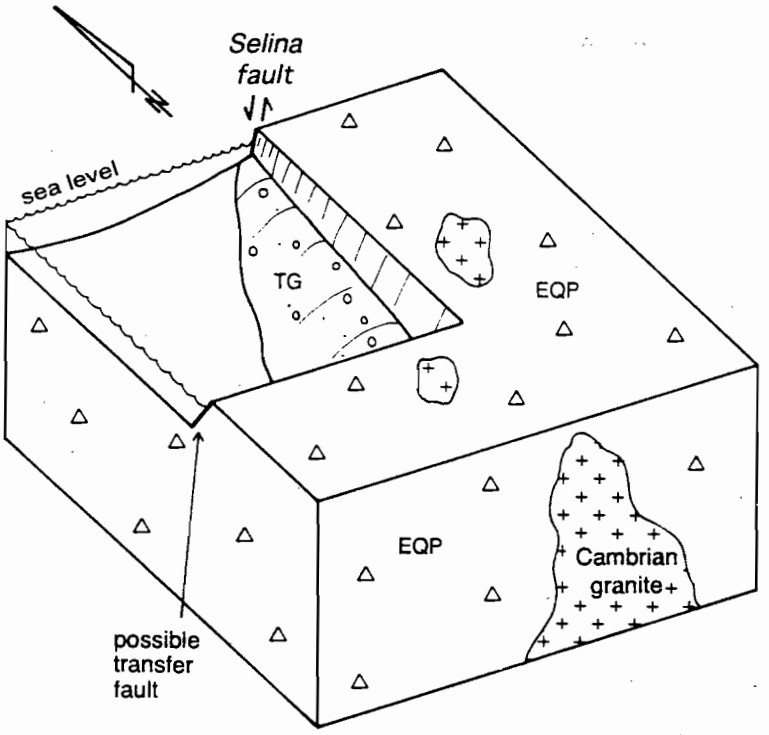

Fig. 8 — Schematic block diagram depicting the preferred model for Tyndall Group deposition in the Anthony River area. The diagram shows the normal growth fault (Selina fault) and a possible transfer fault or growth fault to the south controlling deposition of the Tyndall Group volcaniclastic units. TG = Tyndall Group, EQP = Eastern quartz-phyric sequence.

depth below surface (as implied by the development of hypidiomorphic granular texture). The depth of emplacement is unknown but would be possibly up to several kilometres. Considerable uplift is required to subaerially expose the granite in order to generate the subrounded to rounded clasts present in the Tyndall Group. Relative uplift may have been associated with the south-bounding, inferred east–west transfer fault.

An alternative explanation is that Selina fault was originally a reverse fault involving substantial upward movement of the eastern block. This model solves the problem of uplift, however, the bedding attitudes in the Tyndall Group rocks dip steeply to the west, and when restored to horizontal, the fault is clearly west-dipping, consistent with the normal fault model.

Summary

In summary, geological evidence in the Anthony River area suggests that Cambrian movement was apparent on what is referred to as the Selina fault, during upper Tyndall Group (Middle to Late Cambrian) time. This is consistent with observations of Keele (1991) and Berry & Keele (1993), who interpreted a normal fault on the contact of the Tyndall Group and the Eastern Quartz-phyric sequence in this area. A southern bounding possible transfer fault may have constrained Tyndall Group deposition into a small fault-bounded basin. Reverse movement on the fault involving east-block upward movement is another possibility.

CONCLUSIONS

1. Sedimentological assessments were carried out in four areas to test the structural model of Berry and Keele (1993) that Cambrian growth faults exist on the eastern side of the Dundas Trough.

2. The possible Cambrian growth fault that lies to the west of the Henty Fault Zone (proposed by Berry & Keele 1993) was assessed at three locations (Moxon Saddle–Henty area, Northern Anthony Road–Murchison area, Hanging Rock). In the Moxon Saddle area, crystal-, lithic-bearing volcaniclastic units rich in rhyolite clasts occur in the Tyndall Group, adjacent to the proposed Cambrian growth fault, suggesting that the Tyndall Group rhyolites were probably originally deposited on both sides of the fault, and were subsequently eroded off the northeastern fault block across a normal fault scarp (Fig. 5). South and west of Moxons fault, (downthrow side) rhyolite-clast volcaniclastic units are widespread, being consistent with this interpretation. In the Henty area, feldspar-altered ferromagnesian phyric intermediate volcanic clasts in volcaniclastic units of the upper part of the Tyndall Group, were probably derived from the CVC to the east, being consistent with a west block down, normal fault configuration.

   To the north, in the Murchison area, crystal-, lithic-bearing volcaniclastic facies were located in the Farrell sequence, on the western (downthrown) side of the proposed growth fault, consistent with the interpretation of Berry & Keele (1993). However, the provenance of the clasts cannot be confidently determined, limiting this interpretation. No sedimentological evidence was found to suggest a Cambrian growth fault to the east of Hanging Rock.

3. The Anthony River area contains Tyndall Group volcaniclastic conglomerate and sandstone, in fault contact with the EQPS to the east. The Tyndall Group contains abundant felsic volcanic clasts and granite clasts, suggesting an easterly provenance. The fault contact between the Tyndall Group and the EQPS is interpreted as a Cambrian growth fault with west block down configuration (referred to as Selina fault) (Fig. 8). An east–west transfer may have existed at the southern margin of the Tyndall Group body, controlling deposition into a small basin.

REFERENCES

Baker, B.H., 1986. Tectonics and volcanism of the southern Kenya Rift Valley and its influence on rift sedimentation. *In* Frostick L. E. et al. (eds): Sedimentation in the African Rifts. *Geol. Soc. Spec. Publ.* 25: 45–57.

Berry, R.F., 1989. The history of movement on the Henty Fault Zone, western Tasmania: an analysis of fault striations. *Aust. J. Earth Sci.* 36: 189–205.

Berry, R.F., 1993. Rosebery section. Structure and mineralisation of western Tasmania, AMIRA Project P.291 Final Report: 1–15.

Berry, R.F. & Keele, R.A., 1993. Cambrian structure in western Tasmania. Structure and mineralisation of western Tasmania, AMIRA Project P.291 Final Report: 55–68.

Boyd, D., 1994. Geology of the Moxon Saddle prospect, western Tasmania. RCG Exploration Pty Ltd unpubl. report.

Bull, S.W., 1994. Preliminary report: Sedimentology of the Dundas Group with reference to a possible syn-depositional growth fault west of Rosebery. Structure and mineralisation of western Tasmania, AMIRA Project P.291A Report No. 1: 1–14.

Bull, S.W., 1995. Second report: Sedimentology of the Dundas Group and correlates with reference to a possible syn-depositional growth fault west of Rosebery. Structure and mineralisation of western Tasmania, AMIRA Project P.291A Report No. 3: 35–43.

Corbett, K.D., 1979. Stratigraphy, correlation and evolution of the Mt Read Volcanics in the Queenstown, Jukes–Darwin and Mt Sedgwick areas. Tasmania Department of Mines, Geological Survey Bulletin 58: 1–74.

Corbett, K. D. & McNeill, A. W., 1986. Map 2. Geology of Rosebery–Mt Block area. 1:25 000 Geological Map. Geological Survey of Tasmania, Department of Mines, Hobart.

Corbett, K.D. & McNeill, A.W., 1988. Map 6. Geological compilation map of the Mount Read Volcanicsand associated rocks, Hellyer to South Darwin Peak. 1:100 000 Geological Map. Geological Survey of Tasmania, Department of Mines, Hobart.

Davidson, G.J. & Kitto, P., 1995. Progress Report 3: Detecting Cambrian structures in the Mount Read Volcanic Belt using sulfur isotopes — on-going work at Rosebery. Structure and mineralisation of western Tasmania, AMIRA Project P.291A Report No. 3: 51–61.

Jenkins, D.R., 1991. Volcanology, mineralisation and alteration of the Red Hills, western Tasmania. Unpubl. BSc (Hons) thesis, University of Tasmania, Hobart.

Keele, R.A., 1991. The Zeehan–Red Hills–Lake Selina Traverse — A domain approach to the analysis of structural data. Structure and mineralisation of western Tasmania, AMIRA Project P.291 Report No. 3: 40–56.

McNeill, A.W., 1987. Geology of the Mount Murchison area. 1:25 000 map sheet 4. Geological Survey of Tasmania-Department of Mines, Hobart.

McNeill, A.W. & Corbett, K.D., 1992. Geology and mineralisation of the Mt Murchison area. Mt Read Volcanics project Geological Report 3. Division of Mines and Mineral Resources.

Polya, D.A., 1981. The geology of the Murchison Gorge. Unpubl. BSc (Hons) thesis, University of Tasmania, Hobart.

White, M.J., 1994. Stratigraphy and palaeovolcanology of the Cambrian Tyndall Group, Mount Read Volcanics, western Tasmania. Structure and mineralisation of western Tasmania, AMIRA Project P.291A, second report, October 1994: 37–40.

White, M.J. & McPhie, J. (in prep). Stratigraphy and palaeovolcanology of the Cambrian Tyndall Group, Mount Read Volcanics, western Tasmania. Australian Journal of Earth Sciences.

Progress Report 4: Detecting Cambrian structures in the Mount Read Volcanic Belt using sulfur isotopes — sulfur isotopes of growth faults

Garry J. Davidson and Paul Kitto

Centre for Ore Deposit and Exploration Studies, Geology Department, University of Tasmania

ABSTRACT

Sulfur isotope results from Cambrian growth faults can be tentatively divided according to fault style and fluid history. Those containing base-metal sulfides have values similar to known base-metal deposits in the Mount Read Volcanics (Carters Prospect). These consistently vary from north ($\delta^{34}S$ = 5–9‰) to south ($\delta^{34}S$ = 7–15‰) in the belt (Solomon et al., 1988). Those faults with small displacements, likely original Normal fault geometries, and pyrite rather than base-metal sulfides in the alteration assemblage, contain heavy sulfur (e.g. Comstock-Zig Zag Hill, $\delta^{34}S$ > ~20‰). Some of these have tentatively been identified at the margins of large base metal deposits, such as Rosebery. Thirdly, faults that lie sub-parallel to stratigraphy, are extensively sericite-chlorite altered, and are defined by wide shear zones (e.g. Moxons Saddle), have $\delta^{34}S = 0 \pm 5$‰, and may represent deep rock-buffered fluid circulation, although this conclusion requires confirmation of a Cambrian origin, because these values overlap those expected from Devonian magmatism. These conclusions are very preliminary, and will require detailed work on each scenario in the coming field season.

WORK UNDERTAKEN

Laser sulfur isotope results are now available for some Cambrian growth faults discussed in the March 1995 report. The sampling strategy for these faults was also discussed in this report. Table 1 documents the sampling details and the result of 31 analyses to date, part of an on-going program. Figures 1–7 show the geology of sampled areas.

RESULTS AND BRIEF DISCUSSION

Cambrian faults form an isotopically disparate group, on sample results to date.

Carters Prospect

The Carters Prospect, in which Cambrian Pb-Zn veins and disseminated base metals occur within and immediately above Precambrian basement, expectectedly was characterised by $\delta^{34}S$ = ~5‰ for pyrite, close to the value of other Cambrian massive sulfides in the Southwell Subgroup, such as Hellyer ($\delta^{34}S$ = ~ 7‰). Work in this area will now focus on other growth faults nearby, that do not show evidence of base-metal development, but that were nevertheless fluxed by low temperature Cambrian fluids.

Moxons Fault

Moxons Fault is the largest sampled in this program. Extensive chlorite-sericite alteration occurs on the sub-parallel faulted contact between Tyndall Group and CVC at Moxons Saddle; pyrite here is characterised by sulfides with $\delta^{34}S$ = –4 to +3.5‰, and a dubious population (requiring reanalysis) as light as $\delta^{34}S$ = ~–24‰. The light values of the main population would not normally be interpreted as the product of Cambrian sulfide-forming fluids in the Mt Read Volcanics, despite the typical Cambrian alteration. The values are comparable to those of other "barren" Cambrian alteration zones at Boco Siding, Basin Lake, Chester and Cattley Range (Green & Taheri, 1992). However, Pb isotopes are recommended, to be quite certain that the Moxons Fault sulfides are Cambrian. If these sulfides prove to be Cambrian, then speculatively, they may earmark an area of deeply circulating Cambrian seawater, in which the sulfur isotope values were controlled by reaction with deep wallrocks. It is important to determine if such values are gradational to "normal" Cambrian massive sulfide values somewhere within the growth fault system.

Comstock

The Zig Zag Hill Fault, identified by R. Berry and M. White, is a small scale structure in the Tyndall Group, with no obvious associated shear fabric in its wallrocks, and only a mild Devonian deformational overprint (the structure itself is covered by alluvium). Pyrite is disseminated up to 200 m away from the structure, associated with chlorite alteration. K-feldspar-chlorite alteration occurs lower in the stratigraphy, but no sulfur isotope values have yet been obtained from this. Sulfur isotope values in the disseminated pyrite are heavy ($\delta^{34}S$ = ~ 18.1–24.7‰, n = 4) suggesting a significant contribution from Cambrian seawater, and unequivocally supporting a Cambrian age for the structure, in view of the lack of Devonian fluid overprint.

Pieman River

The proposed Cambrian growth Fault of Bull (1995) and Berry & Keele (1993), 1.5 km west of (and parallel to) the Rosebery Fault was sampled, using disseminated pyrite in siltstones adjacent to vein and faults that showed evidence of Devonian reverse movement. This fault juxtaposes Crimson Creek Formation with Stitt Quartzite, although the exposed outcrop is mainly Crimson Creek Formation (Bull, 1995). Sulfur isotope values are $\delta^{34}S$ = 15.9–33.6‰, (n = 3), consistent either with the direct precipitation of sulfides from Cambrian fluids, or the scavenging of Cambrian sulfides by Devonian fluids. However, very heavy values have only been found in shallow Cambrian convection systems elsewhere in the Mount Read Volcanics, favouring an original growth fault origin.

Dalmeny Street fault, Rosebery hangingwall

Several thin veins and faults occur at a position corresponding to a probable low-angle Cambrian fault separating feldspar-quartz phyric tuff from feldspar-phyric volcanics of the Mount Black Volcanics, 500 m east of the Rosebery lodes. The brittle character, undeformed state, and association with minor reverse faults all suggest that pyrite in these veins was deposited during Devonian deformation. The sulfides were sampled on the premise that the Devonian features would nevertheless have preserved a Cambrian signature from the pre-existing structure. Values of $\delta^{34}S$ = 11.9–15.6, av. 13.5‰ (n = 4) were obtained. These values are similar to normal Rosebery base-metal sulfides, and hence most likely derive directly by the remobilisation of sulfur away from the main Cambrian sulfide body during the Devonian. They do not support local remobilisation of heavy sulfur from a Cambrian growth fault that originally contained heavy sulfur. They do indicate an original Cambrian source for sulfur in these veins. The ambiguity in these conclusions suggest that the variation of sulfur isotopes in Cambrian structures needs to be better understood before routinely examining faults with strong Devonian overprints, and this will be the continuing aim of this sub-project.

FURTHER WORK

The difference of sulfur isotope values for different Cambrian growth faults requires further work on the isotopic variation within each growth fault system, to determine if the signature for each is a uniform feature. The examples to pursue include the Carters Prospect area, where extension of the Pecambrian basement formed many small growth faults, allowing along-strike comparison of sulfides in a well-understood geological environment. Moxons Fault is a second example, which has particular importance given its proximity to the mineralised Henty Fault system, and the possibility that it may represent a deep Cambrian structure which experienced high fluid flows. However, Pb-isotopes will be obtained on pyrite separates to be certain of a Cambrian age, before further sulfur isotope work is undertaken. Thirdly, the Comstock–Zig Zag Hill area will be investigated in detail using drill core samples, to determine the characteristics of systems containing abundant heavy sulfur.

REFERENCES

Berry, R.F. & Keele, R.A. , 1993. Cambrian structure in western Tasmania. AMIRA Project P.291 Final Report: 55–68.

Bull, S.W., 1995. Second report: sedimentology of the Dundas Group and correlates with reference to a possible syn-depositional growth fault west of Rosebery. AMIRA project P.291A, Third Report: 35–44.

Green, G.R. & Taheri, J., 1992. Stable isotopes and geochemistry as exploration indicators. *Bull. Geol. Surv. Tasmania* 70: 84-91.

Solomon, M., Eastoe, C.J., Walshe, J.L. & Green, G.R., 1988. Mineral deposits and sulfur isotope abundances in the Mount Read Volcanics between Que River and Mt Darwin, Tasmania. *Econ. Geol.* 83: 1307–1328.

Table 1 — Sampling details of regional Cambrian Faults.

Fault	Location	Sampling details	Sulfur isotopes (‰)	Nature of samples
Carters Prospect	2km NW of Back Peak, vein-systems transecting the Precambrian/ Cambrian contact	Fault not directly sampled. Samples mainly 30 m east of probable fault trace.	4.3–6.8, av. py =5.5 (n=4)	Some visible disseminated py and galena in silicified areas; Pb-isotopes indicate Cambrian age
Moxons Fault (a Henty Fault splay)	2km NW of Henty mine, on the Tyndall-CVC contact	100m wide intense shearing with severe chlorite, pyrite and sericite alteration	Two populations 1. subhedral –28.7 to 19.9. 2. massive –4.1 to +3.2‰, av. +0.5 (n=6)	Visible pyrite. Samples taken at ~20 m intervals across the shear.
Tullabardine Fault (a Henty Fault splay)	On the northern shore of Lake Macintosh, on the CVC-Dundas Group contact	Fault not directly sampled. Obtained Dundas Group 100m east, and CVC 50m west, and an isolated silica pod in the fault.	no results to date	Visible pyrite nodules in the Dundas Group. No visible pyrite elsewhere.
Dalmeny St Fault	Rosebery township	A brittle fault dipping 80°/076° was sampled, likely to be Devonian, but this corresponds to the Cambrian location	11.9–15.6, av. 13.5‰, n=4.	No visible sulphides; Sample intervals: 0, 1, 5m; weathered.
Pieman River	1.5 km SW of Bastyan Dam	Juxtaposes Crimson Ck Fm with Dundas Group sediments N-S growth fault	15.9–33.6, n=3	Disseminated pyrite in sediments
ZigZag Hill Fault	Comstock Valley, 6 km north of Queenstown	Fault not exposed. Separates Tyndall Group andesites from volcaniclastics. Associated with strong red-K-feldspar alteration	18.1–24.7, av. 22.5 (n=4)	Minor visible py. RGC drillhole with abundant py still needs to be sampled. Have sampled 5, 10 and 100m from fault.

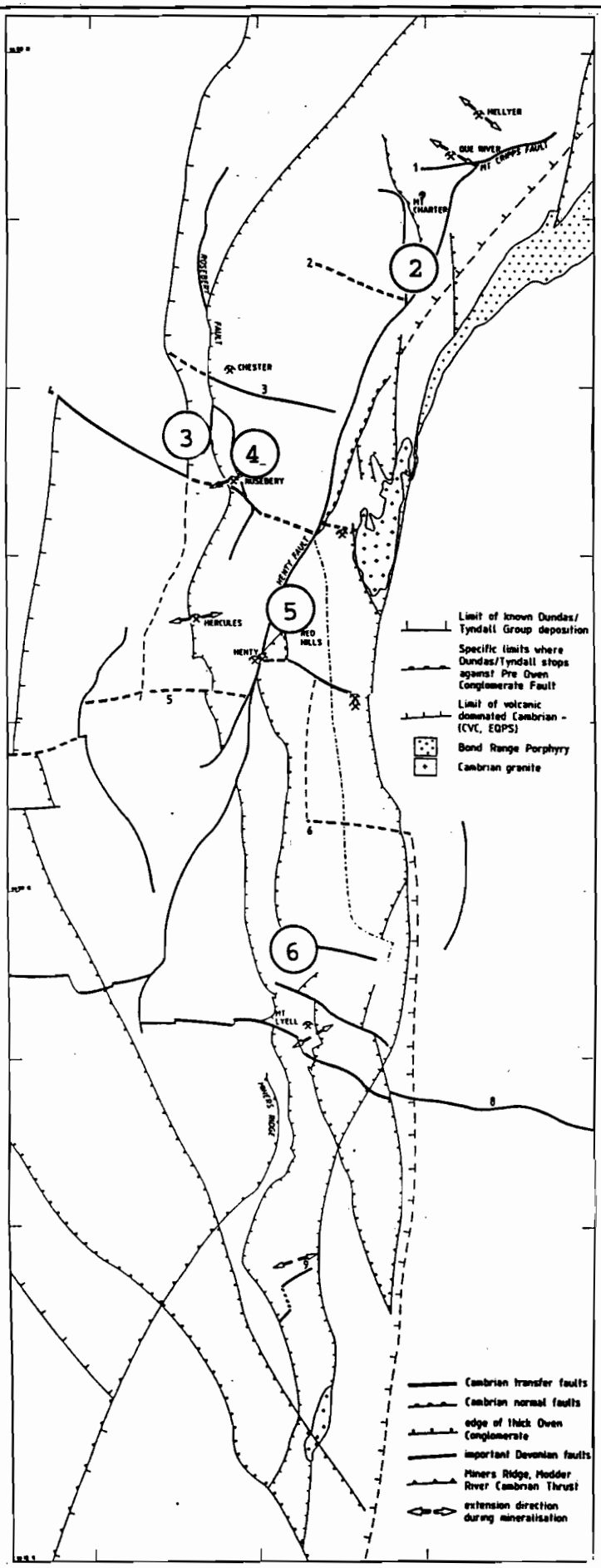

Fig. 1 — Location of sample areas in western Tasmania, showing the positions of probable growth faults (after Berry & Keele, 1993).

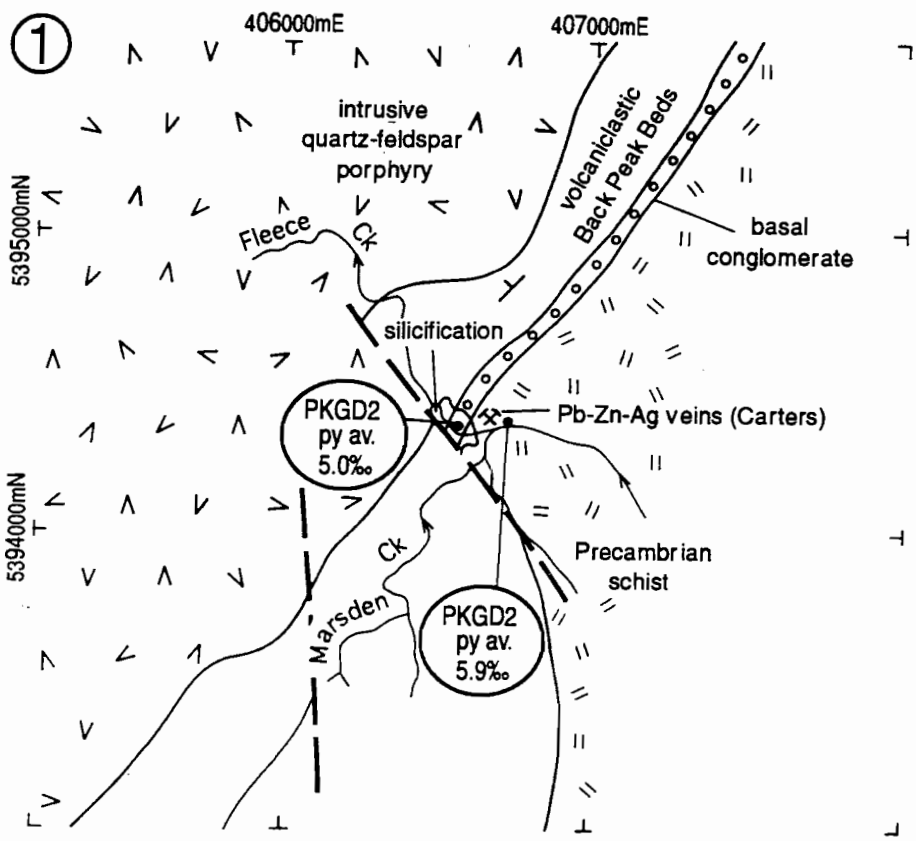

Fig. 2 — Geology of the Carters Prospect.

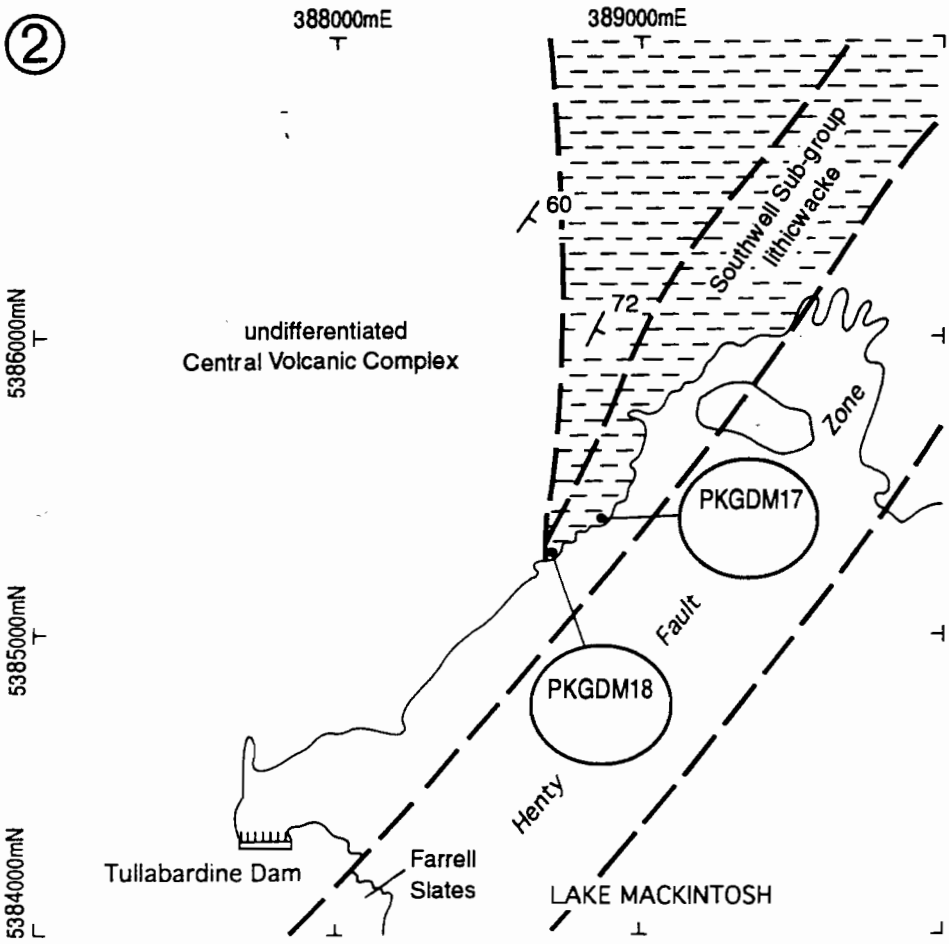

Fig. 3 — Geology of the Tullabadine Dam area.

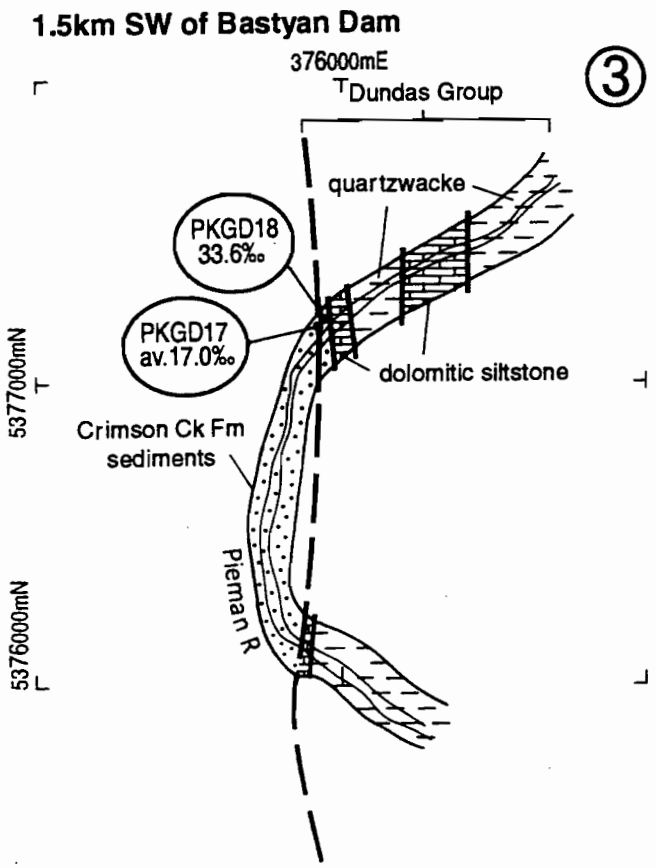

Fig. 4 — Geology of the Pieman River growth fault.

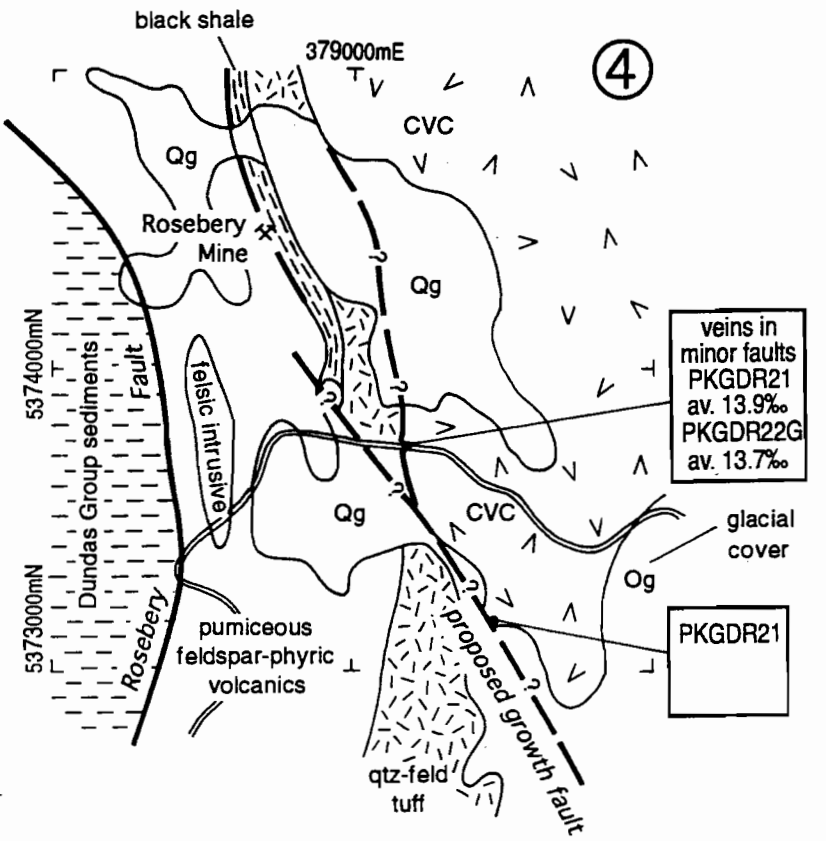

Fig. 5 — Geology of the Rosebery hangingwall (Dalmeny St fault) area.

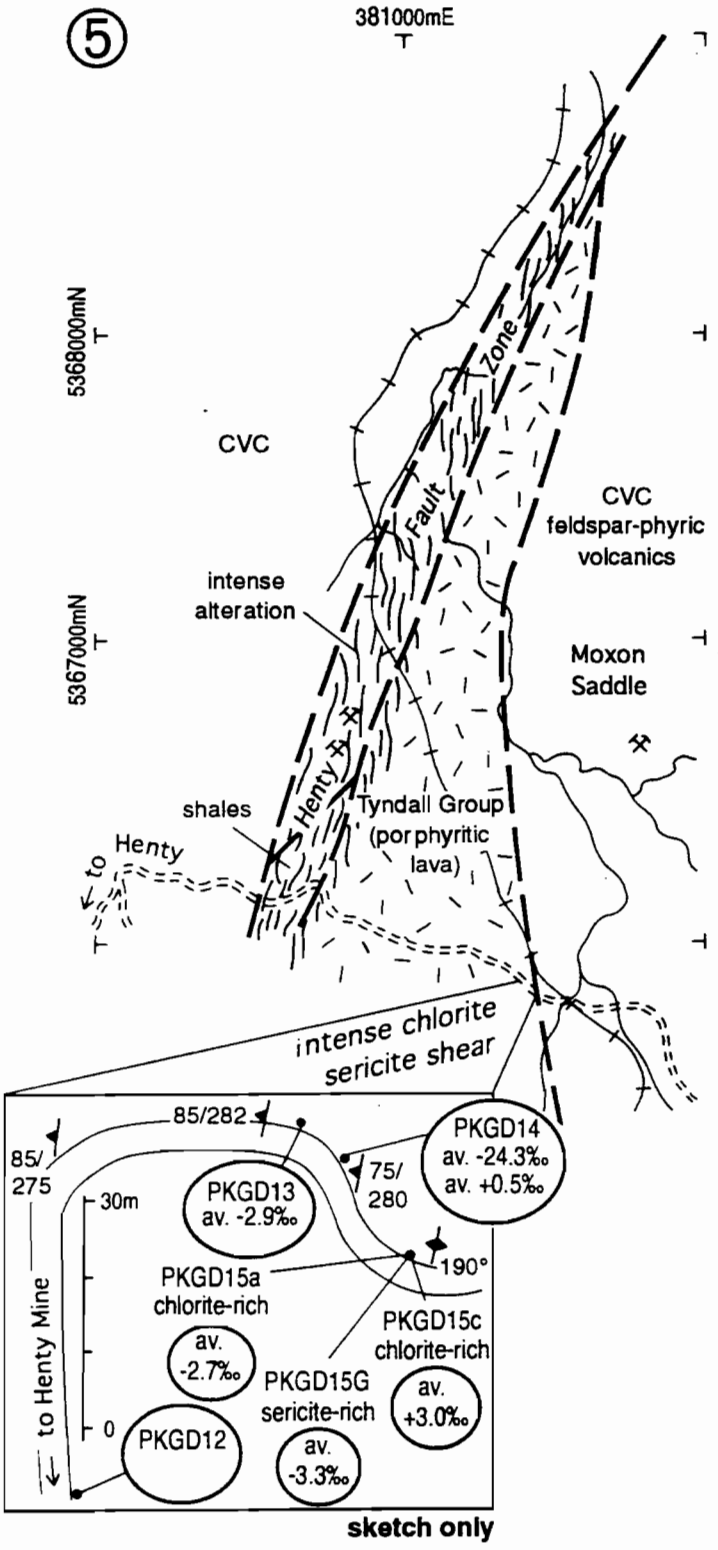

Fig. 6 — Geology of the Moxons Saddle area.

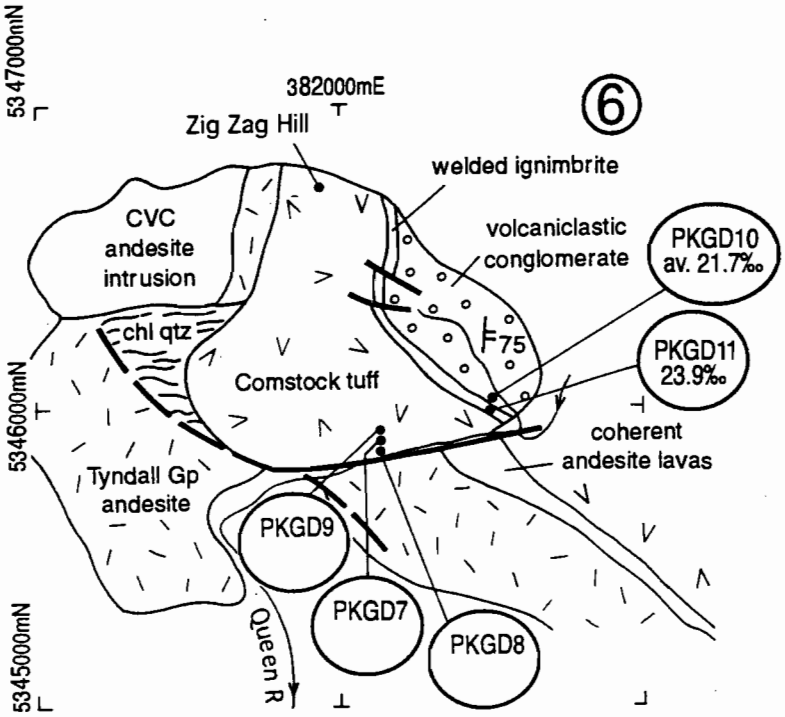

Fig. 7 — Geology of the Comstock–Zig Zag Hill area.

Fluid inclusion microthermometry of Cambrian and Devonian fault structures

Paul A. Kitto

Centre for Ore Deposit and Exploration Studies, Geology Department, University of Tasmania

ABSTRACT

Fluid inclusion microthermometric investigations in conjunction with stable isotopes have been used to successfully characterise the mineralised vein assemblages in the Pieman River - Mackintosh Dam area. Pyrite-sphalerite-quartz±galena±chlorite mineralisation was derived from a KCl-NaCl-H_2O-rich hydrothermal fluid with a salinity that ranged from 4 to 8 eq. wt. % NaCl. $\delta^{18}O_{qz}$ values together with fluid inclusion results indicate that the mineralising fluid was potential derived from a Devonian mixed magmatic - meteoric hydrothermal source. Two further hydrothermal fluids have been recognised. The first is a CO_2-rich, low salinity fluid responsible for quartz-chlorite±pyrite mineralisation in the Murchison Volcanics; and the second is a low temperature highly saline brine responsible for quartz deposition in the Central Volcanic Complex on the Pieman Road.

INTRODUCTION

Fluid inclusion microthermometric investigations of vein material in the Pieman River - Mackintosh Dam area have been undertaken to complement earlier $\delta^{18}O_{qz}$ studies and assist with the interpretation of the isotopic results previously reported in P.291A May 1994.

The initial isotopic study was undertaken to establish the usefulness of $\delta^{18}O_{qz}$ values in defining metal zonation patterns across the buried Devonian granite ridge, and to possibly differentiate Cambrian from Devonian fault structures. A number of syn- to post-tectonic quartz veins of varying mineralogies were sampled across the traverse from various host sequences. The location of samples is shown in figure 1.

The aims of this fluid inclusion study are to describe the fluid inclusions associated with the various vein mineralogies from the sample locations in terms of their classification types, chemical compositions (solids, liquid and gas), salinities, and homogenisation temperatures to try and establish diagnostic Cambrian and Devonian signatures associated with mineralisation.

METHOD OF STUDY

Primary fluid inclusions are visible in zoned quartz, and as isolated primary(?) fluid inclusions in quarz and sphalerite. The majority of the fluid inclusions are typically less than 5 μm but workable fluid inclusions from 5 to 30 μm were recognised. A total of 23 doubly polished sections were prepared for qualitative and descriptive investigation during this study. From these, 11 doubly polished thin sections

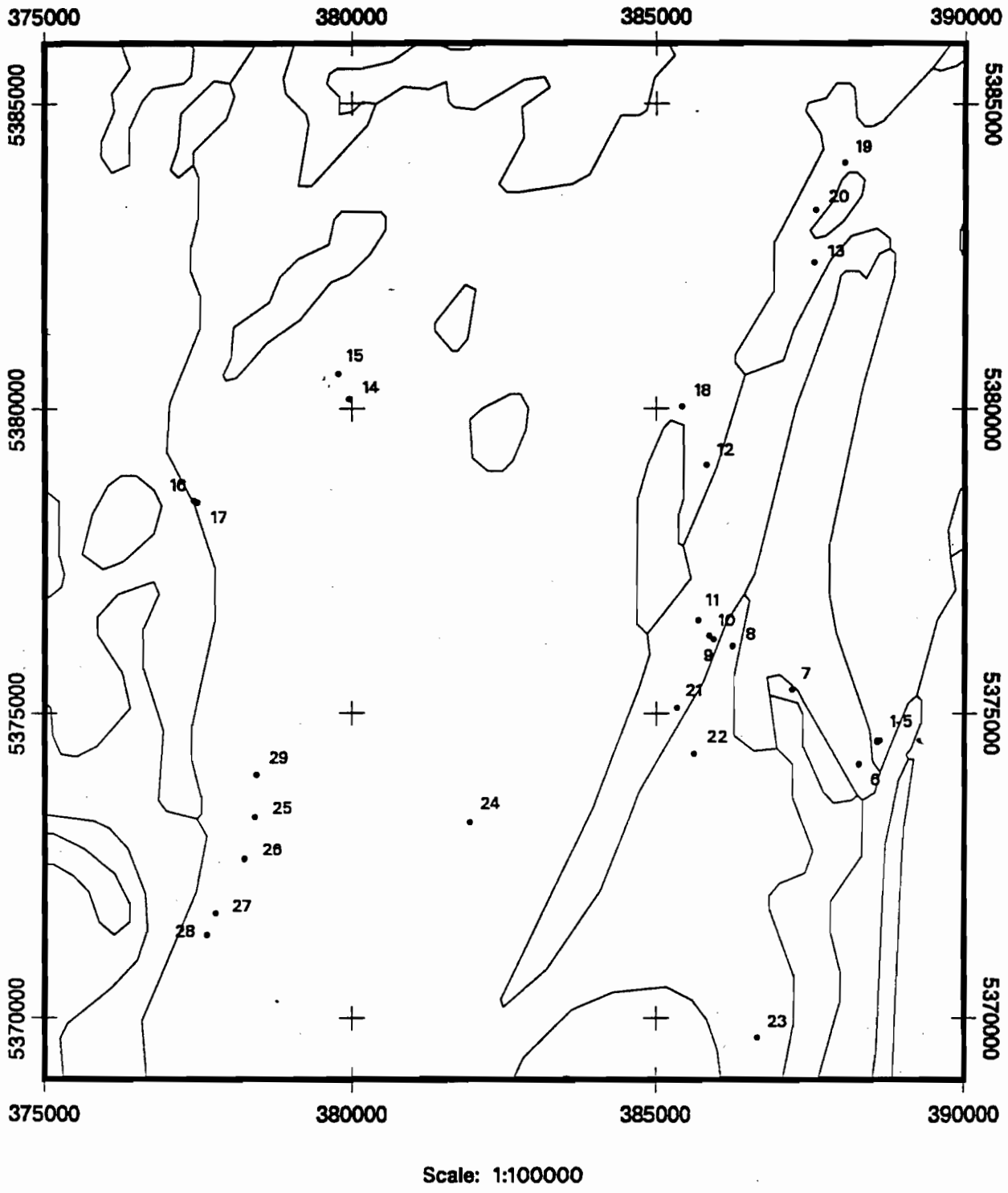

FIG. — Sample location points from the study area.

were selected for heating and freezing experiments. A total of 81 fluid inclusions have been analysed. Fluid inclusions were classified in a temporal sense as primary, or secondary (Table 1) relative to their host mineral and time of trapping. Of those studied, 53 are considered to be primary and the remainder classified as secondary. Minerals hosting fluid inclusions in the study area rarely show growth zoned patterns (quartz) which are typically recognised by alignment of occluded solid phases. Only fluid inclusions formed during this primary growth phase, and isolated solitary fluid inclusions have been classified as primary (e.g., Roedder, 1984; Shepherd et al., 1985; Reynolds, 1990). The remaining fluid inclusions have been grouped together as secondary fluid inclusions for all statistical considerations. All fluid inclusion data collected during this study are tabulated in Table 1.

Microthermometry was performed at the University of Tasmania on a modified USGS gas-flow heating/freezing stage supplied by Fluid Inc (Sterner & Bodnar, 1984; Bodnar & Sterner, 1985). Calibration of the stage was performed using synthetic fluid inclusions manufactured by Syn Flinc, and the precision of measured temperatures are ± 1.0°C for heating and ± 0.3°C for freezing. The accuracy of the Trendicator thermocouple measurements were calibrated against the triple point of CO_2 (-56°C), the freezing point of water (0.0°C), and the critical point of water (374.1°C) in synthetic fluid inclusions.

Homogenisation temperatures, which represent minimum trapping temperatures, have not been corrected for pressure because suitable constraints are not available. Salinity estimates are based on freezing point depressions for undersaturated fluid inclusions. This method provides only a rough estimate of the true salinity. Calcite was the only recognised daughter inclusion in all fluid inclusions studied. A minor number of fluid inclusion from those examined contained *visible* CO_2; salinity estimates were not possible.

Laser Raman microprobe analyses were undertaken at the Australian Geological Survey Organisation's fluid inclusion laboratory under the supervision of Dr. Terry Mernagh. Raman microprobe analyses were obtained from a Microdil 28 spectrometer, using 40 mW of 514.5 nm laser excitation from a Spectra Physics 2020 5W Ar^+ laser. Spectra were typically obtained after 10 accumulations with a 5 second integration time and an approximately 5 cm^{-1} spectral bandpass. The Raman spectra were calibrated using Ar^+ plasma and neon emission lines; wave numbrs were measured from the position of the peak maximum and are accurate to ± 1 cm^{-1}.

CLASSIFICATION OF FLUID INCLUSION TYPES

Only four distinct fluid inclusion types have been identified in the Pieman - Mackintosh Dam area, based on phase relations observed at room temperature (Nash, 1976; Fig. 2). The fluid inclusion types are:

Type 1A: Two-phase liquid-rich fluid inclusions that homogenise by vapour bubble disappearance. Type 1A fluid inclusions are abundant in all vein stages.

Type 3B: Three-phase liquid-rich fluid inclusions (liquid + vapour + carbonate daughters) that homogenise by vapour bubble disappearance. Type 3BV fluid inclusions are most abundant in base metal stage veins.

Type 4: Rare CO_2-rich fluid inclusions that contain visible CO_2 liquid and gas, plus H_2O-liquid (± daughter minerals) are restricted to a single sample (PK7B, Table 1).

Type 5: Rare secondary single-phase liquid only or vapour only fluid inclusions have been noted.

FLUID INCLUSION PETROGRAPHY

1. *Fluid Inclusions In Quartz*

Zoned quartz crystals were difficult to find in the sampled material resulting in only two zoned crystals being suitable for

Table 1. Fluid inclusion microthermometric results for the Pieman River - Makintosh Dam area.

SAMPLE NO.	RING NO.	LOCATION	HOST	TYPE	CRITERIA	PHASES	SIZE	Tm-CO2	Te	Tm	Salinity	Th	O18-qz	O18-fl	RAMAN (Gases)	RAMAN (Daughters)
PK1A	#1	Lake Makintosh - Sofia Tunnel	Qz	1A-LV	P - isolated	L-V	20µ			-5.2	8.1	271.0	13.3	5.3	-	-
	#1	Lake Makintosh - Sofia Tunnel	Qz	1A-LV	P - isolated	L-V	15µ		-23.8			151.8	13.3	-1.9	-	-
	#1	Lake Makintosh - Sofia Tunnel	Qz	1A-LV	P - isolated	L-V	10µ					177.5	13.3	0.2	-	-
	#1	Lake Makintosh - Sofia Tunnel	Qz	1A-LV	P - isolated	L-V	15µ		-23.8	-4.8	7.6	170.2	13.3	-0.4	-	-
	#1	Lake Makintosh - Sofia Tunnel	Qz	1A-LV	P - isolated	L-V	10µ		-23.8	-4.9	7.7	193.4	13.3	1.3	-	-
	#1	Lake Makintosh - Sofia Tunnel	Qz	1A-LV	P - isolated	L-V	10µ		-23.8	-5.1	8.0	148.0	13.3	-2.2	-	-
PK1C	#1	Lake Makintosh - Sofia Tunnel	Qz	3B-LVD	P - isolated	L-V-1D	5µ					280.7	13.3	5.7	-	Calcite
	#1	Lake Makintosh - Sofia Tunnel	Qz	3B-LVD	P - isolated	L-V-1D	6µ					272.9	13.3	5.4	-	Calcite
	#1	Lake Makintosh - Sofia Tunnel	Qz	3B-LVD	P - isolated	L-V-1D	5µ					333.5	13.3	7.5	-	Calcite
	#1	Lake Makintosh - Sofia Tunnel	Qz	3B-LVD	P - isolated	L-V-1D	4µ					263.0	13.3	5.0	-	Calcite
	#1	Lake Makintosh - Sofia Tunnel	Qz	3B-LVD	P - isolated	L-V-1D	4µ					276.0	13.3	5.5	-	Calcite
PK1D	#1	Lake Makintosh - Sofia Tunnel	Qz	1A-LV	P - isolated	L-V	7µ			-1.5	2.6	211.5			CO2	-
	#1	Lake Makintosh - Sofia Tunnel	Qz	1A-LV	P - isolated	L-V	7µ			-1.5	2.6	204.7			CO2	-
	#1	Lake Makintosh - Sofia Tunnel	Qz	1A-LV	P - isolated	L-V	4µ			-1.8	3.1				CO2	-
	#2	Lake Makintosh - Sofia Tunnel	Qz	1A-LV	P - isolated	L-V	5µ					222.2			CO2	-
	#2	Lake Makintosh - Sofia Tunnel	Qz	1A-LV	P - isolated	L-V	5µ					277.1			CO2	-
PK4C	#2	Lake Makintosh Car Park	Sph	3B-LVD	P - isolated	L-V-1D	30µ					252.0	11.7	2.9	-	-
	#2	Lake Makintosh Car Park	Sph	3B-LVD	P - isolated	L-V-1D	30µ					258.6	11.7	3.2	-	-
PK5A(i)	#1	Lake Makintosh Car Park - Shed	Qz-zoned	1A-LV	S - fractured	L-V	10µ			-3.0	4.9	163.7	13.4	-0.8	-	-
	#1	Lake Makintosh Car Park - Shed	Qz-zoned	1A-LV	S - fractured	L-V	12µ			-3.1	5.1	163.7	13.4	-0.8	-	-
PK6A	#1	Tunnel Road Saddle	Qz-zoned	3B-LVD	P - zoned xst	L-V-1D	5µ			-0.9	1.6	243.2	12.1	2.9	CO2	Calcite
	#1	Tunnel Road Saddle	Qz-zoned	3B-LVD	P - zoned xst	L-V-1D	10µ			-1.0	1.7	170.9	12.1	-1.5	CO2	Calcite
	#1	Tunnel Road Saddle	Qz-zoned	3B-LVD	P - zoned xst	L-V-1D	15µ			-0.9	1.6	169.0	12.1	-1.7	CO2	Calcite
	#1	Tunnel Road Saddle	Qz-zoned	3B-LVD	P - zoned xst	L-V-1D	7µ			-1.0	1.7		12.1		CO2	Calcite
	#1	Tunnel Road Saddle	Qz-zoned	3B-LVD	P - zoned xst	L-V-1D	7µ			-1.1	1.9	178.0	12.1	-1.0	CO2	Calcite
	#1	Tunnel Road Saddle	Qz-zoned	3B-LVD	P - zoned xst	L-V-1D	7µ			-0.8	1.4		12.1		CO2	Calcite
	#1	Tunnel Road Saddle	Qz-zoned	3B-LVD	P - zoned xst	L-V-1D	10µ			-0.9	1.6		12.1		CO2	Calcite
PK7B	#1	Murchison Gorge Rd	Qz	4A-CO2	P - isolated	L-V-CO2	15µ	-56.6	-22.4			331.6			CO2	-
	#1	Murchison Gorge Rd	Qz	4A-CO2	P - isolated	L-V-CO2	7µ		-22.4			218.4			CO2	-
	#1	Murchison Gorge Rd	Qz	4A-CO2	P - isolated	L-V-CO2	7µ		-22.4			319.9			CO2	-
	#1	Murchison Gorge Rd	Qz	4A-CO2	P - isolated	L-V-CO2	7µ		-22.4			253.4			CO2	-
	#1	Murchison Gorge Rd	Qz	4A-CO2	P - isolated	L-V-CO2	7µ		-22.4			333.9			CO2	-
	#1	Murchison Gorge Rd	Qz	4A-CO2	P - isolated	L-V-CO2	7µ		-22.4			311.5			CO2	-
	#1	Murchison Gorge Rd	Qz	4A-CO2	P - isolated	L-V-CO2	10µ		-22.4			315.3			CO2	-
PK11B	#2	Murchison Open-cut	Qz	3B-LVD	P - isolated	L-V-1D	5µ			-2.3	3.9	162.0	13.3	-1.0	-	-
	#2	Murchison Open-cut	Qz	3B-LVD	P - isolated	L-V-1D	5µ			-2.1	3.5		13.3		-	-
	#2	Murchison Open-cut	Qz	3B-LVD	P - isolated	L-V-1D	7µ			-2.0	3.4		13.3		-	-
	#2	Murchison Open-cut	Qz	3B-LVD	P - isolated	L-V-1D	5µ			-2.2	3.7		13.3		-	-
	#2	Murchison Open-cut	Qz	3B-LVD	P - isolated	L-V-1D	5µ		-26.4	-2.2	3.7	174.0	13.3	-0.1	-	-

SAMPLE NO.	RING NO.	LOCATION	HOST	TYPE	CRITERIA	PHASES	SIZE	Tm-CO2	Te	Tm	Salinity	Th	O18-qz	O18-fl	RAMAN (Gases)	RAMAN (Daughters)
	#2	Murchison Open-cut	Qz	3B LVD	P - isolated	L-V-1D	7μ			-2.2	3.7	162.6	13.3	-1.0	-	-
	#2	Murchison Open-cut	Qz	3B-LVD	P - isolated	L-V-1D	7μ			-2.2	3.7	172.8	13.3	-0.2	-	-
	#2	Murchison Open-cut	Qz	3B-LVD	P - isolated	L-V-1D	15μ		-25.8	-4.8	7.6	161.7	13.3	-1.1	-	-
	#2	Murchison Open-cut	Qz	3B-LVD	P - isolated	L-V-1D	5μ			-2.3	3.9		13.3		-	-
	#2	Murchison Open-cut	Qz	3B-LVD	P - isolated	L-V-1D	5μ			-2.4	4.0	214.1	13.3	2.5	-	-
	#2	Murchison Open-cut	Qz	3B-LVD	P - isolated	L-V-1D	7μ		-26.2	-2.4	4.0	170.0	13.3	-0.4	-	-
	#2	Murchison Open-cut	Qz	3B-LVD	P - isolated	L-V-1D	7μ		-26.2	-2.4	4.0	170.0	13.3	-0.4	-	-
PK15A	#1	Pieman Road - Boco Creek	Qz	1A-LV	P - isolated	L-V	5μ		-24.2	-18.5	21.6	124.0			-	-
	#1	Pieman Road - Boco Creek	Qz	1A-LV	P - isolated	L-V	5μ		-24.2	-18.5	21.6	124.0			-	-
	#1	Pieman Road - Boco Creek	Qz	1A-LV	P - isolated	L-V	5μ		-23.5	-16.0	19.6	132.2			-	-
	#1	Pieman Road - Boco Creek	Qz	1A-LV	P - isolated	L-V	5μ		-23.5	-16.6	20.0	132.8			-	-
	#1	Pieman Road - Boco Creek	Qz	1A-LV	P - isolated	L-V	5μ		-24.0	-16.7	20.1	132.0			-	-
	#1	Pieman Road - Boco Creek	Qz	1A-LV	P - isolated	L-V	10μ		-24.2	-8.2	12.0	125.0			-	-
PK15B	#1	Pieman Road - Boco Creek	Qz	1A-LV	S - fractured	L-V	15μ		-22.6	-2.3	3.9	142.3	12.1	-4.0	-	-
	#1	Pieman Road - Boco Creek	Qz	1A-LV	S - fractured	L-V	15μ		-22.6	-2.3	3.9	142.3	12.1	-4.0	-	-
	#1	Pieman Road - Boco Creek	Qz	1A-LV	S - fractured	L-V	25μ		-22.6	-2.3	3.9	142.3	12.1	-4.0	-	-
	#1	Pieman Road - Boco Creek	Qz	1A-LV	S - fractured	L-V	5μ		-22.6	-2.3	3.9	142.3	12.1	-4.0	-	-
	#1	Pieman Road - Boco Creek	Qz	1A-LV	S - fractured	L-V	5μ		-22.6	-2.3	3.9	142.3	12.1	-4.0	-	-
	#1	Pieman Road - Boco Creek	Qz	1A-LV	S - fractured	L-V	10μ		-22.6	-2.3	3.9	142.3	12.1	-4.0	-	-
	#1	Pieman Road - Boco Creek	Qz	1A-LV	S - fractured	L-V	5μ		-22.6	-2.3	3.9	142.3	12.1	-4.0	-	-
	#1	Pieman Road - Boco Creek	Qz	1A-LV	S - fractured	L-V	7μ		-22.6	-2.3	3.9	142.3	12.1	-4.0	-	-
	#1	Pieman Road - Boco Creek	Qz	1A-LV	S - fractured	L-V	5μ		-22.6	-2.3	3.9	142.3	12.1	-4.0	-	-
	#1	Pieman Road - Boco Creek	Qz	1A-LV	S - fractured	L-V	5μ		-22.6	-2.3	3.9	142.3	12.1	-4.0	-	-
	#1	Pieman Road - Boco Creek	Qz	1A-LV	S - fractured	L-V	5μ		-22.6	-2.3	3.9	142.3	12.1	-4.0	-	-
	#1	Pieman Road - Boco Creek	Qz	1A-LV	S - fractured	L-V	7μ		-22.6	-2.3	3.9	142.3	12.1	-4.0	-	-
	#1	Pieman Road - Boco Creek	Qz	1A-LV	S - fractured	L-V	5μ		-22.6	-2.3	3.9	142.3	12.1	-4.0	-	-
	#1	Pieman Road - Boco Creek	Qz	1A-LV	S - fractured	L-V	5μ		-22.6	-2.3	3.9	142.3	12.1	-4.0	-	-
	#1	Pieman Road - Boco Creek	Qz	1A-LV	S - fractured	L-V	5μ		-22.6	-2.3	3.9	142.3	12.1	-4.0	-	-
	#1	Pieman Road - Boco Creek	Qz	1A-LV	S - fractured	L-V	10μ		-22.6	-2.3	3.9	142.3	12.1	-4.0	-	-
	#1	Pieman Road - Boco Creek	Qz	1A-LV	S - fractured	L-V	10μ		-22.6	-2.3	3.9	142.3	12.1	-4.0	-	-
	#1	Pieman Road - Boco Creek	Qz	1A-LV	S - fractured	L-V	10μ		-22.6	-2.3	3.9	142.3	12.1	-4.0	-	-
	#1	Pieman Road - Boco Creek	Qz	1A-LV	S - fractured	L-V	10μ		-22.6	-2.3	3.9	142.3	12.1	-4.0	-	-
PK21A(i)	#1	Murchison Hwy - Sth Tullah	Qz	1A-LV	P - isolated	L-V	10μ		-21.3	-2.3	3.9	162.2			-	-
	#1	Murchison Hwy - Sth Tullah	Qz	1A-LV	P - isolated	L-V	10μ		-23.4	-2.4	4.0	152.2			-	-
	#1	Murchison Hwy - Sth Tullah	Qz	1A-LV	P - isolated	L-V	5μ		-21.3	-2.3	3.9	140.6			-	-

INCLUSION TYPE		PHASES AT 25°C	HOMOGENISATION BEHAVIOUR
Type 1A	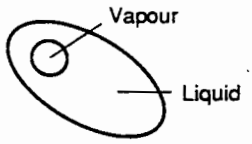	Liquid + vapour	Vapour disappears
Type 1B	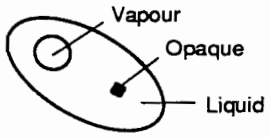	Liquid + vapour + opaque	Vapour disappears
Type 2	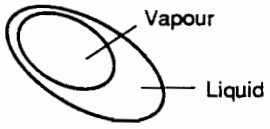	Vapour + liquid	Critical Behaviour
Type 3AD	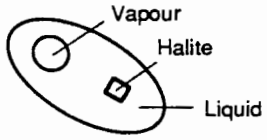	Liquid + vapour + halite (± other daughters)	Vapour disappears
Type 3BV	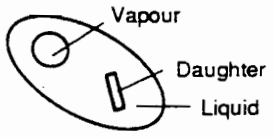	Liquid + vapour + daughter(s) (1 - 5)	Vapour disappears
Type 4	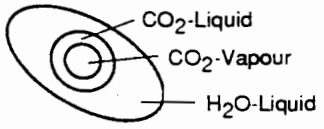	CO_2-liquid + CO_2-vapour + H_2O-liquid	CO_2 disappears
Type 5		Single phase	N.A.

Figure 2. Summary of fluid inclusion types, the phase(s) present at 25°C, and the high temperature homogenisation behaviour.

microthermometric study (e.g., PK5A & PK6A; Table 1). The majority of the material consisted of vein quartz containing isolated solitary fluid inclusions.

Fluid inclusion types 1A and 3B dominate the vein quartz occurrences. Rare Type 4 (CO_2-bearing) and Type 5 (single-phase) fluid inclusions also occur in quartz.

2. Fluid Inclusions In Sphalerite

The iron-rich sphalerite is typically too dark to satisfactorily observe fluid inclusions present, but two analyses of Type 3B fluid inclusions were obtained in a zoned sphalerite specimen (PK4C; Table 1).

FLUID INCLUSION MICROTHERMOMETRY

1. Lake Makintosh

Lake Makintosh mineralisation is dominated by Type 1A and Type 3B fluid inclusions (Fig. 3). Fluid inclusions range in size from 10 to 20 μm in diameter, but are typically ≤ 10 μm. Isolated fluid inclusions are most common and have been classified as primary in this study (Roedder, 1984). Zones quartz crystals with primary fluid inclusions were not observed.

Homogenisation temperatures for primary fluid inclusions range from 148° to 333°C; most occur between 150° and 195°C (Fig. 3A). Primary Type 3B fluid inclusions mostly yield significantly higher homogenisation temperatures than Type 1A fluid inclusions resulting in a bi-modal distribution. Type 3BV fluid inclusion from the Lake Makintosh area typically contain a birefringent daughter mineral. Homogenisation by the vapour bubble to the liquid phase occurs before final dissolution of the daughter mineral. Continued heating results in decrepitation of Type 3BV fluid inclusions prior to daughter dissolution.

Salinity estimates for fluid inclusions in the Lake Makintosh area were only obtained for Type 1A fluid inclusions and were distributed evenly from 2.6 to 8.1 eq. wt. % NaCl (Fig. 3B). Similarly, first melting temperatures were only obtained for Type 1A fluid inclusions. The first melting temperature for the Type 1A fluid inclusions all have values of -23.8°C. (Fig. 3C).

2. Tunnel Road Saddle

Fluid inclusions from the Tunnel Road Saddle only contained Type 3BV fluid inclusions suitable for microthermometric analysis (Fig. 4A). Fluid inclusions range in size from 5 to 15 μm in diameter, but are typically ≤ 7 μm. The only primary fluid inclusions associated with growth zones in the quartz host were observed in the Tunnel Road Saddle material.

Homogenisation temperatures for these primary fluid inclusions ranged from 169° to 243°C (Fig. 4A). A total of only 4 homogenisation temperatures were possible from this material. The Type 3BV fluid inclusions form distinct bimodal populations at 170° and 240° but this is most probably an artifact of the limited data set for the Tunnel Road Saddle. Type 3BV fluid inclusion from the Tunnel Road Saddle area typically contain a birefringent daughter mineral. Homogenisation by the vapour bubble to the liquid phase occurs before final dissolution of the daughter mineral. Continued heating results in decrepitation of Type 3BV fluid inclusions prior to daughter dissolution.

Salinity estimates for fluid inclusions in the Tunnel Road Saddle area were obtained for Type 3BV fluid inclusions and were distributed evenly from 1.4 to 1.9 eq. wt. % NaCl (Fig. 4B). No first melting temperatures were obtained for Type 3BV fluid inclusions.

3. Murchison Gorge Road

Fluid inclusions from the Murchison Gorge Road only contained Type 4 (CO_2-rich) fluid inclusions suitable for microthermometric analysis (Fig. 5A).

Fluid inclusions range in size from 7 to 15 μm in diameter, but are typically 7 μm. Isolated fluid inclusions are most common and have been classified as primary in this study (Roedder, 1984). Zoned quartz crystals with primary fluid inclusions were not observed.

Homogenisation temperatures for Type 4 primary fluid inclusions from the Murchison Gorge Road range from 218° to 334°C. The largest fluid inclusion population homogenises between 311° and 334°C (Fig. 3A). Homogenisation of the CO_2 vapour bubble to CO_2 liquid occurs prior to complete homogenisation.

Salinity estimates on the Murchison Gorge Road fluid inclusions were not possible. A single fluid inclusion yielded a first melting temperature of -56.6°C (Table 1). The remaining fluid inclusions had first melting temperatures of -22.4°C.

4. Murchison Open-cut

Fluid inclusions from the Murchison Open-cut only contained Type 3BV fluid inclusions suitable for microthermometric analysis (Fig. 6A). Fluid inclusions range in size from 5 to 15 μm in diameter, but are typically ≤ 7 μm. Isolated fluid inclusions are most common and have been classified as primary in this study (Roedder, 1984). Zoned quartz crystals with primary fluid inclusions were not observed.

Homogenisation temperatures for these primary fluid inclusions ranged from 162° to 214°C (Fig. 6A). The Type 3BV fluid inclusions form distinct bimodal populations at 170°. Type 3BV fluid inclusion from the Murchison Open-cut area typically contain a birefringent daughter mineral. Homogenisation by the vapour bubble to the liquid phase occurs before dissolution of the daughter mineral. Continued heating results in decrepitation of Type 3BV fluid inclusions prior to daughter dissolution.

Salinity estimates for fluid inclusions in the Murchison Open-cut were obtained for Type 3BV fluid inclusions and ranged from 3.4 to 7.6 eq. wt. % NaCl (Fig. 6B). With the exception of one fluid inclusion the salinity of the fluids from the Murchison Open-cut were between 3.4 and 4.0 eq. wt. % NaCl.

First melting temperatures for the Murchison Open-cut fluid inclusions, where obtained, are very tightly constrained in a range from -25.8° to -26.4°C (Fig. 6C).

5. Pieman Road - Boco Creek

Microthermometric analysis was only possible on Type 1A fluid inclusions from the Pieman Road - Boco Creek area (Fig. 7). Isolated primary fluid inclusions range in size from 5 to 10 μm in diameter, but most are typically ≤ 5 μm. Zoned quartz crystals with primary fluid inclusions were not observed. Secondary fracture controlled Type 1A fluid inclusions in the Pieman Road - Boco Creek area range in size from 5 to 25 μm in diameter, but the majority are ≤ 10 μm.

Homogenisation temperatures for the primary Type 1A fluid inclusions form a very tight low temperature population that ranges from 124° to 132°C (Table 1; Fig. 7A). Similarly, secondary Type 1A fluid inclusions have low homogenisation temperatures (142°C; Table 1).

Salinity estimates for the Pieman Road - Boco Creek area exhibit vastly different values depending whether they are primary or secondary fluid inclusions. The primary fluid inclusion population has a very distinctive salinity range between 12 and 22 eq. wt. % NaCl; dominated by salinities near 20 eq. wt. % NaCl (Fig. 7B). Whereas the secondary fluid inclusion population has a much lower salinity at 4 eq. wt. % NaCl (Fig. 7B).

First melting temperatures range from -23.5° to -24.2°C for the primary fluid inclusions, and remain constant at -22.6°C for secondary fluid inclusions (Fig. 7C).

6. Murchison Highway - South Tullah

Limited microthermometric analyses were possible on the Type 1A fluid inclusions from the Murchison Highway - South Tullah area (Fig. 8). The three isolated primary fluid inclusions range in size from 5 to 10 μm in diameter. Zoned quartz crystals with primary fluid inclusions were not observed.

Homogenisation temperatures for the three primary Type 1A fluid inclusions ranges from 140° to 162°C (Table 1; Fig. 8A). Salinity estimates are constant for these fluid inclusions with values from 3.9 to 4.0 eq. wt. % NaCl (Fig. 8B), and the first melting temperatures ranged from -21.3° to -23.4°C.

DISCUSSION

The fluid inclusion results for the vein material from the Pieman River - Makintosh Dam has been summarised into figures 9 (A, B, C) and 10 (A, B, C) and is discussed below.

1. *Lake Makintosh*

The fluid inclusion data from the five sample locations at Lake Makintosh dominate the higher temperature end of the Pieman River - Makintosh Dam data set, from 150° to 330°C (Fig. 9A). Salinity estimates for these hydrothermal fluids, based on ice melting temperatures, range from approximately 3 to 8 eq. wt. % NaCl which covers the dominant range for most of the fluid inclusion data gathered for the Pieman River - Makintosh Dam region (Fig. 9B). Based on limited first melting temperatures of -23.8°C the hydrothermal fluids responsible for quartz-pyrite-sphalerite±chlorite mineralisation at the contact between the Murchison Volcanics and the Owen Conglomerate are potentially KCl-NaCl-H_2O-rich brines (Fig. 9C). Minor CO_2 was detected in the vapour phase of these hydrothermal fluids in a single specimen (PK1D) using the laser Raman technique. The high spatial resolution of the laser Raman microprobe, which allows *in situ* identification of non-ionic daughter minerals, indicated that Type 3BV daughters minerals in fluid inclusions from the Lake Makintosh region were calcite. A spectral analysis of CO_2 vapour and a calcite daughter using the laser Raman is shown in figures 11A and 11B, respectively.

2. *Tunnel Road Saddle*

Homogenisation temperatures for the Tunnel Road Saddle fall within the middle temperature range for the Pieman River - Makintosh Dam data set (169° - 243°C; Fig. 9A). The low salinity (1.4 - 1.9 eq. wt. % NaCl) for the Tunnel Road Saddle hydrothermal fluids, however, are anomalous (Fig. 9B). Absence of first melting data for the Tunnel Road Saddle prevents speculation of the fluid compositions responsible for quartz-pyrite-galena mineralisation, except to say that laser Raman analyses detected significant CO_2 vapour not visible at room temperature (Table 1). The Type 3BV daughters minerals in fluid inclusions from the Tunnel Road Saddle area are calcite.

3. *Murchison Gorge Road*

The Murchison Gorge Road Type 4 (CO_2-rich) fluid inclusions are some of the highest homogenisation temperature fluids in the Pieman River - Makintosh Dam area (218° to 334°C; Fig 9A). These are the only truely CO_2-rich fluid inclusions observed and they were also the only fluid inclusions analysed associated with quartz-chlorite±pyrite mineralisation in the Murchison Volcanics.

4. *Murchison Open-cut*

The sphalerite-pyrite-quartz-carbonate mineralisation in the Murchison Open-cut is considered to be Devonian in origin based on Pb isotopes. The homogenisation temperatures (162° to 214°C; Fig. 9A) overlap the lower end of the spectrum for mineralisation in the Pieman River - Makintosh Dam area. Salinity estimates of approximately 4 eq. wt. % NaCl are some of the lowests, and indicate a

significant meteoric input to the likely magmatic hydrothermal fluids responsible for mineralisation (Fig. 9B). First melting temperatures indicate that the mineralising fluids were potentially KCl-NaCl-H_2O-rich brines (Fig. 9C).

5. Pieman Road - Boco Creek

The quartz only veins in the Central Volcanic Sequence at Pieman Road - Boco Creek have the lowest homogenisation temperature of all the fluid inclusions studies in the the Pieman River - Makintosh Dam area (124° to 142°C; Fig. 9A). The salinities of the primary and secondary fluid inclusions are extremely interesting in that the primary fluid inclusions are high saline brines (~20 eq. wt. % NaCl) and the secondary fluid inclusions are low saline brines (~4 eq. wt. % NaCl). The low salinity fluids overlap the majority of the fluid inclusion data from the Pieman River - Makintosh Dam area but the high saline brines are unique to the area (Fig. 9B). The first melting temperatures (~23°C) for the primary and secondary fluid inclusions indicate that both mineralising fluids were potentially KCl-NaCl-H_2O-rich brines (Fig. 9C).

6. Murchison Highway - South Tullah

Quart-pyrite-galena mineralisation in veins along the Murchison Highway south of Tullah have been described by previous researchers as Devonian mineralisation, based on Pb isotopes. Homogenisation temperatures from the fluid inclusions range from 140° to 162°C and fall at the lower temperature range within the Pieman River - Makintosh Dam data set but just overlap the temperatures from the Murchison Open-cut (Fig. 9A). Salinity estimates of 4 eq. wt. % NaCl are identical to the Devonian mineralisation in the Murchison Open-cut, and the fluids compositions are also thought be potentially KCl-NaCl-H_2O-rich brines (Fig. 9B, C).

CONCLUSIONS

Based on fluid inclusion microthermometric data collected for vein material from the Pieman River - Makintosh Dam area a number of conclusions can be drawn. It would appear that the pyrite-sphalerite-quartz±galena±chlorite mineralisation sampled across the area has been derived from a hydrothermal fluid which has a number of common features. Firstly, the composition of the hydrothermal fluids would appear to be KCl-NaCl-H_2O-rich brines with a salinity that ranges from 4 to 8 eq. wt. % NaCl. CO_2 is not a significant component of this hydrothermal fluid. Fluid inclusion homogenisation temperatures associated with this style of mineralisation vary from as low as 140° to as high as 330°C. Similar fluids have been recorded at Renison and at Lakeside associated with Devonian base metal mineralisation (Taheri and Green, 1990; Kitto, 1994). Figure 12 (A & B) summarise the nature of the fluid inclusion data from the the Pieman River - Makintosh Dam area and illustrates the homogeneity in first melting temperatures across the region and the range in salinity of fluid inclusions with temperature. With the exception of the high salinity data (~20 eq. wt. % NaCl; discussed below) such results are not too dissimilar to the base metal stage fluid inclusion data from Renison (Fig. 13A & B).

Calculation of the oxygen isotope compositions for the hydrothermal fluids responsible for mineralisation are presented in Table 2. Pyrite-sphalerite-quartz±galena±chlorite mineralisation appears to be associated with $\delta^{18}O_{fluid}$ (SMOW) values that are intermediate between magmatic and meteoric in composition (7.5‰ to -1.7‰). A spacial distribution of this data relative to the underlying Devonian granite body is not possible at this stage.

The hydrothermal fluids responsible for quartz-chlorite±pyrite mineralisation in the Murchison Volcanics is unique in this study by the fact that it is associated with CO_2-rich fluids. Such fluids are not characteristic of Devonian hydrothermal

fluids associated with base metal mineralisation in the Renison region and do not correspond to those hydrothermal fluids responsible for pyrite-sphalerite-quartz±galena±chlorite mineralisation in the Pieman River - Makintosh Dam area. $\delta^{18}O_{fluid}$ (SMOW) values and homogenisation temperature do, however, overlap the higher temperature hydrothermal fluids observed in the Pieman River - Makintosh Dam area.

Finally, the quartz mineralisation sampled in the Central Volcanic Complex at Pieman Road - Boco Creek would appear to have originated from a hydrothermal fluid derived from a different source to that reponsible for mineralisation sampled elsewhere in the Pieman River - Makintosh Dam area. The hydrothermal fluid responsible for quartz precipitation was low temperature, highly saline, and possessing a negative $\delta^{18}O_{fluid}$ (SMOW) value. The origin of this fluid is uncertain.

Figure 3.

Lake Makintosh

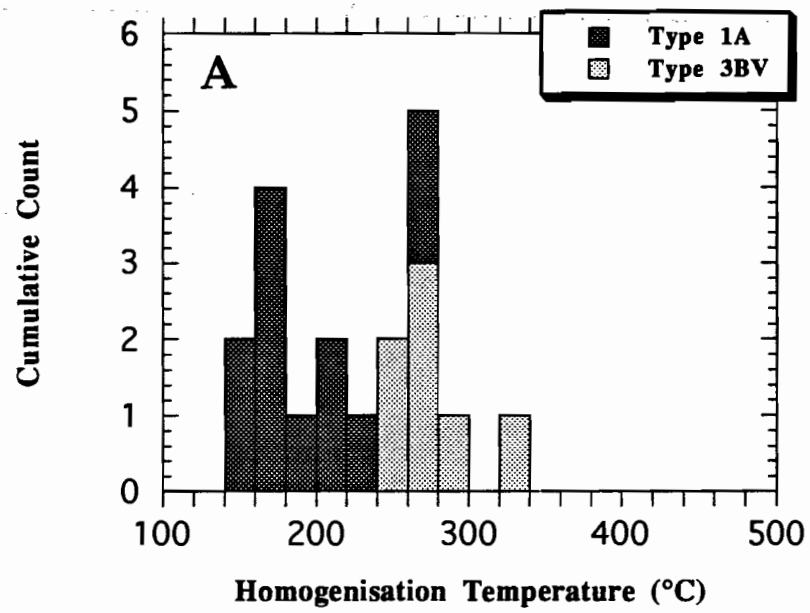

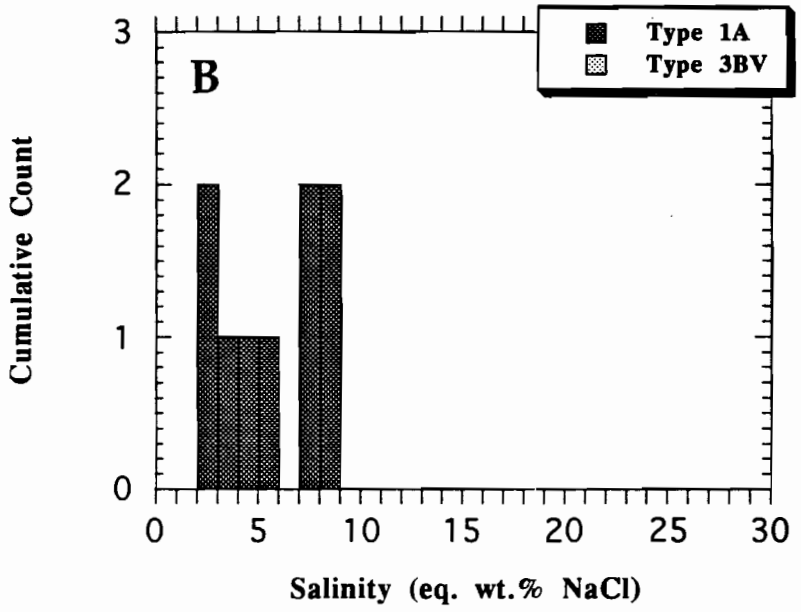

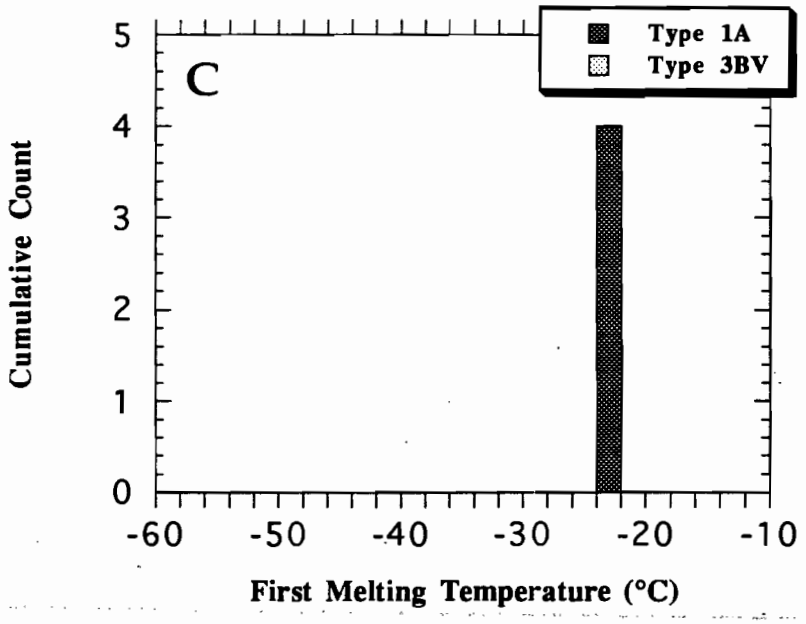

Figure 4.

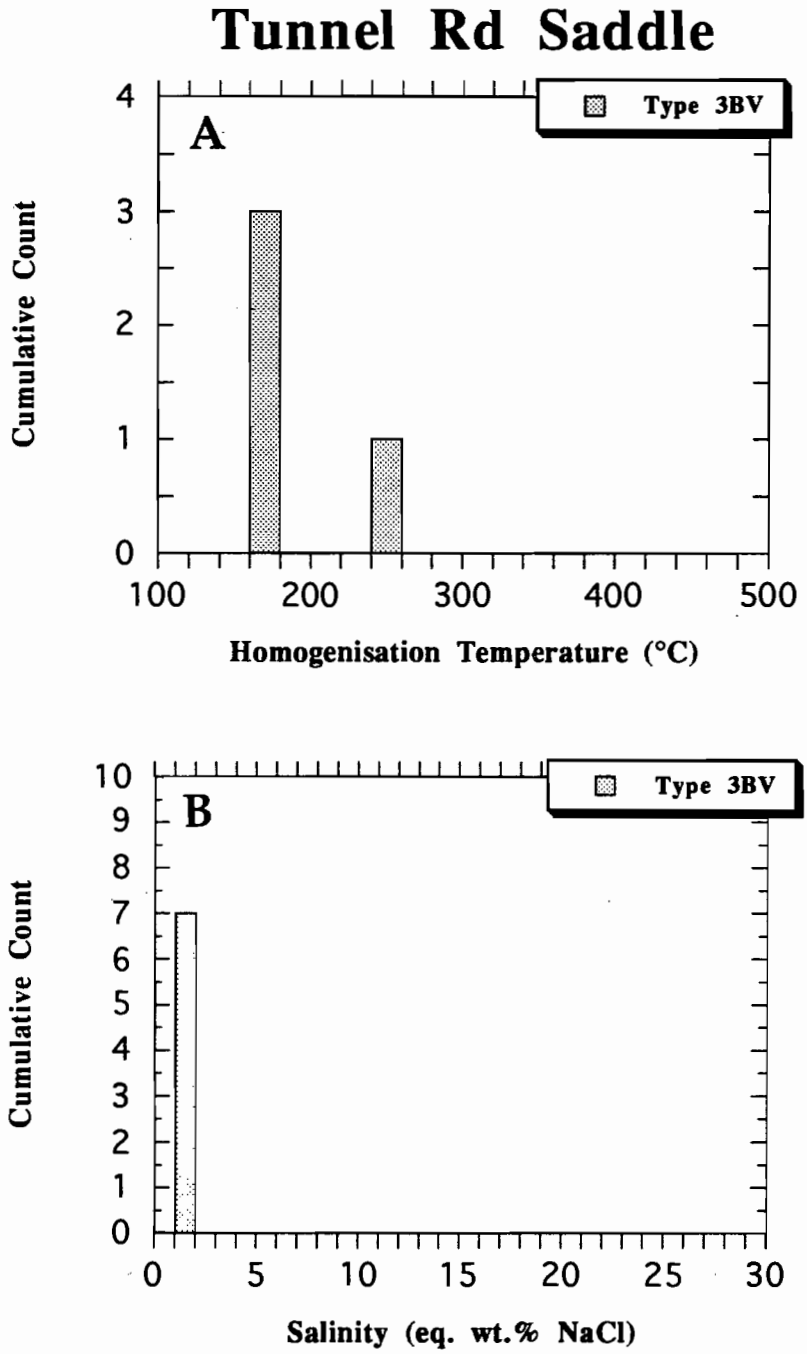
Tunnel Rd Saddle
A
Type 3BV
Cumulative Count
0
1
2
3
4
100
200
300
400
500
Homogenisation Temperature (°C)
B
Type 3BV
Cumulative Count
0
1
2
3
4
5
6
7
8
9
10
0
5
10
15
20
25
30
Salinity (eq. wt.% NaCl)

Figure 5.

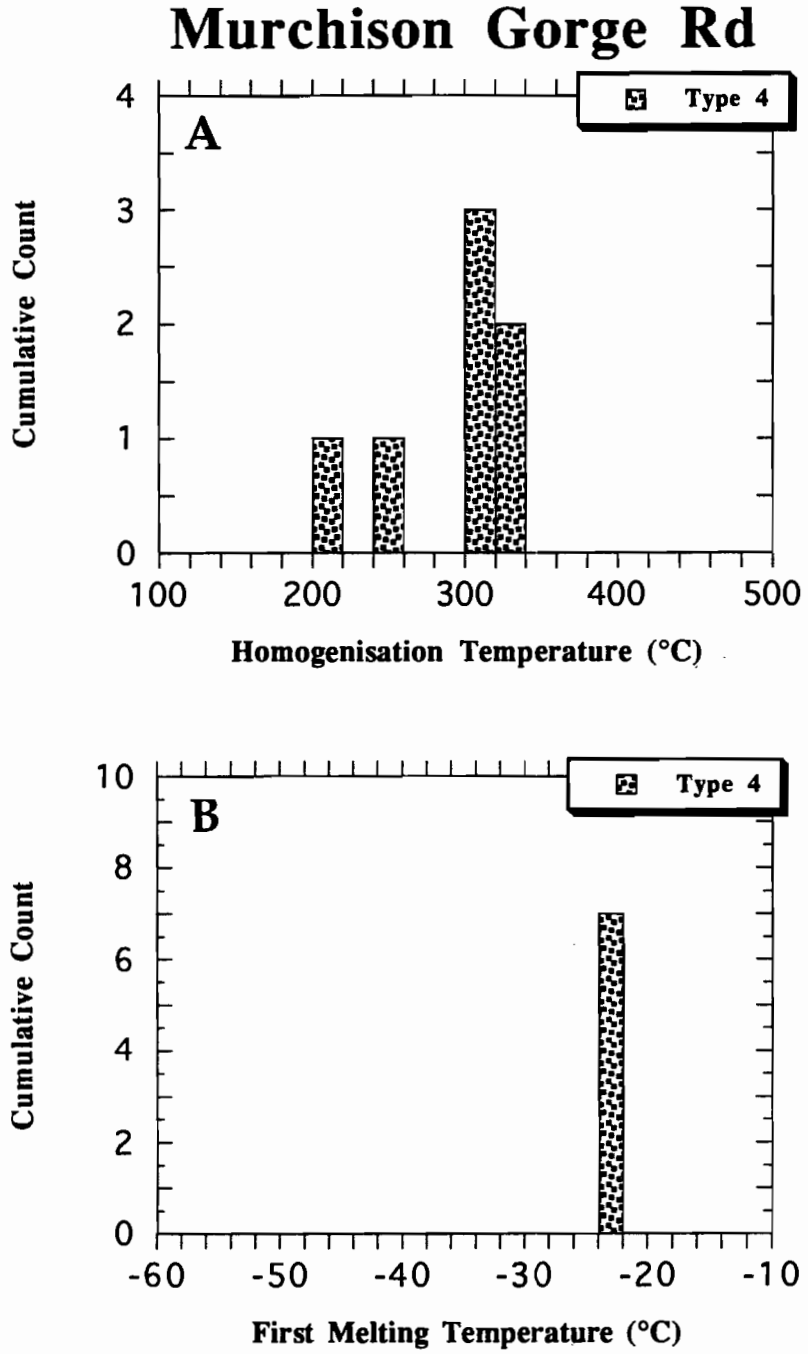
Murchison Gorge Rd
A
Type 4
Cumulative Count
0
1
2
3
4
100
200
300
400
500
Homogenisation Temperature (°C)
B
Type 4
Cumulative Count
0
2
4
6
8
10
-60
-50
-40
-30
-20
-10
First Melting Temperature (°C)

Murchison Opencut

Figure 6.

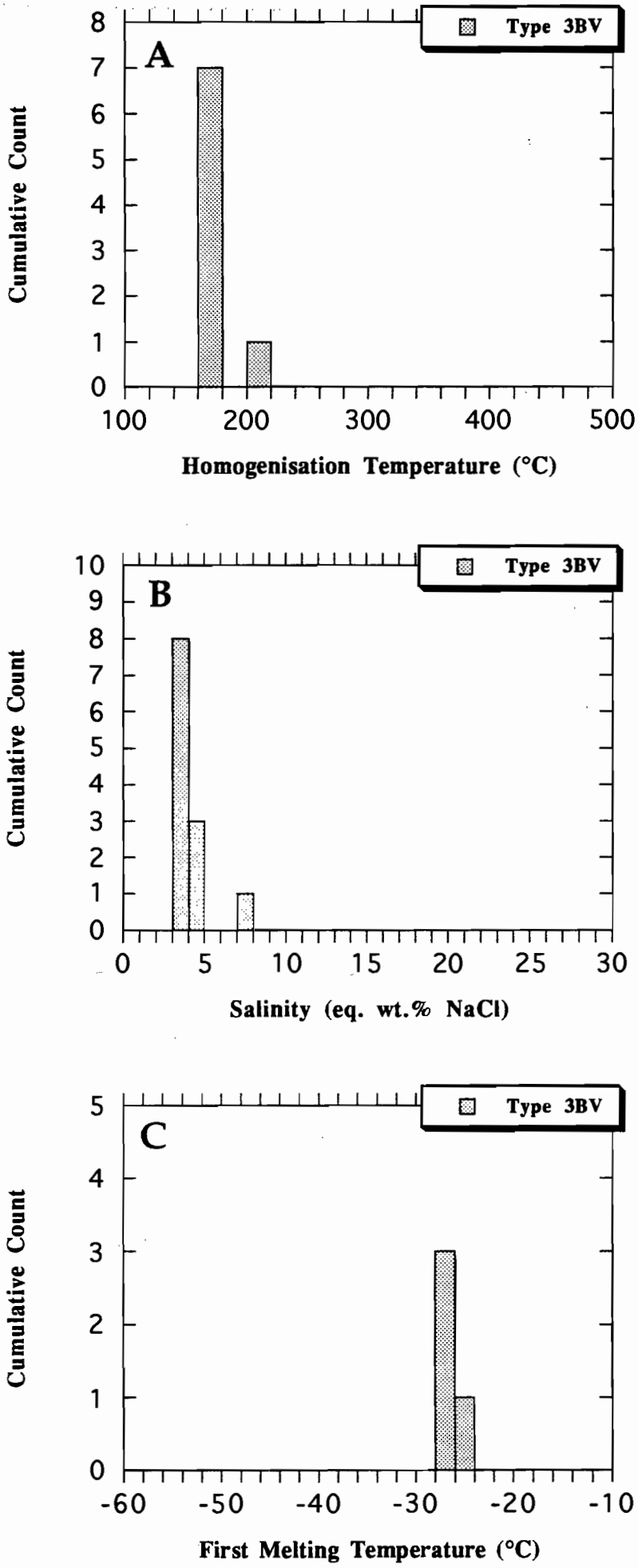

Figure 7.

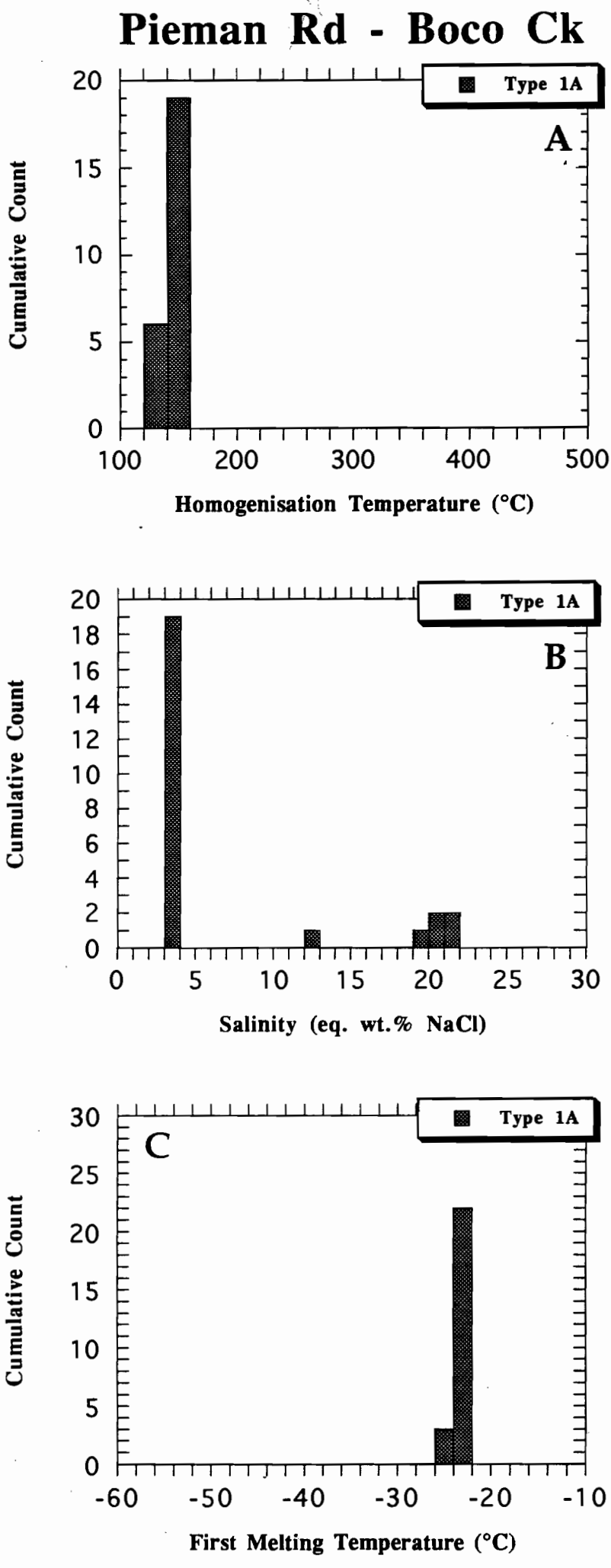
Pieman Rd - Boco Ck
Type 1A
A
Cumulative Count
Homogenisation Temperature (°C)
B
Salinity (eq. wt.% NaCl)
C
First Melting Temperature (°C)

Figure 8.

Murchison Hwy

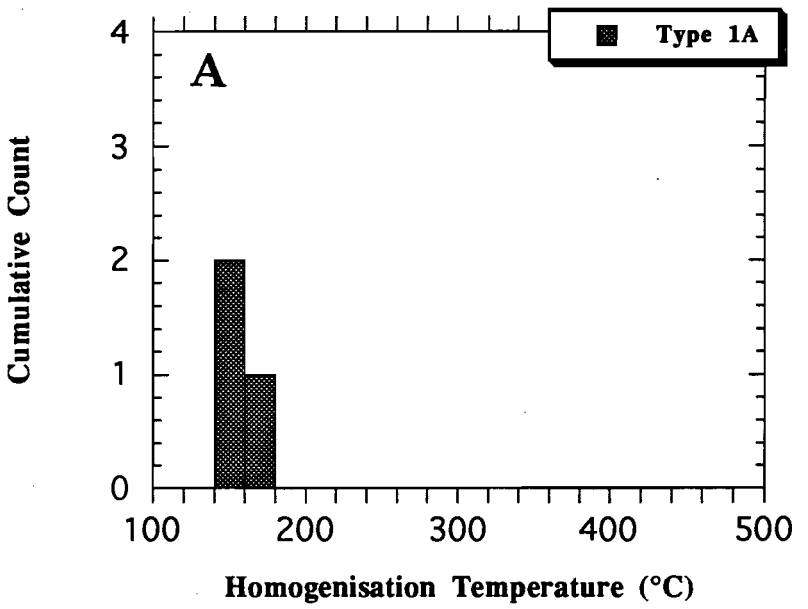

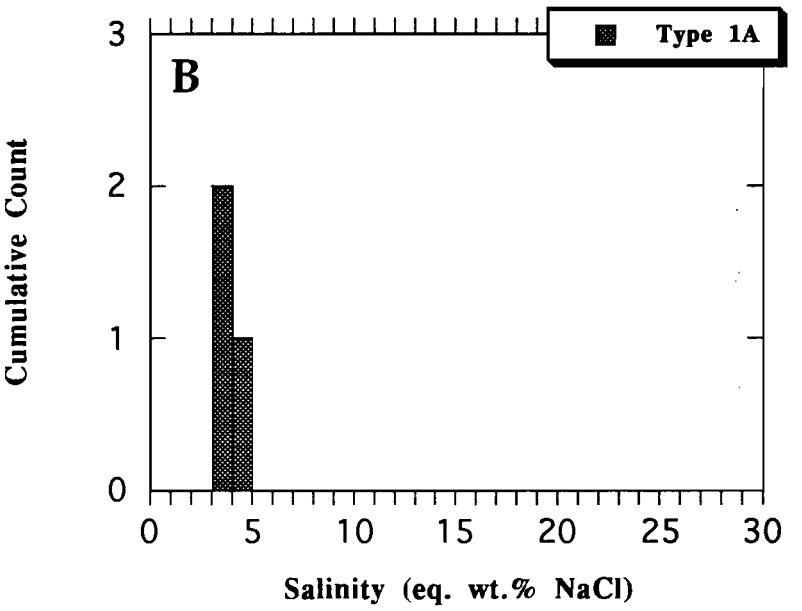

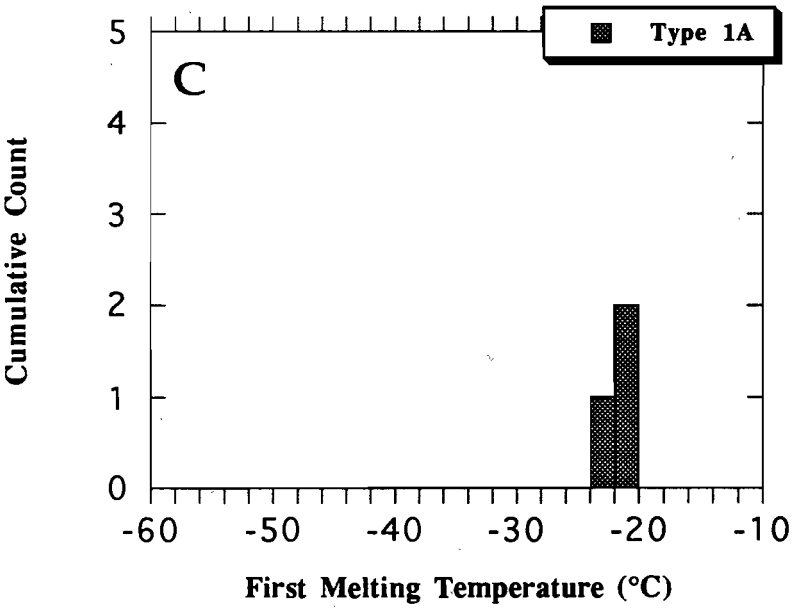

Figure 9

Locations - F.I. Data

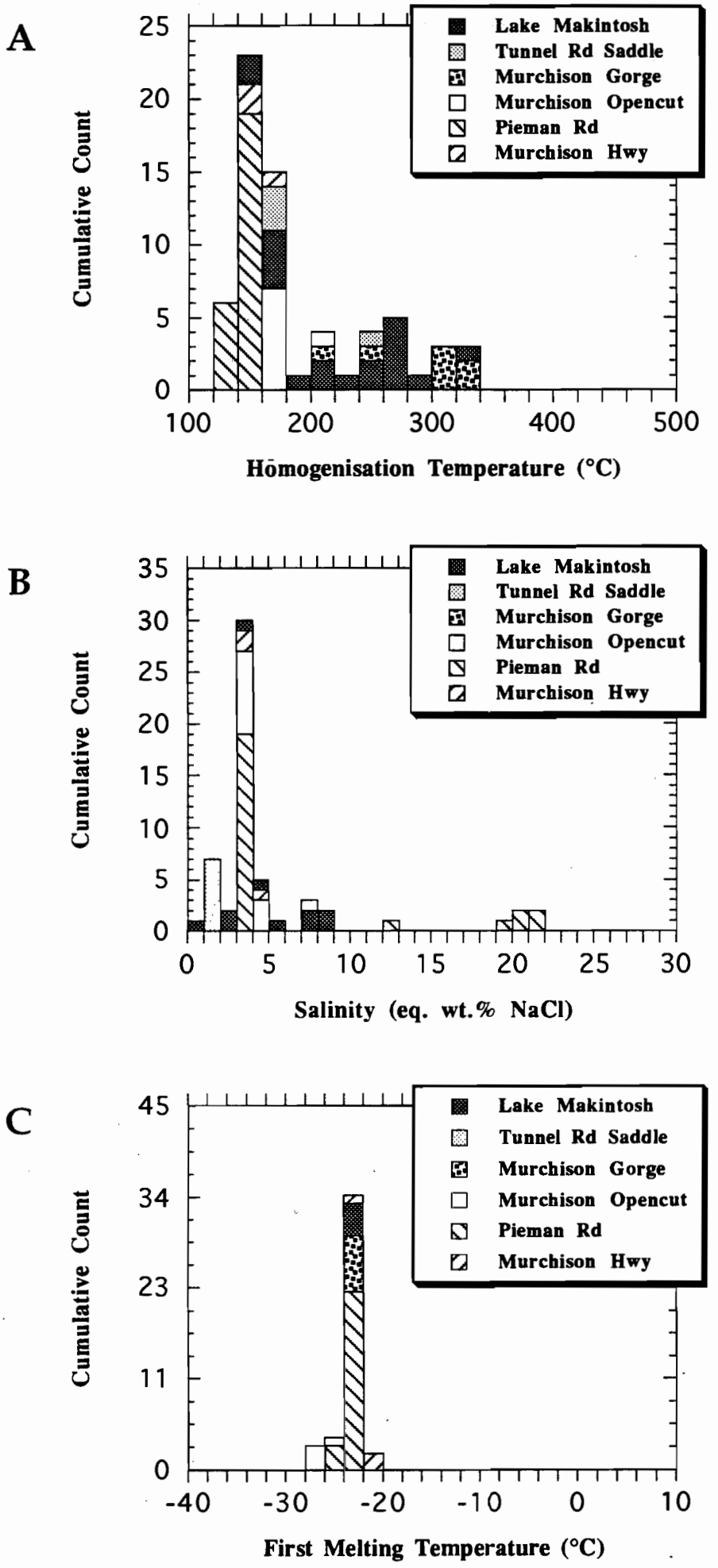

Distribution Of F.I. Types

Figure 10.

A

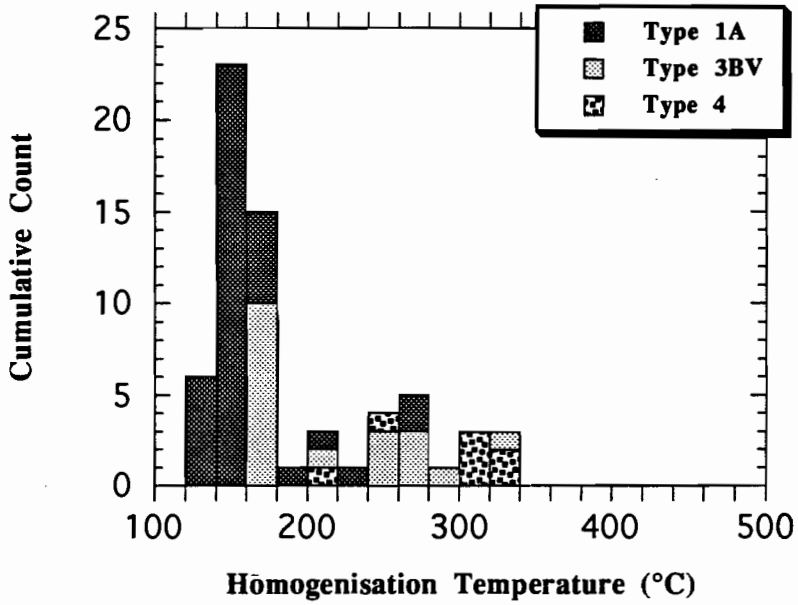

B

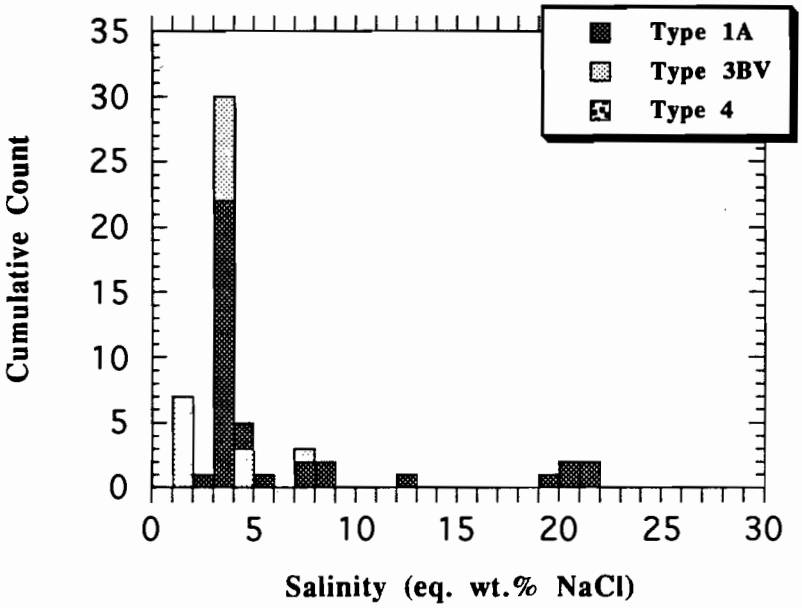

C

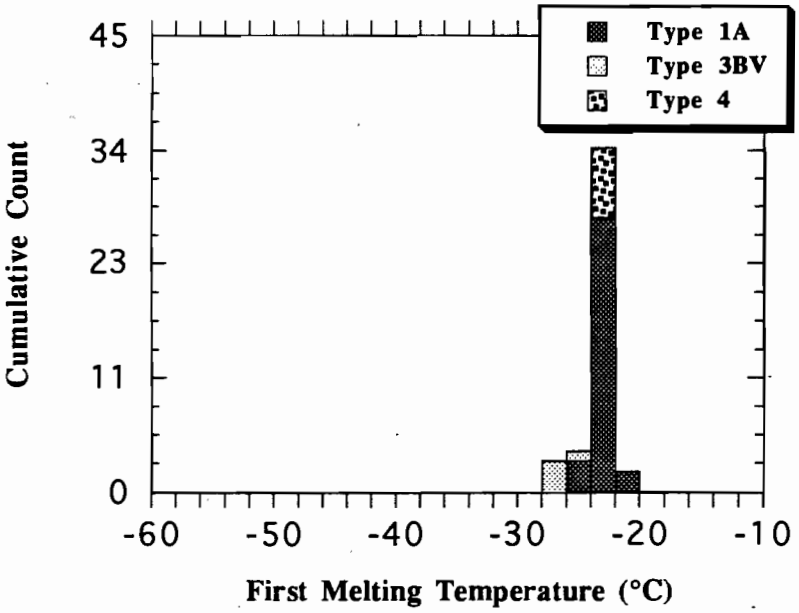

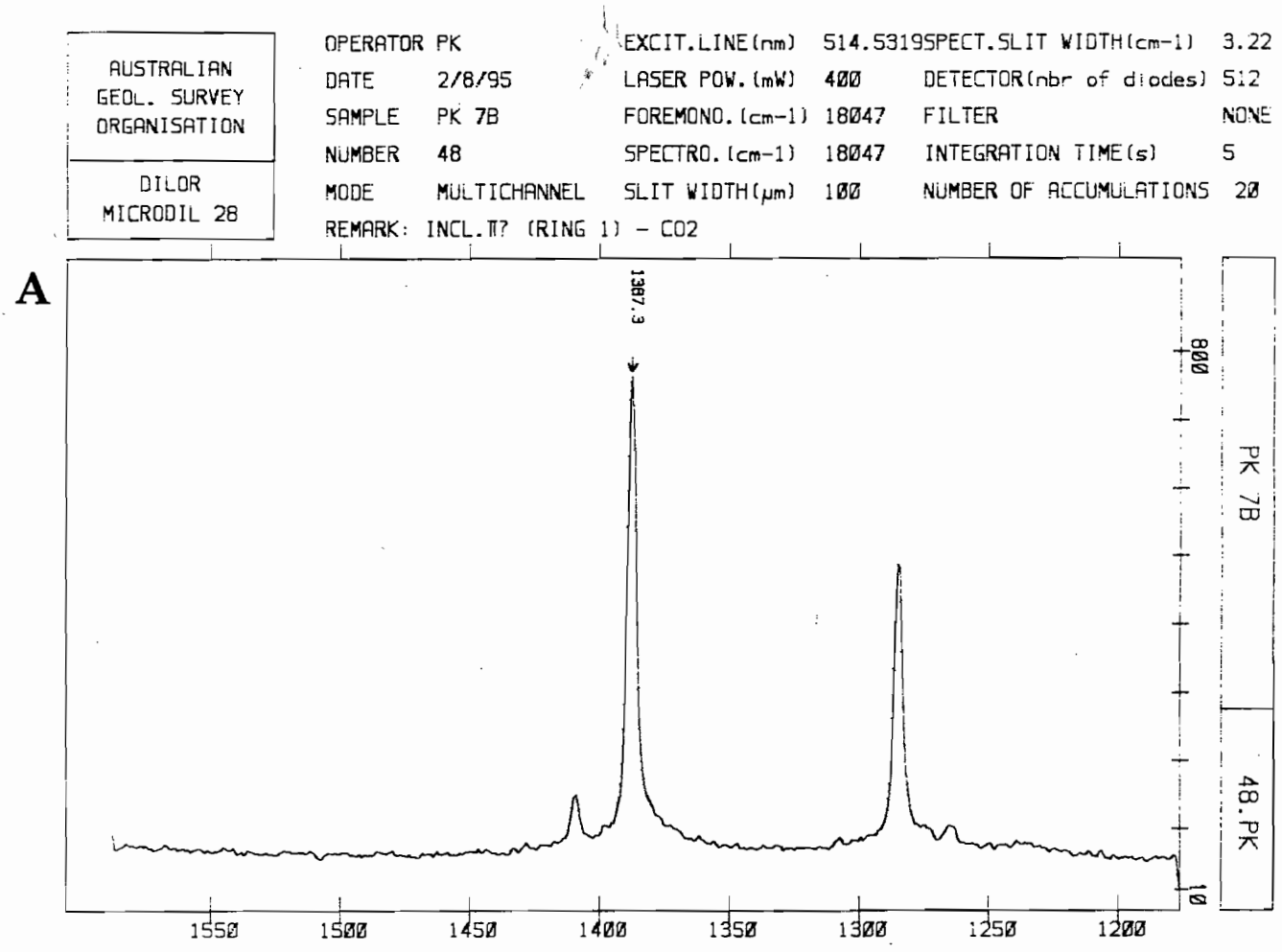
AUSTRALIAN GEOL. SURVEY ORGANISATION
DILOR MICRODIL 28
OPERATOR PK
DATE 2/8/95
SAMPLE PK 7B
NUMBER 48
MODE MULTICHANNEL
REMARK: INCL.?? (RING 1) - CO2
EXCIT.LINE(nm) 514.5319
LASER POW.(mW) 400
FOREMONO.(cm-1) 18047
SPECTRO.(cm-1) 18047
SLIT WIDTH(µm) 100
SPECT.SLIT WIDTH(cm-1) 3.22
DETECTOR(nbr of diodes) 512
FILTER NONE
INTEGRATION TIME(s) 5
NUMBER OF ACCUMULATIONS 20
A
1387.3
800
10
PK 7B
48.PK
1550
1500
1450
1400
1350
1300
1250
1200

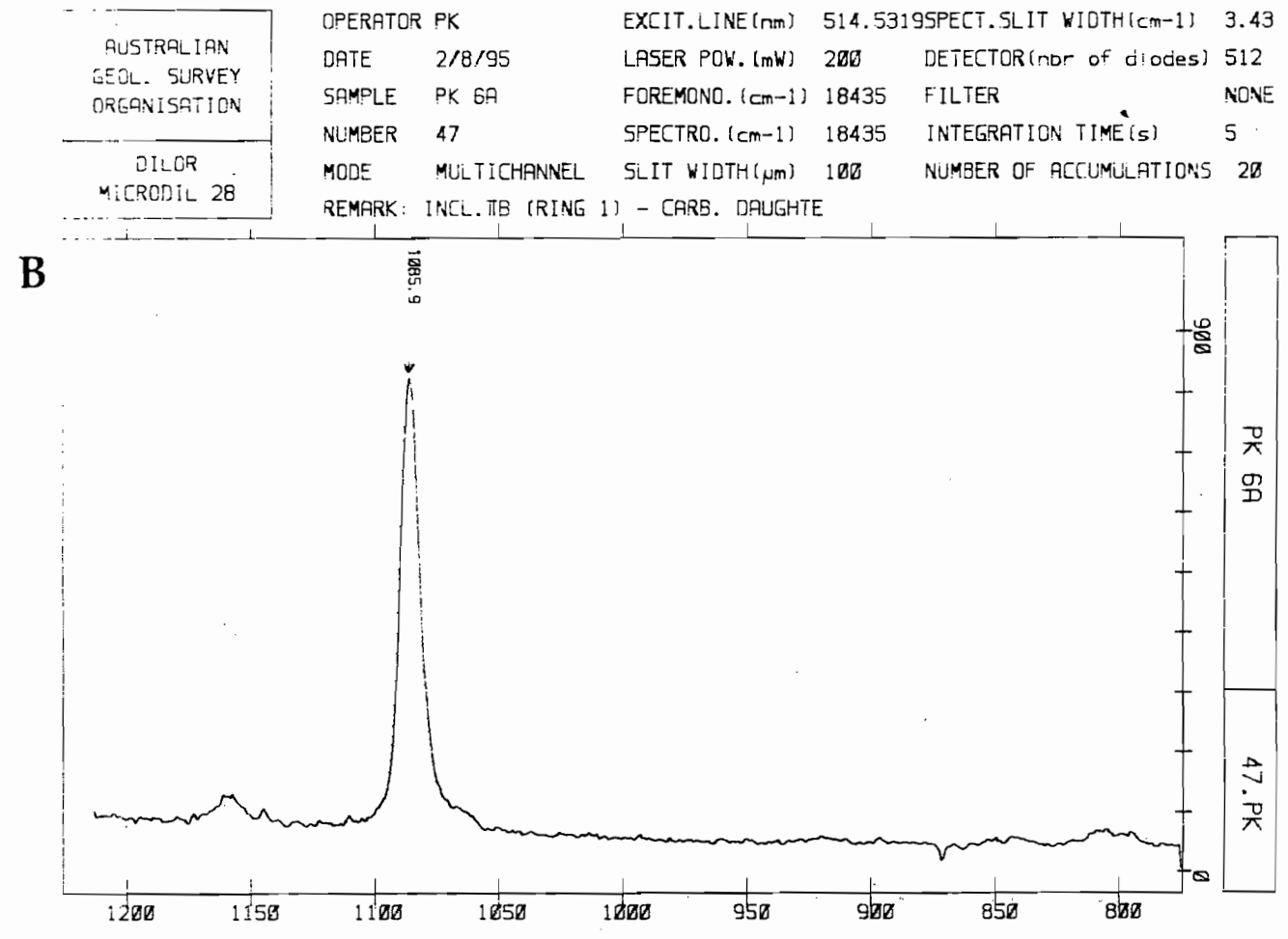
AUSTRALIAN GEOL. SURVEY ORGANISATION
DILOR MICRODIL 28
OPERATOR PK
DATE 2/8/95
SAMPLE PK 6A
NUMBER 47
MODE MULTICHANNEL
REMARK: INCL.?B (RING 1) - CARB. DAUGHTE
EXCIT.LINE(nm) 514.5319
LASER POW.(mW) 200
FOREMONO.(cm-1) 18435
SPECTRO.(cm-1) 18435
SLIT WIDTH(µm) 100
SPECT.SLIT WIDTH(cm-1) 3.43
DETECTOR(nbr of diodes) 512
FILTER NONE
INTEGRATION TIME(s) 5
NUMBER OF ACCUMULATIONS 20
B
1085.9
900
0
PK 6A
47.PK
1200
1150
1100
1050
1000
950
900
850
800

Figure 11.

Figure 12.

A

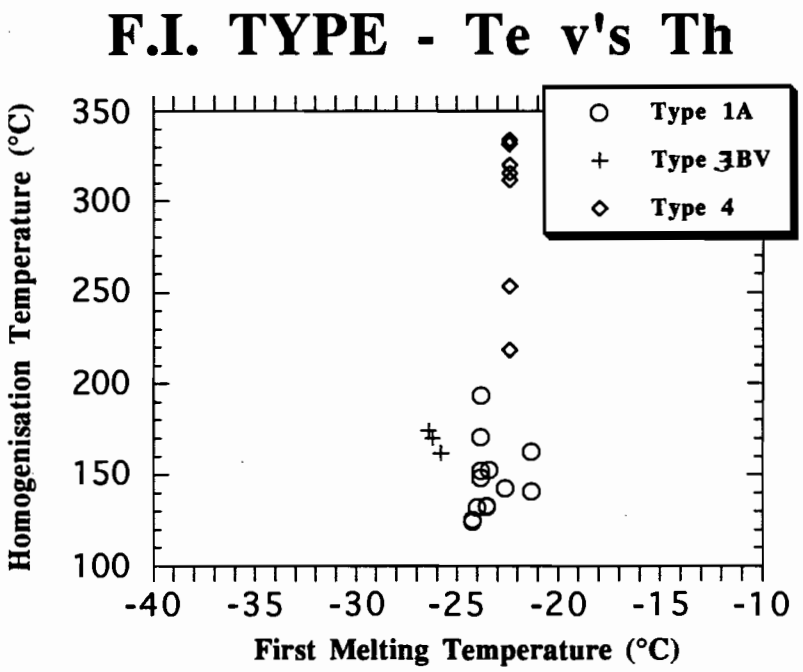
F.I. TYPE - Te v's Th
Homogenisation Temperature (°C)
350
300
250
200
150
100
-40
-35
-30
-25
-20
-15
-10
First Melting Temperature (°C)
Type 1A
Type 3BV
Type 4

B

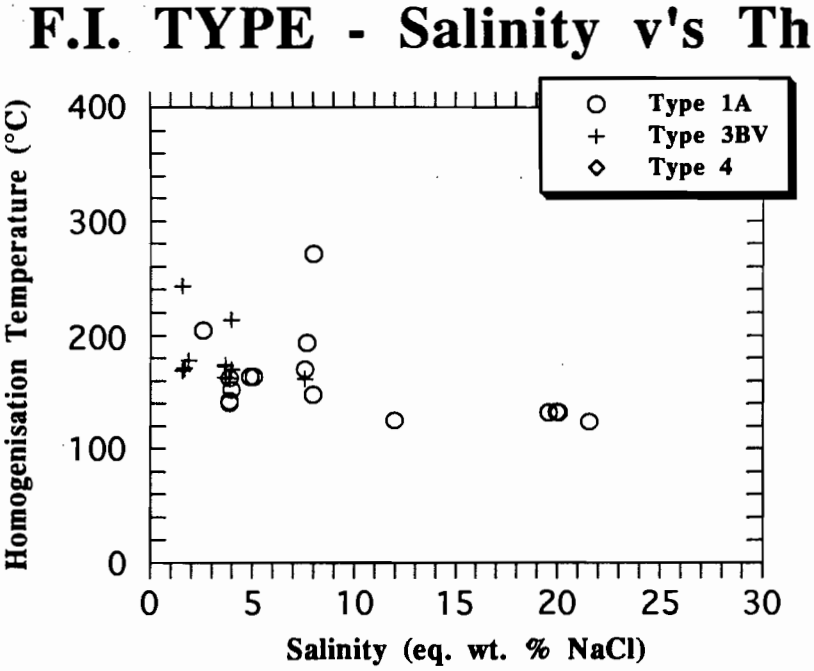
F.I. TYPE - Salinity v's Th
Homogenisation Temperature (°C)
400
300
200
100
0
0
5
10
15
20
25
30
Salinity (eq. wt. % NaCl)
Type 1A
Type 3BV
Type 4

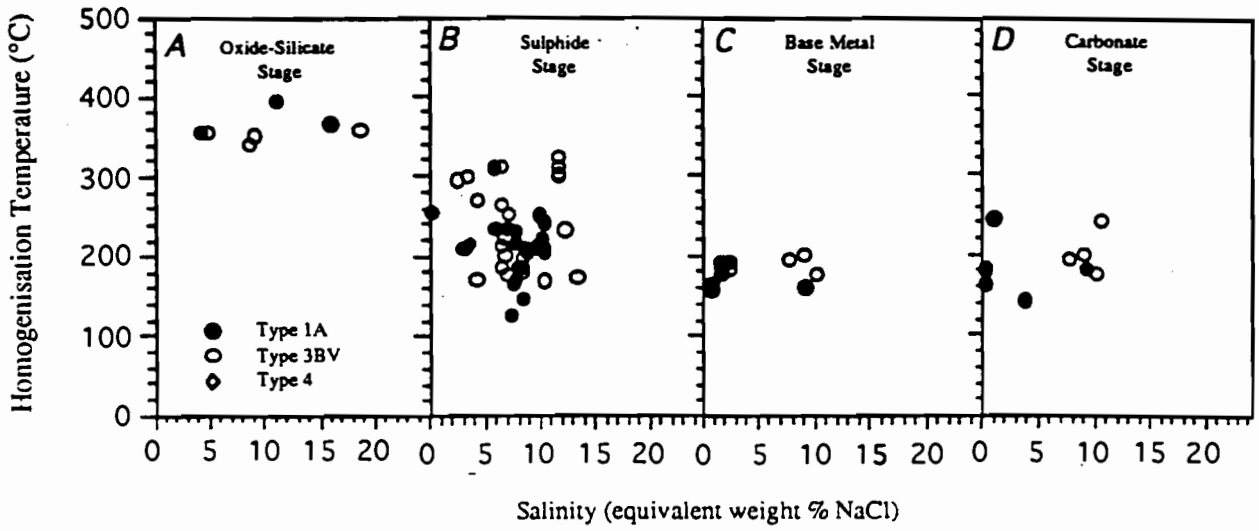

Figure 13. A Salinity v's homogenisation temperature for primary fluid inclusions from the vein stages of mineralisation. *A* : Oxide-silicate stage. *B* : Sulphide stage. *C* : Base metal stage. *D* : Carbonate stage.

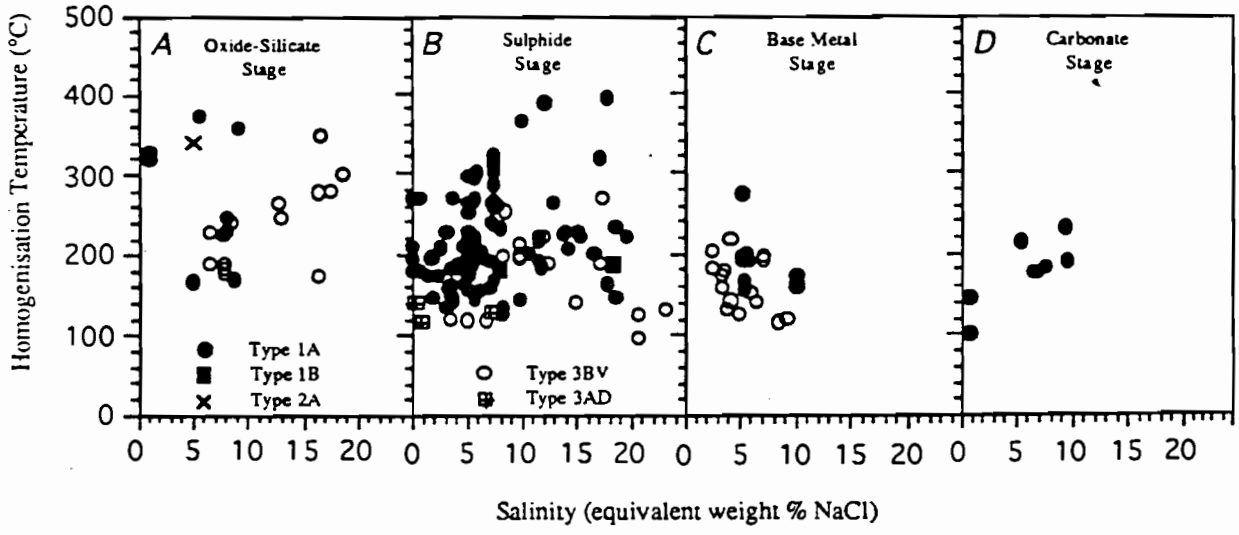

Figure 13. B Salinity v's homogenisation temperature for secondary fluid inclusions from the vein stages of mineralisation. *A* : Oxide-silicate stage. *B* : Sulphide stage. *C* : Base metal stage. *D* : Carbonate stage.

Table 2. Oxygen isotope analyses from quartz samples and their equilibrating fluids at indicated temperatures (°C).

FIELD NO.	LOCATION	MINERALOGY	TEMP (°C)	$\delta^{18}O_{qz}$ (SMOW)*	$\delta^{18}O_{fluid}$ (SMOW)	FLUID TYPE
PK-1A	388640E/5374560N Lake Makintosh-Sofia Tunnel	Py-Qz-Sph-Chl vein in Murchison volcanics	271.0	13.3	5.3	KCl-NaCl-H2O 8wt% NaCl eq.
PK-1C	388640E/5374560N Lake Makintosh-Sofia Tunnel	Qz-Sph-Py alteration in Owen conglomerate	333.5	13.3	7.5	?
PK-4C	388600E/5374530N Lake Makintosh car park	Qz-Sph-Py vein in Murchison granite	258.6	11.7	3.2	?
PK-5A	388600E/5374560N Lake Makintosh next to shed	Qz-Py-Sph-Chl vein in Murchison granite	163.7	13.4	-0.8	5wt% NaCl eq.
PK-6A	388300E/5374170N Tunnel Road Saddle	Qz-Py-Gal vein at contact b/w Owen congl. & Murch. gr.	243.2	12.1	2.9	Minor CO2 2wt% NaCl eq.
PK-7B	387220E/5375390N Murchison Gorge Rd.	Qz-Chl vug in Murchison volc. with dissem. Chl-Py	333.9	11.0	5.2	CO2-NaCl-H2O
PK-11B	385690E/5376530N Murchison Opencut	(i) Sph-Py-Qz-Carb	214.1	13.3	2.5	KCl-NaCl-H2O 4wt% NaCl eq.
PK-15B	379780E/5380570N Pieman Rd - Boco Ck	Qz vein in CVC	142.3	12.1	-4.0	KCl-NaCl-H2O 20wt% NaCl eq.
PK-21A	385340E/5375090N Murchison Hwy-Sth Tullah	Qz-Py-Gal-(Bte)? vein in Farrell Slates	162.2	12.6	-1.7	KCl-NaCl-H2O 4wt% NaCl eq.

* Analytical error is ± 0.2‰

Geochemical and isotopic signatures associated with Cambrian and Devonian fault structures

Paul A. Kitto

Centre for Ore Deposit and Exploration Studies, Geology Department, University of Tasmania

INTRODUCTION

Identification and classification of Cambrian and/or Devonian deformation structures using geochemical and isotopic signatures should assist/test the tectonic models proposed in the AMIRA Project P291 extension - *Structure and Mineralisation in Western Tasmania.* Ore deposit research has already shown that the source of ore fluids responsible for both Cambrian and Devonian mineralisation are substantially different. As a consequence, both the geochemical and isotopic signatures of vein material precipitated within faults should record the structural history of the fault; be it active in the Cambrian, Devonian or throughout major tectonic events.

PREVIOUS WORK

Initial geochemical and isotopic investigations were undertaken in a transect from the Pieman River to the Murchison Dam. It was reported that **oxygen isotope studies** of Devonian quartz bearing veins in association with detailed gravity interpretations of the underlying Devonian granite can be used to predict district scale telescoped Sn-Cu-Pb-Zn metal zonation patterns. This has been shown to be true for the Dundas mineral field and investigations continue in the Zeehan and Farrell mineral districts. **Microthermometric** results on fluid inclusions in quartz samples from the Pieman River - Murchison Dam transect indicate that base metal mineralisation resulted from a mixed magmatic and possibly meteoric source (Table 1). Such findings agree with late base metal stage fluid inclusion studies at Renison and Lakeside. These results, however, do not differentiate Cambrian styles of base metal mineralisation. Preliminary **PIXE Probe** and **Laser Raman** investigations on fluid inclusions from Devonian and Cambrian styles of mineralisation are currently being undertaken and it is considered that the results from such studies will assist in characterising the geochemical signatures of mineralised fault structures. **D/H isotope** studies on fluid inclusions should also assist in identifying the source(s) for hydrothermal fluids. Efforts are being undertaken to establish a facility capable of D/H isotope analysis in the CSL at the University of Tasmania.

Previous investigations on carbonate bearing vein assemblages, which typically post-date the main stages of mineralisation, show that the carbonates have unique isotopic signatures ($\delta^{18}O_{carb}$ & $\delta^{13}C_{carb}$) that can differentiate Cambrian hydrothermal carbonates from Devonian hydrothermal carbonates. **Sr and C isotopic** variations in marine carbonates have been suggested by Kaufman et al (1993) to indicate significant environmental and tectonic changes. Preliminary investigations of Sr and C isotopic variations in fault controlled carbonate will proceed when suitable analytical facilities can be located.

Pb isotope investigations by Gulson and co-workers on western Tasmanian deposits show that Devonian and Cambrian styles of mineralisation have distinct Pb isotope signatures. This technique has already been used to identify Cambrian growth structures in the Mt Read Volcanics (Davidson & Kitto, this report). Similarly **S isotopes** are being used to identify fluid flow directions responsible for Cambrian VHMS mineralisation north of Rosebery, and recognition of a Devonian overprint is also apparent.

CONCLUSIONS

In conclusion, it is apparent that no single geochemical or isotopic technique can itself differentiate those structures that have been active in Cambrian &/or Devonian periods. However, a number of approaches can be systematically undertaken depending whether the mineralised structure contains **quartz** (O, D/H isotopes; fluid inclusion microthermometry, PIXE Probe, Laser Raman), **carbonate** (C/O, Sr/C, D/H isotopes; fluid inclusion microthermometry, PIXE Probe, Laser Raman), **galena** (Pb, S isotopes), or **sulphides** (S isotopes, trace elements in pyrite). The implementation of an integrated investigative approach to the recognition of possible Cambrian growth structures within the Mt Read Volcanic belt will be the major thrust of on going research in the next 6 month period.

Table 1. Oxygen isotope analyses from quartz samples and their equilibrating fluids at indicated temperatures (°C).

FIELD NO.	LOCATION	MINERALOGY	TEMP (°C)	$\delta^{18}O_{qz}$ (SMOW)*	$\delta^{18}O_{fluid}$ (SMOW)
PK-1A	388640E/5374560N Lake Makintosh-Sofia Tunnel	Py-Qz-Sph-Chl vein in Murchison volcanics	271.0	13.3	5.3
PK-1C	388640E/5374560N Lake Makintosh-Sofia Tunnel	Qz-Sph-Py alteration in Owen conglomerate	333.5	13.3	7.5
PK-4C	388600E/5374530N Lake Makintosh car park	Qz-Sph-Py vein in Murchison granite	258.6	11.7	3.2
PK-5A	388600E/5374560N Lake Makintosh next to shed	Qz-Py-Sph-Chl vein in Murchison granite	163.7	13.4	-0.8
PK-6A	388300E/5374170N Tunnel Road Saddle	Qz-Py-Gal vein at contact b/w Owen congl. & Murch. gr.	243.2	12.1	2.9
PK-7B	387220E/5375390N Murchison Gorge Rd.	Qz-Chl vug in Murchison volc. with dissem. Chl-Py	333.9	11.0	5.2
PK-11B	385690E/5376530N Murchison Opencut	(i) Sph-Py-Qz-Carb	214.1	13.3	2.5
PK-15B	379780E/5380570N Pieman Rd - Boco Ck	Qz vein in CVC	142.3	12.1	-4.0
PK-21A	385340E/5375090N Murchison Hwy-Sth Tullah	Qz-Py-Gal-(Bte)? vein in Farrell Slates	162.2	12.6	-1.7

* Analytical error is ± 0.2‰

ISOTOPES	POTENTIAL INFORMATION	RELATED STUDIES
$\delta^{18}O_{quartz}$, $\delta^{18}O_{fluid}$	• Metal Zonation • Type of Fluids • W/R ratios	• Microthermometry • PIXE Probe • Laser Raman
$\delta^{18}O_{carb}$, $\delta^{13}C_{carb}$	• Source of Fluids • W/R ratios	• Microthermometry • PIXE Probe • Laser Raman
D/H	• Sources of Fluids	• Microthermometry • PIXE Probe • Laser Raman
Sr/C	• Environmental Changes • Tectonic Changes	• Microthermometry • PIXE Probe • Laser Raman
Pb	• Source of Fluids	
S	• Source of Fluids	• Trace Element Geochem.

SIGNATURE	CAMBRIAN	DEVONIAN
$\delta^{18}O_{quartz}$, $\delta^{18}O_{fluid}$	POTENTIALLY	YES
$\delta^{18}O_{carb}$, $\delta^{13}C_{carb}$	YES	YES
D/H	POTENTIALLY	POTENTIALLY
Sr/C	?	?
Pb	YES	YES
S	YES	POTENTIALLY
FLUID INCLUSIONS		
• Microthermometry	POTENTIALLY	POTENTIALLY
• PIXE Probe	POTENTIALLY	POTENTIALLY
• Laser Raman	POTENTIALLY	POTENTIALLY